# Thermal Desalination: Structural Optimization and Integration in Clean Power and Water

by

Gina Marie Zak

B.S., University of Illinois at Urbana-Champaign (2010)

Submitted to the Department of Mechanical Engineering
in partial fulfillment of the requirements for the degree of

Master of Science in Mechanical Engineering

at the

MASSACHUSETTS INSTITUTE OF TECHNOLOGY

June 2012





Author .....
Department of Mechanical Engineering
May 11, 2012

Certified by .....
Alexander Mitsos
Rockwell International Assistant Professor
Thesis Supervisor

Accepted by .....
David E. Hardt
Ralph E. and Eloise F. Cross Professor of Mechanical Engineering
Chairman, Department Committee on Graduate Theses

# Thermal Desalination: Structural Optimization and Integration in Clean Power and Water

by

Gina Marie Zak

Submitted to the Department of Mechanical Engineering
on May 11, 2012, in partial fulfillment of the
requirements for the degree of
Master of Science in Mechanical Engineering

## Abstract

A large number of resources are dedicated to seawater desalination and will only grow as world-wide water scarcity increases. In arid areas with high temperature and salinity seawater, thermal desalination and power plants (dual-purpose/co-generation plants) are often employed for the production of power and water. In other areas, reverse osmosis is commonly employed. However, both technologies are inherently challenged with economic and performance issues. Seawater desalination methods, in particular thermal desalination methods, are highly energy intensive and are associated with $CO_2$-emitting electricity production. This thesis is presented with three chapters, each of which is self-contained, but have a unifying goal of improving industrial-scale thermal desalination and its integration with power production or other technologies.

The first chapter presents a critical review of hybrid desalination systems for co-generation of power and water. Hybrid desalination, i.e., employing both thermal and mechanical desalination methods, is a response to the issues associated with existing seawater desalination technologies and has been increasingly utilized over thermal desalination plants alone. An overview of thermal desalination, seawater reverse osmosis, and co-generation of power and water is presented, specifically with regards to the motivation for utilizing hybrid plants, e.g., process limitations and areas of potential improvement. In addition, a review of the considerations for design and economics of hybrid desalination plants is presented, e.g., existing system configurations, thermoeconomic analyses, and improvements of seawater pretreatment are discussed. Finally, studies for the optimization of hybrid desalination systems are reviewed. Specifically, the use of objective functions, continuous optimization methods, and optimal hardware configurations are discussed with respect to the key considerations of hybrid desalination plants.

The purpose of the second chapter is to investigate the integration of thermal desalination methods with carbon capture and sequestration (CCS) electricity production in order to implement emissions-free thermal desalination facilities. Specifically,

the Advanced Zero Emissions Plant (AZEP) oxy-combustion concept is utilized for integration in this study. The performance of several bottoming cycle integrations coupled to multi-effect distillation (MED) with and without thermal vapor compression (TVC) is estimated in order to evaluate the thermodynamic and economic feasibility of such emissions-free power and water plants. It is found that AZEP plants could utilize industry-standard dual-purpose technology and produce water near power-to-water ratios typical of dual-purpose plants without CCS.

Finally, the structural optimization of thermal desalination is investigated. Many configurations of thermal desalination technologies exist, each with trade-offs in operational performance and required economic investment. Further, the optimization of hybrid or dual-purpose desalination is informed by the configuration and operation of thermal desalination as a subsystem. In this study, thermal desalination technologies are analyzed by a control volume perspective in order to identify physical processes which are shared among all technologies. A superstructure is then developed to express connectivity possibilities between these physical processes. The resulting superstructure encompasses existing thermal desalination configurations as well as the possibility for novel configurations. Informed by the superstructure, three non-standard configuration case studies are presented; the case studies demonstrate better performance with respect to performance ratio and/or specific heat transfer surface area than existing thermal desalination configurations. These studies indicate promising alternatives to standard configurations, but also identify the need for numerical optimization and detailed modeling in order to determine optimal thermal desalination structures in conjunction with dual-purpose and/or hybrid integrations.

Thesis Supervisor: Alexander Mitsos
Title: Rockwell International Assistant Professor

# Acknowledgments

There are many people who have contributed to the success of this undertaking. I cannot fully express my gratitude in these short sentences, but I will be forever indebted to those who motivated me to find personal strength I did not know I possessed.

To my advisor, for steadily guiding me and always having my best interests in mind. You are an inspirational thinker, and you have taught me many skills which I will utilize throughout my career.

To my family, who has given me unrelenting encouragement throughout the course of this endeavor and my life. To my Mom, for instilling in me dedication and the courage to move forward. To Nicole, for your willingness to listen and being a best friend as well as a sister.

To Katie, I am so grateful for the time I have spent with you. You have been an unwaivering source of support and happiness.

To Greg, you have been an amazing friend in many ways. You always encouraged me to push for success, and it contributed greatly to where I am now.

To my friends, you made this experience a time that I will not forget. To Enrique, Dan, Nick, Elysia, Tawfiq, and the rest of my labmates, you have helped me think about my project in new ways and provided many thoughtful discussions.

To Mr. Bob Coverdill, Dr. Andrew Alleyne, and Dr. Kimani Toussaint, for honing my skills as an engineer and always motivating me to utilize my talents.

To Nicholas D. Mancini, Dr. Amin Ghobeity, and Dr. Mostafa H. Sharqawy for their contributions to the work which is presented herein.

Finally, I thank the King Fahd University of Petroleum and Minerals in Dhahran, Saudi Arabia, for funding the research reported in this thesis through the Center for Clean Water and Clean Energy at MIT and KFUPM.

*— In memory of Joseph R. Zak —*

THIS PAGE INTENTIONALLY LEFT BLANK

# Contents


**1 A Review of Hybrid Desalination Systems for Co-Production of Power and Water: Analyses, Methods, and Considerations 17**

1.1 Introduction . . . . . 17

1.2 Overview of Thermal Desalination in Large Scale Applications . . . . 19

1.2.1 Overview of the MED Process . . . . . 20

1.2.2 Overview of the MSF Process . . . . . 24

1.2.3 Electrical Energy Consumption in Thermal Desalination . . . . 26

1.2.4 Common Models to Describe Thermal Desalination . . . . . 28

1.3 Overview of Seawater Reverse Osmosis . . . . . 28

1.3.1 Limitations of SWRO . . . . . 29

1.3.2 SWRO System Configuration . . . . . 30

1.4 Overview of Co-Generation for Power and Water . . . . . 30

1.4.1 Steam supply design . . . . . 31

1.4.2 Power-to-Water Ratio . . . . . 32

1.5 Scaling and Fouling in Desalination . . . . . 33

1.5.1 Scaling in Thermal Desalination . . . . . 33

1.5.2 Scaling and Fouling in Seawater Reverse Osmosis . . . . . 34

1.6 Considerations for Hybrid Desalination Systems . . . . . 35

1.6.1 Configurations of Hybrid Systems . . . . . 36

1.6.2 Thermoeconomic Analyses . . . . . 40

1.6.3 Pretreatment Improvement Through Nanofiltration . . . . . 43

1.7 Optimization Methods . . . . . 45
1.7.1 Objective Functions . . . . . 46
1.7.2 Continuous Optimization Methods . . . . . 47
1.7.3 Fixed versus Flexible Hardware Configurations for Optimization 50
1.8 Conclusion . . . . . 53

**2 Integration of Thermal Desalination Methods with Membrane-Based Oxy-Combustion Power Cycles 55**

2.1 Introduction . . . . . 55
2.2 Plant Descriptions and Simulation of Thermodynamic Performance . 58
2.2.1 Advanced Zero Emissions Plant Description and Simulation . . 59
2.2.2 Thermal Desalination Method Descriptions and Simulations . 63
2.3 Estimation of Capital Expenditures . . . . . 70
2.4 Bottoming Cycle Integrations . . . . . 71
2.4.1 MED Back-Pressure Bottoming Cycle . . . . . 72
2.4.2 MED-TVC Extraction Bottoming Cycle . . . . . 73
2.4.3 Water-Only Bottoming Cycle . . . . . 74
2.5 Results and Discussion . . . . . 76
2.5.1 Thermodynamic Performance and Water Production . . . . . 76
2.5.2 Capital Expenditures . . . . . 78
2.5.3 Specific Lost Work and Power-to-Water Ratios . . . . . 80
2.6 Conclusion . . . . . 81

**3 Structural Optimization of Thermal Desalination 83**

3.1 Introduction . . . . . 83
3.2 Thermal Desalination by Physical Processes . . . . . 86
3.2.1 Multi-Stage Flash by Physical Processes . . . . . 87
3.2.2 Multi-Effect Distillation by Physical Processes . . . . . 89
3.2.3 Thermodynamic Modeling of Physical Processes . . . . . 92

3.3 Thermal Desalination Superstructure . . . . . 97
3.3.1 Evaporation Unit and Down Condensing Unit . . . . . 97
3.3.2 Steam Supply Interface . . . . . 103
3.3.3 Configuration Examples . . . . . 105
3.4 Case Studies of Non-Standard Configurations . . . . . 109
3.4.1 Forward to Parallel-Cross MED . . . . . 110
3.4.2 MSF to FF-MED . . . . . 117
3.4.3 MSF to FF-MED-TVC . . . . . 121
3.5 Conclusion . . . . . 125

THIS PAGE INTENTIONALLY LEFT BLANK

# List of Figures


1-1 Schematic of MED process. . . . . 21

1-2 Schematic of MED-TVC process. . . . . 21

1-3 Schematic of MED-MVC process. . . . . 21

1-4 Forward-feed MED configuration . . . . . 23

1-5 Backward-feed MED configuration . . . . . 23

1-6 MSF process with once through cooling . . . . . 24

1-7 MSF process with brine recirculation . . . . . 25

1-8 Reported values of MED and MED-TVC electrical consumption . . . 27

1-9 Examples of hybrid configurations . . . . . 37

1-10 MSF/SWRO hybrid experimental plant, El-Sayed et al. [73] . . . . . 39

2-1 AZEP Topping Cycle; zero emission cycles do not include an after-burner (block "AFTERBRN"). . . . . 60

2-2 Triple pressure bottoming cycle for AZEP100/72: Pressure levels for AZEP100 are 100/20/5 bar and AZEP72 are 100/25/5 bar. . . . . 61

2-3 $CO_2$ Compression and Purification Unit (CPU). . . . . 62

2-4 Unit Model of MED Effect "N" modeled in ASPEN Plus®. . . . . 65

2-5 Parallel-cross MED with feedwater heaters. . . . . 66

2-6 Parallel-cross MED-TVC with feedwater heaters. . . . . 69

2-7 MED Back-pressure bottoming cycle, AZEPXX-BST-MED, flowsheet. 73

2-8 MED-TVC extraction bottoming cycle, AZEPXX-EST-TVC, flowsheet. 74

2-9 Triple pressure TVC water-only bottoming cycle, AZEPXX-3TVC, flowsheet. . . . . 75

2-10 First Law efficiency and water production results for proposed bottoming cycle integrations. The baseline efficiencies of AZEP100 and AZEP72 are 48.9% and 53.4%, respectively. . . . . 77

2-11 Capital expenditures of proposed bottoming cycle integrations. . . . . 79

3-1 Once-through multi-stage flash (MSF). . . . . 87

3-2 Single stage of MSF with depiction of physical processes. . . . . 88

3-3 Parallel feed multi-effect distillation (PF-MED). . . . . 90

3-4 Parallel feed multi-effect distillation with thermal vapor compression (PF-MED-TVC). . . . . 90

3-5 Single effect of PF-MED with depiction of physical processes. . . . . 91

3-6 First effect of MED-TVC with depiction of physical processes. . . . . 92

3-7 Thermal desalination structure: Evaporation unit, Unit N. . . . . 98

3-8 Thermal desalination structure: down condensing unit. . . . . 102

3-9 Down condensing unit as a subset of evaporation unit. . . . . 102

3-10 Thermal desalination structure: Steam supply interface, Unit 0. . . . . 103

3-11 Example connectivity of unit N: a stage of once-through MSF. . . . . 105

3-12 Example connectivity: Heat rejection section of brine-recirculating MSF. 106

3-13 Example connectivity of unit N and unit 0: Effect 1 and 2 of MED parallel configuration. . . . . 106

3-14 Backward-feed MED configuration. . . . . 107

3-15 Example connectivity: Last two effects of backward MED configuration. 107

3-16 Evaporation section of hybrid MED-MSF configuration discussed by Nafey et al. [138]. . . . . 108

3-17 Hybrid MED-MSF configuration [138] expressed by repeating superstructure units. . . . . 108

3-18 Transition from forward to parallel-cross configuration of FF-PC-MED concept depicted by thermal desalination superstructure. . . . . 111
3-19 Forward to parallel-cross MED concept . . . . . 111
3-20 Performance of FF-PC-MED (Figure 3-19) configuration with varying number of effects and transition effects. . . . . 116
3-21 Transition from MSF configuration to MED configuration in MSF-MED concept. . . . . 118
3-22 MSF to FF-MED concept with alternative vapor routing of MSF for unit ($N_s$-1). . . . . 118
3-23 Performance of MSF-MED concept as compared to MSF-OT for fixed operating conditions and total number of units ($N_t$=24) with varying transition unit from $N_s$=12 to $N_s$=24. . . . . 120
3-24 Transition from MSF configuration to MED configuration in MSF-MED-TVC concept, shown with MED steam supply configuration. . 121
3-25 MSF to MED-TVC concept . . . . . 121
3-26 Performance of MSF-MED-TVC concept as compared to FF-MED-TVC and PC-MED-TVC with varying TVC compression ratio and fixed number of stages/effects. . . . . 125

THIS PAGE INTENTIONALLY LEFT BLANK

# List of Tables


1.1 Main features of MED-TVC plant [36] . . . . . 23

1.2 Main features of MSF Plant [36] . . . . . 25

1.3 Typical steam conditions for thermal desalination plants [63, 109] . . 32

2.1 Performance results of zero and partial emissions AZEP cycles from Mancini and Mitsos [116]. . . . . 63

2.2 Thermal desalination operating parameters for integration with AZEP. 67

2.3 ASPEN Plus® Simulation Results of MED and MED-TVC. . . . . 69

2.4 HRSG economic parameters [50]. . . . . 71

2.5 Power and water production performance results of bottoming integrations; the negative bottoming work of 3TVC is due to HRSG pumping requirements. . . . . 77

2.6 Capital expenditures of bottoming cycle components (million $US). . 78

2.7 Specific lost work and PWR results of proposed bottoming cycle integrations (kWh/m$^3$). . . . . 81

3.1 Superstructure stream types, associated variables, and figure keys. . 98

3.2 Operating parameters for PC-MED, FF-MED, and FF-PC-MED (Figure 3-19) configurations. . . . . 113

3.3 Forward-feed MED results. 12 effects, PR=9.47, SA=439 m$^2$/(kg/s), Area of down condenser=1009 m$^2$. . . . . 114

3.4 Parallel-cross MED results. 12 effects, PR=10.32, SA=525 m$^2$/(kg/s), Area of down condenser=895 m$^2$. . . . . 114

3.5 Forward to parallel-cross MED results, 12 effects with transition at effect 6. PR=10.19, SA=491 $m^2/(kg/s)$, Area of down condenser = 912 $m^2$. . . . . 115

3.6 Operating parameters for MSF-MED (Figure 3-22) and MSF-OT configuration. . . . . 119

3.7 MSF-MED results for $N_t$=24 with transition unit $N_s$=12. PR=9.75, SA=238 $m^2/(kg/s)$, RR=17.6%. . . . . 120

3.8 Operating parameters for FF-MED-TVC, PC-MED-TVC, and MSF-MED-TVC (Figure 3-25) configurations. . . . . 122

3.9 Variation of TVC compression ratio for $P_{m,sat}$ = 0.175 MPa ($T_{m,sat}$ = 116°C), $P_{e,sat}$ = 0.00732 MPa ($T_{e,sat}$ = 40°C), with resulting entrainment ratio, discharge temperature, MED TBT, and MSF last effect brine temperature. . . . . 123

3.10 MSF-MED-TVC results for MSF $N_t$=15, MED $N_t$ = 12, and CR=4. PR=13.0, SA=418.1 $m^2/(kg/s)$. . . . . 124

# Chapter 1

# A Review of Hybrid Desalination Systems for Co-Production of Power and Water: Analyses, Methods, and Considerations*

## 1.1 Introduction

Seawater desalination processes are highly energy intensive, and the need for freshwater procurement has been of growing importance over the past several decades. In the Middle East and other regions with water of high salinity (total dissolved solids (TDS) of $\approx 35-45$ g/kg) and high temperature ($\approx 30-35$°C during summer), thermal desalination methods, in particular multi-stage flash (MSF), have historically been favored. The energy consumption of thermal desalination methods is independent of the feedwater salinity to a first order. Typically, these regions also have difficult water pretreatment issues due to seasonal algae growth, and pre-treatment in MSF is less critical since scaling in MSF is minimal.

*This chapter includes contributions by Dr. Amin Ghobeity (MIT) and Dr. Mostafa H. Sharqawy (KFUPM). Specifically, Dr. Ghobeity contributed to Section 1.3 and 1.5. Dr. Sharqawy contributed to Section 1.2, 1.4, and 1.5.

These thermal desalination plants are usually integrated as a dual-purpose scheme (also called co-generation), i.e., simultaneous production of power and water, which increases the thermal efficiency of the plant as compared to a standalone thermal desalination plant. However, high capital and maintenance costs are associated with the use of thermal desalination and issues, e.g., mismatch in production ratio to meet electrical/water demand, exist when integrated as a dual-purpose plant. As a result, improvements to existing desalination technologies and novel integration schemes have been increasingly investigated.

Hybrid desalination systems, i.e., the combination of thermal and mechanical desalination technologies, in addition to integration with electrical power production is a promising solution to the difficulties associated with conventional dual-purpose plants. The purpose of this article is to review investigations of hybrid desalination and dual-purpose integrations; specifically, studies relating to the analyses and methods used to optimize such systems will be reviewed. Because of the high investment and long-term maintenance costs involved in large scale dual-purpose plants, the optimization of potential hybrid schemes is of high importance. Further, both the concerns and potential advantages or ideas relating to hybrid desalination systems shall be reviewed within the context of existing literature.

As a precursor to the discussion on hybrid dual-purpose desalination systems, the desalination technologies typically suggested for hybrid integration shall be overviewed. The most popular industrial scale desalination systems, i.e., MSF, multi-effect distillation (MED) and seawater reverse osmosis (SWRO), shall be presented for the reason that MSF is the most popular technology utilized in dual-purpose schemes and MED and SWRO are the fastest growing technologies to be implemented in seawater desalination applications. The interest in hybridization has been increasing over the past decade, and the focus of this article shall be mainly on recent publications.

In this article, a dual-purpose plant shall refer to a system that produces both power and water. In most contexts, a dual-purpose plant refers to one utilizing thermal desalination because of the thermodynamic benefit of integration (to be summarized later). A hybrid desalination system shall refer to the combination of more

than one desalination technology, typically thermal distillation combined with mechanical desalination. An example of a single-purpose hybrid desalination system is multi-stage flash with reverse osmosis and nanofiltration (NF-SWRO-MSF). The details of each technology and subsequent integration schemes will be summarized in the following sections.

## 1.2 Overview of Thermal Desalination in Large Scale Applications

Thermal desalination has been applied in large scale production, especially in the Middle East and North African countries, since the mid-twentieth century. This is because this region has a lack of fresh water resources and requires large scale desalination plants to meet the water demand of the increasing population and development. MSF is the dominating technology within thermal desalination with multiple installations in the countries of Gulf Cooperation Council (GCC), where the energy cost is low. Thermal desalination technologies produce high quality product water with very low salinity, and the efficiency and production rate are not affected by the quality of feed water (to a first order). As a result, the majority of large scale desalination plants in the GCC countries use thermal desalination processes. About 77% of the total water production in this region is produced by thermal desalination processes [88].

MSF is more reliable and simpler in operation than other desalination processes. In the 1960's, the unit capacity of MSF Plant was 500 $m^3/d$ (0.1 MIGD), and later in the late 1970's, the capacity increased to 27,000-32,000 $m^3/d$ (6-7 MIGD) [12]. Current MSF capacities have increased to 50,000-75,000 $m^3/d$ (11-16.5 MIGD) [2]. This increase in unit capacity of MSF was achieved through improvements in the construction materials and by newly designed and streamlined components, which includes tubing, demisters, venting systems, partitions, and pumping units. The MSF technology has excellent process reliability and the ability to continuously operate

for durations of more than 2 years, has encouraged the continued maintenance and updating of existing MSF plants. It requires minimal feedwater pre-treatment and has low potential of bio-fouling and scaling. However, MSF is highly energy intensive and requires large investment cost.

MED (also known as multi-effect evaporation, MEE or multi-effect boiling, MEB), is another thermal desalination process which has been used in large scale production. MED was the first proposed thermal desalination technology (before MSF), but due to severe scaling and fouling problems the plants experienced frequent shutdowns [17]. Presently, MED does not have large market share as compared to MSF, especially in GCC countries. However, MED has increasingly been installed in large scale water production due to improvements in enhanced heat transfer surfaces and anti-scalants. Furthermore, due to reduced pressure drop in pipes and ducts of the MED, the electrical power consumption for pumping in MED is claimed to be lower than MSF. The unit capacity of MED systems have significantly increased up to 45,000-68,000 $m^3/d$ (10-15 MIGD) as compared to market introduction of 4,500 $m^3/d$ (1 MIGD) [17].

### 1.2.1 Overview of the MED Process

In the MED plant, seawater is desalinated by means of evaporation in a series of evaporators (effects); then the vapor is condensed to be collected as distillate. To increase the efficiency as compared to a single effect process, the vapor formed in one effect is used to vaporize seawater in the next effect. This procedure is repeated from one effect to another with gradually decreasing temperature and pressure due to the decrease in the formed vapor saturation temperature. The process is driven by a heat source from steam that evaporates the seawater in the first effect. Figure 1-1 shows a simplified schematic of a MED process. Each effect is composed of heat transfer tubes wherein vapor is condensed and seawater evaporates outside the tubes. The vapor formed outside the tubes is transferred to flow inside the tubes of the next effect to vaporize more seawater. The vapor inside the tubes is condensed and collected in the

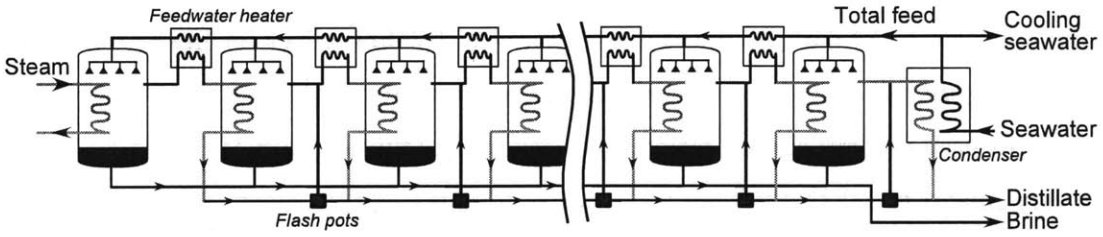


**Figure 1-1:** Schematic of MED process.

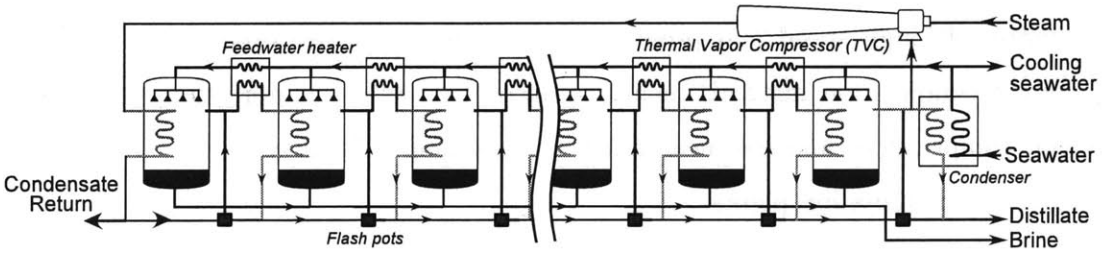


**Figure 1-2:** Schematic of MED-TVC process.

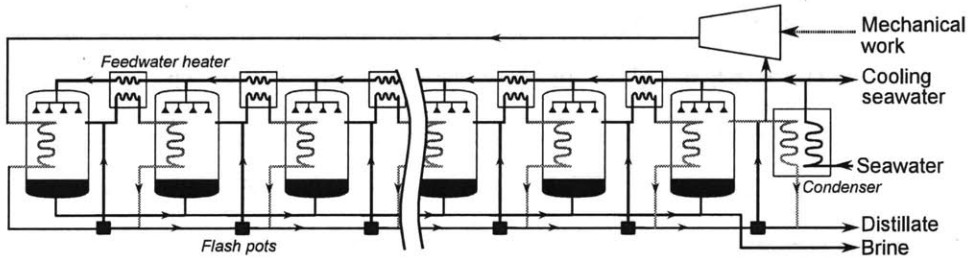


**Figure 1-3:** Schematic of MED-MVC process.

distillate line. The vapor at the last effect (lowest temperature) is condensed using cooling seawater. Part of the seawater which is preheated in the last condenser is fed to the effects and the remaining part is discharged back to the sea.

There are three main types of MED processes. The first type is the low-temperature MED process (Figure 1-1) in which low pressure steam (typically less than 0.5 bar) is the main heating source. The second type is MED-TVC (thermal vapor compression) in which moderate pressure steam (2.5-3 bar) is used as motive steam of an ejector. The ejector entrains the vapor from the last effect (condenser) and mixes it with the

motive steam to be compressed and introduced to the first effect for heating the seawater (Figure 1-2). Table 1.1 summarizes the key features of MED-TVC plants, which are most used in large co-generation production. The third type is MED-MVC, which is very similar to MED-TVC but the vapor is compressed by a mechanical compressor (Figure 1-3). This type eliminates the need for moderate-pressure steam and therefore can be utilized when there is no steam available since the compression process raises the temperature of the vapor. However, MVC requires compressor operation at extremely high speed and pressure ratios. There are also other types that use different compression methods including absorption vapor compression, adsorption vapor compression, and chemical vapor compression. These types are not used in large scale desalination plants.

For MED (with or without TVC/MVC), there are different configurations for the flow arrangement of both the feed seawater and the vapor in each effect. These configurations are parallel (Figure 1-1), forward (Figure 1-4) and backward (Figure 1-5). In the parallel configuration, the feed seawater is sprayed in near equal amounts in each effect over the bank of tubes. In the forward configuration, the feed seawater is pumped to the first (highest temperature) effect; then the brine and vapor flow in the same direction to the last effect (condenser). In the backward configuration, the feed seawater enters the last (lowest temperature) effect; then the brine from that effect is pumped to the next effect (higher temperature) until reaching the first (highest temperature) effect. In the backward configuration, vapor flows in the opposite direction of the feed flow.

The forward feed configuration can operate at high top brine temperature since the salt salinity is minimum [68] which results in higher performance ratio. However, from a thermodynamic point of view, the forward configuration has a large temperature difference between the heating steam in the first effect and feed seawater which increases the irreversibility. From this aspect, the backward configuration performs better, but the major disadvantage of the backward system is the high pumping power as compared to other configurations required to pump the feed seawater to the higher pressure effects. The other disadvantage of this system is that the brine with the

**Table 1.1:** Main features of MED-TVC plant [36]

| | |
|---|---|
| Seawater salinity | 30-47 g/kg |
| Top brine temperature (TBT) | 63-75 °C |
| Steam supply | 2.5-3 bar |
| Steam consumption | 15.8 Tons/MIGD |
| GOR | 12-15 |
| Capital cost | 4.5-9.0 US$ MM per MIGD |
| Capital cost - Intake/Outfall | 0.1-2.0 US$ MM per MIGD |
| Chemicals cost | 40,000 US$/yr per MIGD |
| Labor cost | 40,000 US$/yr per MIGD |

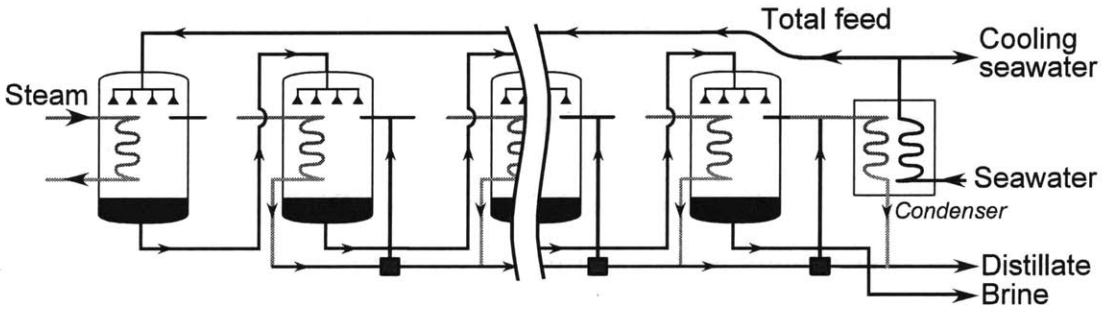


**Figure 1-4:** Forward-feed MED configuration

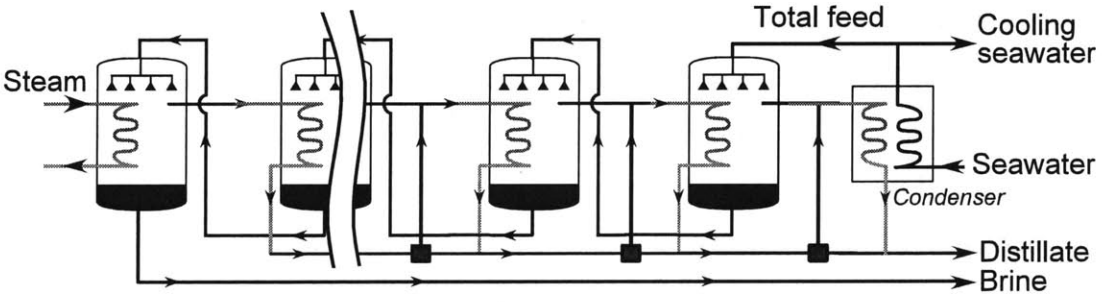


**Figure 1-5:** Backward-feed MED configuration

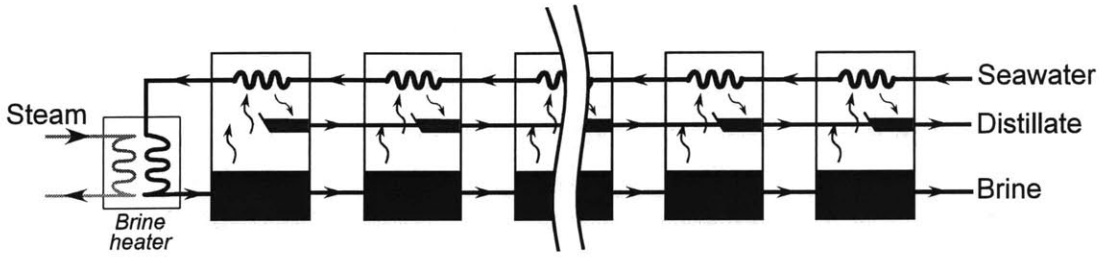


**Figure 1-6:** MSF process with once through cooling

highest salinity is subjected to the highest temperature which easily allows the brine to exceed the solubility limits of seawater salt constituents. Moreover, analysis of the heat transfer surface areas shows that more total area is required with backward feed than the forward feed due to the difference in effect temperature profiles [58].

### 1.2.2 Overview of the MSF Process

MSF desalination is the most common thermal desalination process employed in large scale co-generation plants. In this process, seawater is evaporated at sub-atmospheric pressure by reducing the pressure in a flashing chamber. The flashing method reduces scale formation significantly as compared with evaporation on tubes or a hot surface. The MSF process, shown in Figure 1-6, consists of three major sections: the brine heater, the heat recovery section, and the heat rejection section.

In the brine heater, steam from the power plant is used to heat preheated seawater to the top brine temperature. The heat recovery section consists of a series of flashing chambers in which the hot brine is allowed to flow freely and evaporate through reducing pressure. Flashing occurs in each stage, where a small amount of vapor is generated and is used to preheat the feed seawater flowing in the tubes at the top of the chamber. The feed seawater is preheated, and the generated vapor is condensed and collected in the distilled tray. At the last flash chamber, an extra amount of seawater is needed to condense the entire vapor generated in this stage and to remove the energy added in the brine heater. This cooling seawater is heated and part of it is rejected back to the sea while the other part is introduced to the previous stage as

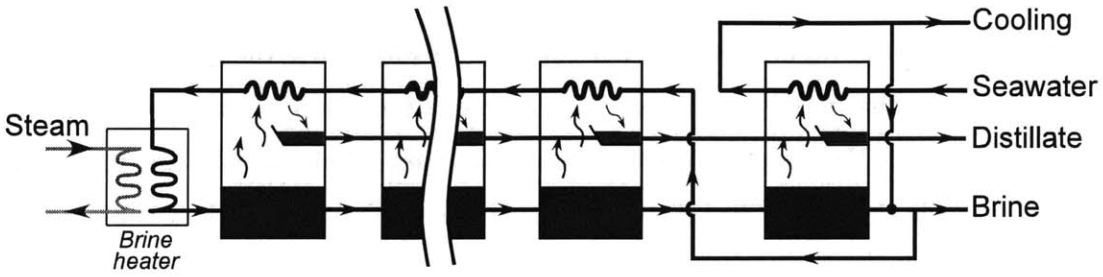


**Figure 1-7:** MSF process with brine recirculation

the feed. This type is called the once through MSF. Another type which is commonly used is the brine recirculation (Figure 1-7). In this method, the hot cooling seawater is mixed with the brine pool in the last flashing stage. Then the feed is taken from this pool to be preheated in the previous stages. This method controls the feed seawater temperature to the flashing stages, especially when the intake seawater has large temperature variations. The key features and operating parameters of MSF plant are given in Table 1.2.

The flashing process is a simple process where the inlet brine stream flashes off because the saturation pressure of the brine is higher than the stage pressure. This feature makes the MSF process robust regarding the salinity of the seawater and reduces the water treatment requirements. MSF produces high quality fresh water (salinity ≤0.01 g/kg) from feed of high salinity seawater. MSF has low potential for scale formation since the evaporation of seawater occurs from the bulk of water by

**Table 1.2:** Main features of MSF Plant [36]

| Seawater salinity | 30-47 g/kg |
|---:|---:|
| Top brine temperature (TBT) | 100-112 °C |
| Steam supply | 2.5-3 bar |
| Steam consumption | 23.7 Tons/MIGD |
| GOR | 8 |
| Capital cost | 5.5-10 US$ MM per MIGD |
| Capital cost - Intake/Outfall | 0.1-2.0 US$ MM per MIGD |
| Chemicals cost | 40,000 US$/yr per MIGD |
| Labor cost | 40,000 US$/yr per MIGD |

flashing instead of evaporation on a hot surface. This feature is the main reason why MSF has been the popular and primary technology for desalination of seawater for several decades. However, the MSF process has many limitations. The top brine temperature is limited to 90-120 °C [87] due to the precipitation of salts at higher temperatures.

The velocity of flashed vapor should be maintained below 6 m/s [99] to limit entrainment of brine droplets in the vapor stream. This is done by appropriate design of the flashing chamber geometry (width and length) which results in high volume and construction cost. The MSF plants cannot be operated below 70-80% [56] of the design capacity for the reason that the flashing process will not be efficient.

### 1.2.3 Electrical Energy Consumption in Thermal Desalination

Although the separation process in thermal desalination is driven by a heat source, i.e., thermal power, the electrical power required is still significant. Electrical energy is required for the high pressure pumps of the feed, the brine recycling, the brine blowdown, the seawater intake, the distillate, and other auxiliary pumps. In MSF, pressure drops in the flashing chambers contribute substantially to the pumping necessary. The pumping energy in MSF is higher than that of MED, especially with the brine recirculation configuration. This difference is because the amount of the circulated brine is much more than the amount of the feed.

In literature, authors have most often used constant electrical energy consumption values per unit volume of water produced ($kWh/m^3$). Some published values are taken from industrial installations, e.g., [59, 63]. However, to the authors knowledge, there are no published models for electrical energy consumption that capture the dependence on design and part load. The use of an electrical energy consumption model by the characterization of MSF or MED pressure drops, and thus the required pumping, would allow for models which could reflect part loading of systems. These models are necessary for a system level model used for optimization of design and operation,

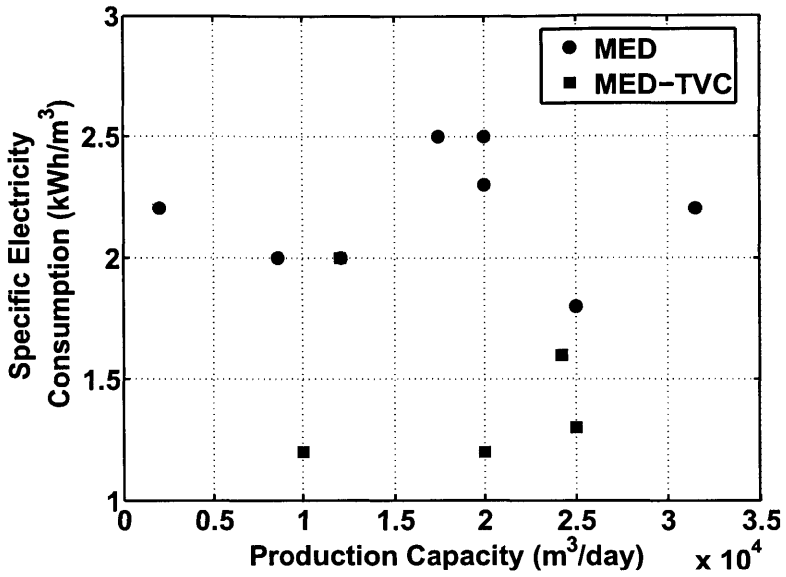


**Figure 1-8:** Reported values of MED and MED-TVC electrical consumption

especially when considering varying loads. Further, a model should accurately reflect the variation of electrical energy consumption with unit capacities. Currently, most constant electrical consumption values utilized in thermal desalination models do not appear to scale with the unit capacities. Figure 1-8 shows reported specific electricity consumption for MED and MED-TVC [125, 15, 24, 29, 30, 49, 52, 63, 146, 61, 59, 142]. As shown in Figure 1-8, the range of reported values in MED systems varies from 1.2-2.5 kWh/m$^3$ for unit capacities of 1992-31499 m$^3$/day and have no notable correlation with respect to production capacity. In the GCC countries, the specific electrical energy consumption range is reported as 2.5-4.5 kWh/m$^3$ of product water [13, 60, 15, 24, 29, 106]. It is important to note that the estimated values of electrical energy consumption make a large difference in thermal desalination perhaps being competitive to SWRO, whose electricity consumption is typically reported as 3-4 kWh$_e$/m$^3$ [155].

### 1.2.4 Common Models to Describe Thermal Desalination

Modeling of the thermal desalination processes is well established in literature [2, 11, 27, 33, 39, 41, 74, 97, 101, 147, 22, 57, 58, 59, 62]. The governing equations of the mathematical models are most often energy balance, mass balance, and heat transfer equations. There are some empirical correlations and short cut techniques summarized in [67], which are useful to provide quick estimates of process parameters, i.e., performance ratio, condenser heat transfer area, and flow rates of various streams. However, detailed analyses are required for accurate thermo-economical calculation, feasibility studies [152], and numerical optimization.

The following are the key assumptions that are frequently used to model MSF and MED processes: *i*) the plant is working in steady state operation at the design point; *ii*) heat losses to the surroundings are negligible; *iii*) the distillate product is salt free; *iv*) equal temperature difference on each stage.

In addition to these assumptions, empirical correlations are used to calculate the overall heat transfer coefficients in the evaporators and condensers which depend on flow rate and temperature of the condensing vapor, flow rate and temperature of the brine inside the condenser tubes, physical properties of the condensing vapor and the brine, the tube material, diameter, and wall thickness, the fouling resistance, and the percentage of non-condensable gases. Some models consider other effects such as boiling point elevation, non-equilibrium allowance, and demister losses. The solution of the energy and mass balance equations define the temperature, flow rate, and salinity profiles across the stages. It is important to note that these equations are non-linear and coupled [137, 168].

## 1.3 Overview of Seawater Reverse Osmosis

Seawater reverse osmosis (SWRO) is the most popular membrane-based desalination method, and a fast growing seawater desalination technology. The membranes used in SWRO have high permeability for water and low permeability for dissolved

substances. Feedwater in SWRO is pressurized such that the pressure difference across the membrane is higher than the osmotic pressure difference between the feedwater (significant) and the permeate water (negligible). As a result, the feed water pressure can be as high as 85 bar. The performance of SWRO (e.g., recovery ratio and power consumption) depends on parameters such as the feed pressure, TDS of the feedwater, membrane characteristics (e.g., salt rejection and material), membrane fouling and concentration polarization [64]. Membrane fouling, i.e., the accumulation of foreign materials on the active surface of the membrane, increases the energy requirement of SWRO significantly. Similarly, concentration polarization, i.e., creation of a boundary layer at the membrane surface, increases the osmotic pressure near the membrane surface, and consequently the energy consumption of the separation process. More on SWRO can be found in [178]; herein, the focus is on SWRO in the context of hybrid desalination and co-generation schemes and more specifically on limitations (process and mechanical), energy consumption, and system configuration.

### 1.3.1 Limitations of SWRO

The permeate flow rate in SWRO can be enhanced via a number of methods such as increasing feedwater pressure and temperature. However, a number of mechanical and process constraints need to be considered. For instance, preheating feedwater to SWRO enhances salt passage [94, 104] and likely membrane degradation. As such, membrane manufacturers recommend a maximum feedwater temperature. Such constraints must be taken into account in synthesizing the hybrid desalination system, where multiple feedwater arrangements are possible. There are also mechanical constraints associated with SWRO. The vessel containing the membranes has a pressure rating which puts a limit on the feedwater pressure. A key performance limitation of SWRO is the inability of a single-stage SWRO to meet a maximum allowable boron concentration in the product water [150, 108]. As such, SWRO plants employ additional steps to increase boron reject, such as pH adjustment of feedwater, and blending of SWRO permeate with other sources. However, in most cases a multi-

stage SWRO has been implemented [150, 108], where an increased boron reject and the overall recovery ratio has been achieved at a significant added capital cost. A key advantage of a hybrid desalination system is the opportunity to blend the product water from a low-cost, single stage SWRO with relatively low product quality with the high-quality permeate flow from an energy-intensive thermal desalination method.

### 1.3.2 SWRO System Configuration

System configuration in SWRO has effect on performance and economics of the plant. A key design decision is whether to build a single or multi-stage system. Single-stage SWRO has a lower capital cost, but yields a lower recovery ratio and a faster membrane degradation. A single-stage SWRO also requires more frequent membrane cleaning, which can be a costly process depending on feedwater quality. A key motivation in use of multi-stage SWRO has been the need to meet stringent permeate water quality, and in many cases a minimum desired boron reject that is not achievable in a single-stage SWRO, e.g., Ashkelon plant [150, 108]. A multi-stage SWRO, however, has a higher overall specific electricity requirement [179]. Recent advances in membrane technology resulting in a reduced cost and energy efficient membranes with high salt rejection are the reason that most new SWRO plant are single stage [179, 182].

## 1.4 Overview of Co-Generation for Power and Water

Co-generation is the simultaneous generation of electrical energy and thermal energy in one power plant. It has been used in many industrial applications including, chemical industries, paper mills, food processing, and district heating. Seawater thermal desalination processes (MSF and MED) are most often combined with power generation in large scale dual-purpose co-generation plants. The combined efficiency of a dual-purpose plant is higher than the efficiency if the production of electricity

and water is carried out separately, i.e., fuel consumption is reduced as compared to utilizing separate boilers for the production of steam for a power cycle and thermal desalination. The design of co-generation plants is an important subject due to the difficulties in satisfying the dynamic variation of both the electrical load and water demand with economically effective plant operation. For example, during off-peak hours or when the power demand is changing, it is essential to provide an auxiliary boiler to provide additional fuel for energy in order to keep water production at a constant level. This additional fuel results in the increase of water costs significantly, and the electricity and water production process can become unprofitable [48].

### 1.4.1 Steam supply design

Large thermal desalination plants are most often coupled with power plants. The steam required for the thermal desalination process can be extracted from the steam turbine in several ways. In general, the steam temperature required to heat the feed seawater in the brine heater, i.e., the minimum approach temperature (pinch) in the brine heaters, should be 5-7°C higher than the top brine temperature [58]. There are many commercially available configurations that provide both electrical power and the steam for the thermal desalination process. These configurations are as follows [71, 113, 110]: *i*) steam cycle with back-pressure steam turbines (BST) where the exhaust steam from the steam turbine is used in the desalination process where it condenses and returns back to the steam cycle; *ii*) steam cycle with extraction/condensing steam turbines (EST) where the steam for the desalination process is extracted from the steam turbine at the appropriate pressures (and temperatures) needed for the desalination process; *iii*) gas cycle with gas turbines connected to heat recovery steam generators (with or without supplementary firing) which use energy from the exhaust gases to generate steam for the desalination process (GT-HRSG); *iv*) combined gas and steam cycle where a heat recovery steam generator (with or without supplementary firing) is used to produce steam at medium or high pressure that is supplied to a back-pressure steam turbine discharging into the thermal de-

salination plant (CC-BST); *v*) combined gas and steam cycle that is similar to the previous one except that an extraction/condensing steam turbine is used (CC-EST).

In all of these configurations, some high pressure steam is required to activate a thermocompressor (steam ejector) in order to purge the system during start-up and to remove non-condensable gases [105]. The supplied steam in the steam ejector compresses the entrained vapor from the flashing stages of the MSF plant or the effects of MED plant and then uses it in the brine heater. The temperature and pressure of the steam required for the desalination process differs according to the desalination process. Table 1.3 shows the typical temperature and pressure ranges as well as the top brine temperature for MSF, MED-TVC, and MED [63, 109]. Each of the above mentioned dual-purpose configurations has its own performance characteristics regarding the part load operation, efficiency, and power-to-water ratio [71].

**Table 1.3:** Typical steam conditions for thermal desalination plants [63, 109]

| Process | Steam temp., °C | Steam pressure, kPa | Top brine temp., °C |
|---|---|---|---|
| MSF | 100-130 | 250-350 | 90-120 |
| MED-TVC | 120-150 | 250-350 | 70-80 |
| LT-MED | 70-90 | 20-40 | 60-80 |

### 1.4.2 Power-to-Water Ratio

A key parameter for dual-purpose plants is the power to water ratio (PWR), which is the ratio of the power produced to the fresh water produced. Spiegler and El-Sayed [165] cite a range of 50-500 kJ/kg for the PWR of dual-purpose plants. In the GCC countries, the rated PWR for the majority of the dual-purpose plants is between 115-230 kJ/kg [165]. The rated PWR is chosen based on the power and water demand of the customer region, i.e., the amount of power and water produced must meet the demand of approximately the same population size. Between 1980 and 2010, the variation for all co-generation plants in Saudi Arabia was ±20%, mostly due to variation in power and water demand from year to year. However, the ability of a

dual-purpose plant to meet a desired PWR is dependent on the power cycle design as well as part-load and supplementary firing characteristics.

Obviously, in extracting steam from an extraction turbine or using steam from a back pressure turbine for a thermal desalination process, the power produced by the turbine is reduced as compared to a power cycle without thermal desalination integration. This reduction increases with increased extraction pressure and amount of steam extracted. However, simultaneously, the amount of water produced increases. Consequently, the combination of these two effects determines the instantaneous PWR of a dual-purpose cycle.

## 1.5 Scaling and Fouling in Desalination

Scaling and fouling in both thermal desalination and seawater reverse osmosis are of major concern in the design and operation of such systems. The performance of desalination technologies is limited by the precipitation of salts and impurities present in seawater. Uncontrolled scaling and fouling leads to failure and plant shutdowns. Therefore, small improvements in scaling and fouling treatments, e.g., seawater additives and scaling inhibitors, can drastically improve process reliability and economics. The following sections present a short overview on scaling/fouling concerns in seawater reverse osmosis and thermal desalination.

### 1.5.1 Scaling in Thermal Desalination

Scale is the formation of seawater salt deposits on process surfaces. Scale forms when a given salt exceeds its saturation limit, which depends on both temperature and salinity. Salts of particular concern in seawater desalination are calcium carbonate ($CaCO_3$), magnesium hydroxide ($Mg(OH)_2$), and calcium sulfate ($CaSO_4$). The solubility of these salts decreases with increasing temperature and salinity, thus limiting the operating range of thermal desalination. Scale formed on heat transfer surfaces reduces their effectiveness and increases the necessary pumping power.

As a result of these solubility problems, thermal desalination operation is limited to a top brine temperature (TBT) and a maximum brine salinity of effects/stages in order to avoid violation of solubility limits. Seawater pretreatment additives are utilized in order to increase the TBT and thus decrease the specific power consumption of the process. Common MSF additives are polyphosphate additives, high temperature additives, and acid treatment methods; these increase the maximum TBT to approximately 90°C, 100°C, and 120°C, respectively [145]. However, the effectiveness of scale control is dependent on many factors, e.g., optimal dosing (especially under varying seawater conditions) [89, 45].

In addition to the scale formation, it is important to mention that the presence of dissolved non-condensable gases in process water is a serious problem in thermal desalination [10]. Even low concentrations can significantly reduce the overall heat transfer coefficient and hence the performance of desalination evaporators. In addition, $CO_2$ dissolves in the condensate and lowers its pH which with the presence of $O_2$, may cause corrosion of the condenser tubes. The release of $CO_2$ from the evaporation process considerably influences concentrations of the carbonate ions and thus plays an important role in scale formation. Furthermore, in MSF, the accumulation of non-condensable gases may disturb the brine flow through the flash chambers. Therefore, a deaerator and a decarbonator is installed to avoid the accumulation of non-condensable gases in thermal desalination systems.

### 1.5.2 Scaling and Fouling in Seawater Reverse Osmosis

In SWRO, membrane fouling, membrane scaling, and concentration polarization affect the performance and cost significantly. Membrane fouling, i.e., the accumulation of foreign materials on the active surface of the membrane, increases the energy requirement of SWRO significantly. Similarly, concentration polarization, i.e., creation of a boundary layer at the membrane surface, increases the osmotic pressure near the membrane surface, and consequently the energy consumption of the separa-

tion process. Membrane scaling of $CaSO_4$ and other salts reduces permeate flux and can reduce the lifetime of the membranes [140].

The silt density index (SDI) is an empirical parameter used by SWRO plant operators as an indicator of the quality of a feedwater to foul membranes [64, 83]. SDI is also referred to as the fouling index in membrane industry. A typical maximum allowable SDI for feedwater in SWRO is 5.

Fouling in SWRO is minimized through pretreatment of the feedwater and periodic membrane cleaning. To minimize consumption of chemicals and maximize plant availability, it is desired to minimize the frequency of membrane cleaning. As such, care is taken in designing efficient and cost effective pre-treatment processes for SWRO. Feedwater pretreatment in SWRO is a combination of media filtration (removal of colloidal particles), microfiltration (removal of suspended solids), and ultrafiltration (removal of organics). SDI's as low as 1 can be achieved with a well designed and properly maintained microfiltration or ultrafiltration system, while traditional pre-treatments (mainly media filtration) can only achieve a SDI near 5 [64]. Recently NF has been suggested as a promising pre-treatment not only for SWRO, but also for pretreating the feedwater to a hybrid SWRO/MSF desalination plant [19, 20, 21, 90, 91, 92, 93].

## 1.6 Considerations for Hybrid Desalination Systems

Hybridization of thermal and mechanical desalination technologies integrated with power plants is a proposed improvement over the standard dual-purpose plant. Several potential integration schemes of brine or permeate flow between MSF or MED and SWRO have been envisioned. The benefits of hybridization, as discussed by Awerbuch et al. [37, 38], include reduction of capital costs through eliminating the need for second-stage SWRO and a decrease in required heat transfer area in thermal desalination. Others benefits [37, 38] are improvement of overall performance by load

shaving of electrical production under time-varying demands, potential for reduced pretreatment, and the increase top brine temperature in thermal desalination systems, which will be discussed within the context of current literature in the coming sections.

The current literature typically focuses on aspects of research which would make hybrid desalination feasible for more widespread industrial scale implementation. Specifically, these include *i*) how thermal and mechanical desalination technologies are combined and their subsequent merits; *ii*) the importance of thermoeconomic analyses; and *iii*) use of nanofiltration for pretreatment in hybrid desalination systems. These points will be discussed in the following sections.

### 1.6.1 Configurations of Hybrid Systems

A main advantage of hybrid desalination systems lies in the flexibility of connectivity between thermal and mechanical desalination; these options for connectivity lead to integration which can minimize the disadvantages and maximize the advantages associated with each technology. Further, it can reduce capital costs for fixed production of water as compared to a dual-purpose plant utilizing thermal desalination alone by sharing some necessary installations between technologies such as intake/outfall facilities and portions of the pre- or post-treatment systems [37].

There are many possibilities for routing of brine and permeate between thermal desalination and reverse osmosis in a hybrid plant, and subsequently, the integration of thermal desalination with a power plant can also vary. Two general routing schemes are commonly employed in literature, namely, parallel [77, 79, 115, 125, 146, 173] or series configuration [47, 72, 73, 121]. Shown in Figure 1-9 are simple examples of parallel and series configurations; other more complicated integrations have been employed in open literature.

In parallel configuration, shown in Figure 1-9(a), intake feed is split between thermal desalination and SWRO, then permeate and brine streams are blended at the outlet. Operation of the desalination modules is primarily independent, and the rela-

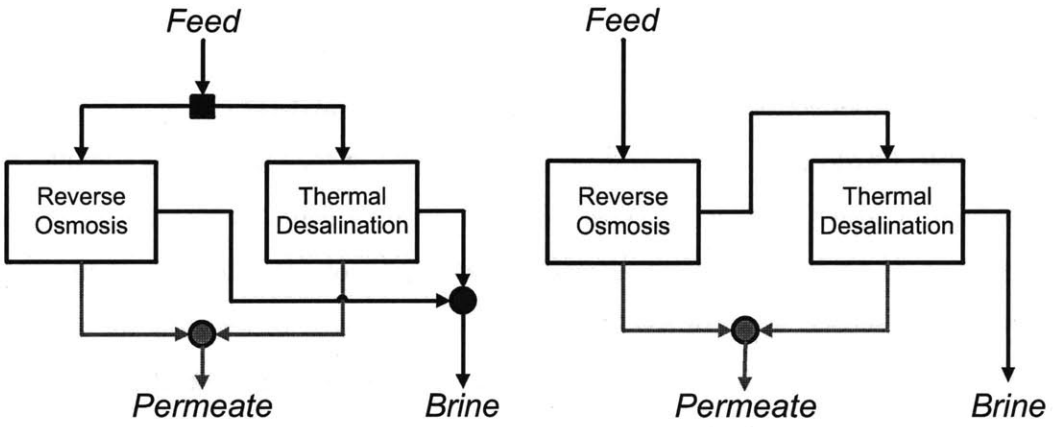


(a) Parallel configuration (b) Series configuration

**Figure 1-9:** Examples of hybrid configurations

tive production capacities of each module is the most important design consideration. The independence of operation in parallel configuration can be advantageous, in that these systems can be easily adjusted to respond to variation in the demand of power and water, i.e., the performance of thermal desalination and SWRO do not depend on each other and thus can be independently adjusted for given plant conditions.

In choosing a ratio of production between thermal desalination and SWRO, the blended permeate salinity should be taken into account. Over operation life, the salt passage of SWRO increases due to membrane degradation; in a standalone SWRO system, the membranes would need to be replaced once the permeate is above acceptable drinking quality, i.e., a TDS above 0.5 g/kg [178]. These replacements incur high maintenance costs over the total lifetime of the plant. In contrast, the permeate obtained through thermal desalination methods is a constant, near-zero TDS. Therefore, the low TDS permeate of thermal desalination can be blended with SWRO permeate in order to extend the usable lifetime of the membranes and reduce maintenance costs. It is important to note that the target recovery ratio for the SWRO system contributes to SWRO membranes degradation, since higher recoveries imply higher feedwater pump pressures which limit membrane lifetime [178]. Therefore, the SWRO recovery for these systems is critical to consider.

Series configuration can involve many integration strategies involving either permeate or brine connections between thermal and mechanical desalination technologies. For example, Cardona et al. [47] propose that the brine of reverse osmosis could be fed to the inlet of either MSF or MED, as shown in Figure 1-9(b). Cardona et al. proffer this scheme as an alternative to using a second stage of SWRO. As mentioned in Section 1.3, a second stage of SWRO is typically employed to increase the recovery of water to values as high as 85% and therefore reduces the amount of feedwater to be pretreated. Cardona et al. claim that it is desirable to use thermal desalination, so as to reduce the electrical energy consumption that is associated with the high feedwater pressure necessary in a second stage of SWRO. Similarly to the parallel configuration, blending of the thermal desalination and SWRO permeate can be employed and thus reduce maintenance costs. It is important to note that the trade-off between electricity consumed by SWRO and the lost work of the power plant turbine to provide steam for thermal desalination is essential to consider. Further, as afore mentioned, the electrical work for pumps in MSF or MED is significant. Therefore, while this particular scheme is beneficial in some ways, the energetic and economic benefits cited by Cardona et al. may not be as substantial once a detailed analysis for given plant conditions is performed.

El-Sayed et al. [73] experimentally investigate another simple series configuration scheme. Shown in Figure 1-10, the pilot-scale plant (20 $m^3/d$) studied preheats the SWRO feed through the heat rejection section of an existing MSF plant. El-Sayed et al. specifically investigate the SWRO performance gains, the product flow rate and the specific energy consumption. The results of the study are compared to a standalone SWRO system. It is reported that a feedwater temperature range of 15 to 33°C can reflect an average product flow rate gain of 42-48%. Also, it is asserted that this can amount to a 45% decrease in specific energy consumption for SWRO.

El-Sayed et al. [72] investigate the effects of SWRO feed temperature experimentally using a similar configuration as in [73] (Figure 1-10). In these experiments, a larger SWRO test rig (300 $m^3/d$) than [73] is used. After testing both spiral wound and hollow fiber membranes, it is found that only a 2.2% average increase in permeate

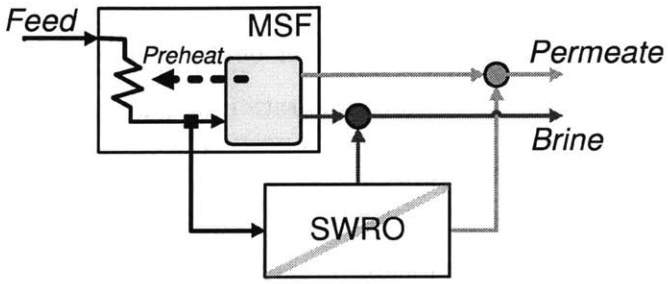


**Figure 1-10:** MSF/SWRO hybrid experimental plant, El-Sayed et al. [73]

recovery per degree Celsius increase in feedwater temperature is achieved. Furthermore, both show an approximately 25% decrease in specific energy consumption, which is less than the decrease reported by the pilot scale testing in [73]. Because there is variation of results with respect to experiment scale for this hybrid scheme, it is unclear whether an industrial-scale implementation would see similar performance.

An advantage of this scheme (Figure 1-10) is that existing MSF or MED plants could be retrofit to integrate SWRO without major changes in the existing plant. However, SWRO membranes are limited to a maximum operating temperature in order to avoid membrane degradation (typically $\approx 45°C$ [64]); in climates where summer seawater temperatures can reach $\gtrsim 35°C$, this scheme as it is, is not necessarily practical. Further, an increase in membrane temperature also increases salt passage, and the resulting quality of SWRO permeate should be considered. In this series configuration, the performance of MSF and SWRO is not independent as it is in the parallel scheme and so responding to changes in plant conditions could be more complicated.

The parallel and series hybrid configuration schemes presented herein are rather simple; investigations regarding more complex configurations will be discussed in coming sections. While these simple configurations may be relatively easy to implement in terms of minimizing the complexity of stream connections, these configurations are not optimized to maximize all potential improvements available through hybridization, e.g., overall reduction of costs, reduced scaling and fouling in both thermal desalination and SWRO, and increased energetic performance. Further, depending

on the location of plant installation and other design constraints, it is not immediately clear whether parallel or series configuration is the most appropriate scheme. Therefore, systematic strategies for developing and implementing novel configurations to fully utilize the potential of the hybridized desalination concept should be employed. While more complex configurations could exploit possible improvements, it is important to note that there are limits to the practicality of such schemes, e.g., increasing complexity has economic and operational disadvantages with regards to system construction and maintenance.

### 1.6.2 Thermoeconomic Analyses

The installation of seawater desalination systems are highly cost intensive. Since hybridized desalination systems are promising in reducing the costs of production, many authors have conducted studies with detailed economic analyses. Mainly, these analyses quantify the total annualized cost (TAC) of water for a given system design.

The TAC includes both capital and operating expenses, of which the operating expenses are calculated based on an availability of the plant, i.e., the number of days the plant is expected to operate. The TAC is highly dependent on the specific conditions of an installation. Common economic factors considered in thermoeconomic models are: *i*) power and water demand and their time dependence [24, 81]; *ii*) fuel prices [46, 114]; *iii*) capital and maintenance costs of equipment [5, 130]; *iv*) interest rate and tax structures [7, 9].

The citations in the list above indicate articles in which the relevant economic factor is a main focus of the authors. [81, 130, 114] study systems without hybridization, but their analysis is relevant to the economic factors to be considered for a hybridized dual-purpose plant. It is important to note that many authors present an analysis method and calculate a TAC of water with the caveat that their solution could be substantially different had other parameter values been considered in their calculations, e.g., fuel prices, seawater temperatures, capital costs of equipment [5, 106, 134, 146, 169].

Hybridized desalination plants coupled to power production are advantageous in responding to the time-varying demands of power and water. In many locations, the demand for water is relatively constant throughout the year, but the demand for electricity is high in the summer and low in the winter. Traditional dual-purpose plants employing a power cycle and thermal desalination system suffer from a mismatch in power and water production during winter months [113], i.e., in order to satisfy winter water demands, more electricity than needed is generated so that steam can be provided to the thermal desalination system. Steam could be provided directly from an auxiliary boiler; however, the thermodynamic advantage of the dual-purpose production is lost, and the cost of producing water subsequently becomes high. The benefit of hybridization in this regard, i.e., integrating SWRO, is that the SWRO system can essentially levelize the demand between power and water through its utilization of surplus electricity [148]. However, uncertainties in demand make the optimal integration of SWRO with the overall system economically complex.

Recent work by Ghobeity and Mitsos [81] finds that it is economically advantageous to design an optimal schedule for SWRO production when considering hourly variation in electricity prices including reducing production and even completely shutting down the SWRO system while electricity prices peak midday. Further, it is found that an oversized system with respect to a fixed water output per day could be economically favorable when there are high energy prices and/or high fluctuations in hourly electricity price. These concepts could be expanded to consider not only the SWRO system but also an entire hybrid system including thermal desalination and power production.

Almulla et al. [24] investigate the seasonal variation of electricity demand as opposed to hourly. In this article, a hybrid CC-MSF-SWRO system is considered with the possibility of energy storage in a spinning reserve; alternatives in the time-varying operation of SWRO are explored, i.e., coupling the spinning reserve to SWRO operation for six months of the year, all year, or not at all or by only using plant surplus power. This study is conducted within the context of an existing plant in the United Arab Emirates, and it is concluded that using spinning power reserve for six months

of the year is the cheapest integration scheme. The best time-dependent integration scheme is not immediately evident in cases such as these and therefore, as is shown in [24] and [81], detailed economic analysis and optimization applied to hybrid system should be further explored.

The optimal design of a plant also depends on the region of installation due to available fuel prices, feedwater quality, etc. For example, the work presented by Cali et al. [46] considers the design of hybrid MSF and SWRO systems in locations where fuel prices are relatively high, unlike regions of the Middle East where primary energy sources are abundant; [46] assume that the cost of using low sulfur fuel oil is 0.02 €/kg and 0.2 €/kg, in OPEC and non-OPEC countries, respectively. Cail et al. determine that economies of scale is an important factor in making hybrid systems economical in regions with high fuel prices. However, [46] does not offer optimization analysis for determining alternative hybrid configurations which minimize production costs in markets with high fuel prices. This type of analysis may be useful for non-OPEC regions which have high temperature, difficult seawater and subsequently cannot exclusively use SWRO, e.g., the Mediterranean.

Economic analyses often reveal the economic disadvantages of a technology; in the context of hybridized desalination systems, analyses can quantify the economic trade-offs of utilizing both thermal and mechanical desalination. For example, [97] and [8] recognize that MSF generally imparts high capital costs and is sensitive to the cost of producing steam with regards to fuel prices and steam quality. On the other hand, SWRO can be utilized to reduce this sensitivity via balancing of capital costs and production during varying loads. These conclusions clearly show that there is an optimal allocation of water production between thermal desalination and SWRO in a hybrid system which will minimize TAC. Therefore, it is of paramount importance that detailed thermoeconomic modeling frameworks, such as those in [7] and [9], are developed for use in optimization of hybrid desalination systems.

### 1.6.3 Pretreatment Improvement Through Nanofiltration

A major goal in the hybridization of thermal and mechanical desalination technologies is to reduce the pretreatment burden of influent feedwater as compared to standalone desalination systems. As discussed in Section 1.5, scaling and fouling in both thermal and mechanical desalination can greatly impede system performance through reduced hardware life causing frequent shutdowns or large expenses for equipment replacement. Pretreatment of feedwater is subsequently necessary but requires auxiliary equipment and recurring operational expenditures for pretreatment chemicals such as scale inhibitors and acid dosing. The integration of nanofiltration (NF) in hybrid systems, however, is a promising solution for addressing scaling and fouling issues.

NF is a membrane filtration technology with a filtering ability between ultrafiltration (UF) and reverse osmosis. NF preferentially removes divalent ions from feedwater, thereby reducing the content of dissolved salts such as $CaSO_4$ and $CaCO_3$ [16]. As discussed herein, the solubility of salts is a function of both temperature and salinity, and these particular ions limit the performance of thermal desalination primarily through a maximum TBT and recovery ratio and reverse osmosis through a maximum recovery ratio. Besides the removal of low solubility salts in order to improve system reliability, NF is also advantageous in that it can reduce the overall TDS of the feedwater [86].

The effectiveness of NF for reducing the potential for scaling and fouling is experimentally investigated in a series of articles by the Saline Water Conversion Corporation (SWCC) of Saudi Arabia [19, 20, 21, 90, 91, 92, 93]. Although most experiments are conducted at a pilot plant scale, key findings show superior performance for NF-SWRO, NF-MSF, and NF-SWRO-MSF systems as compared to standalone MSF or SWRO systems. For example, [91] achieves an operation period of over 1600 hours for an NF-MSF system with NF make-up and 270 hours with NF-SWRO reject at a temperature of 120°C without the addition of antiscalant chemicals. [90] investigates a NF-SWRO-MSF system operating in series; SWRO recovery is reported as 45% at

an operating pressure of 60 bar, and MSF is successfully operated up to a temperature of 130°C with an 9% increase in recovery over standalone MSF operation at 120°C.

Similar experimental results are shown by Awerbuch [35]. Through a series of demonstration trials of a NF-MSF system, Awerbuch reports successful operation at a maximum TBT of 118°C and a 24% increase in plant output over a standalone MSF plant. A study conducted by Al-Rawajfeh [14] models the potential of sulfate scaling in NF-MSF and NF-SWRO-MSF systems. Al-Rawajfeh finds that with 100% of feedwater pretreated by NF in the NF-MSF system, no anti-scalants would be needed for TBTs up to 175°C and for only 30% NF make-up, a TBT of 135°C could be reached.

From the above studies, NF is clearly beneficial for hybrid desalination system performance. However, few studies have been conducted which examine the most effective way to integrate NF and/or quantify the maximum achievable performance and economic improvement of an overall system. Studies regarding optimal integration of NF have focused on maximum water recovery, which implies overall increase in production for the same capacity of equipment and minimal water to pretreat, i.e., reduction of operational expenses.

In [170, 171, 172], Turek et al. discuss the merits of hybrid UF-NF-SWRO-MSF or MED-crystallization schemes. Turek et al. claim that such systems can reach overall recoveries up to 80% and substantially reduce the cost of water production. The cost of water which Turek et al. calculate relies on producing commodity salts through the crystallization process and brings the price below the best standalone SWRO systems. However, Turek et al. do not offer a rigorous economic model for their estimates of water costs which incorporate the addition of NF to hybridization nor is optimization of configuration performed.

In a two-part study by Abdullatef et al. [3, 4], the optimal configuration of NF modules for maximum membrane life and water recovery, with a goal of over 80%, is studied. In these articles, the configuration of NF is not considered in relation to either thermal desalination or SWRO. Rather, the optimal number of elements within a stage and the choice of one NF stage or two is experimentally investigated.

While Abdullatef et al. demonstrate the ability to reach NF recoveries above 80%, systematic modeling and optimization techniques are not utilized.

The result of the above studies show that the performance and configuration optimization of the individual NF module is important, but also that its interaction with coupled desalination technologies must also be considered. Rigorous optimization analyses which include detailed performance metrics and economic models will be necessary to truly characterize the maximum benefit of NF integration in hybrid desalination systems.

## 1.7 Optimization Methods

As shown herein, hybrid co-generation plants offer benefits over traditional dual-purpose plants. However, it is clear that there is much to be investigated in regards to the optimal design and performance of such systems. Because desalination systems require such high investments for each project, it is not practical to experimentally test every potential system improvement. Further, testing performance at a lab-scale is not entirely useful since the performance of desalination systems is strongly scale dependent. Therefore, the use of systematic optimization methods to develop and quantify optimal performance criteria is critical for the understanding and practical implementation of dual-purpose hybrid desalination systems.

The following discussion is a survey of literature which employs methods for optimizing hybrid and dual-purpose systems. Specifically, the following sections examine *i*) the choice of objective function(s); *ii*) which methods are used to optimize operational performance, i.e., the selection of continuous optimization methods; *iii*) how to choose the best hardware and subsequently its connectivity, i.e., the merits of fixed versus flexible configuration frameworks. In regards to the considerations discussed in the previous section, systematic use of optimization methods will address issues and improve upon benefits of hybridized desalination systems.

### 1.7.1 Objective Functions

The choice of an objective function for optimization has a substantial impact on the optimal operating parameters of a system. An objective function is a mathematical formulation of what is desired to be maximized or minimized in order to obtain an "optimal" system. Within the context of hybrid desalination systems, economic considerations are usually of paramount importance when designing a system. Because of this fact, minimizing the cost of water in some form is a common objective function defined for optimization studies. The minimization of TAC of water has been employed by several authors [96, 119, 120, 121, 130, 156].

Thermoeconomic optimization, which weighs the impact of exergy destruction through cost-based component models, has also been used to approach the dual-purpose and hybrid optimal design problem [30, 48, 146, 174]. In this case, the objective function quantifies the cost of exergy destruction expressed in terms of the cost of water or other parameters. For example, Rensonnet et al. [146] study the differences between minimizing electricity cost versus water cost versus the total combined cost within the context of a hybrid plant of power-MSF/MED-SWRO. Rensonnet et al. [146] conclude that optimizing for the total combined cost of electricity and water is most appropriate because of the strong interdependence between the two systems. As expected, this result implies that for given electricity/water demands, a specific PWR must be met in an optimal (most economical) fashion by the plant, and for certain time varying loading cases, the optimal condition may be to produce either no power or no water.

Because of the different objective functions, some authors have proposed multi-objective optimization (MOO) for dual-purpose and hybrid systems [5, 175]. By employing MOO, the trade-offs between competing criteria can be quantified. For example, Abdulrahim et al. [5] compare the maximization of distillate production and gain ratio and the minimization of product cost and exergy destruction as objectives in hybrid MSF-SWRO systems. In this study, it is found that the most influential trade-offs lie between minimization of cost and exergy destruction. Vince et al. [175]

develop a general framework for MSF-SWRO systems and uses MOO to minimize the TAC of water and the water resource consumption, i.e., the water drawn from a water source per cubic meter of water desalinated. In this study, less expensive solutions compete against solutions with less environmental impact. Although the results of these articles which employ MOO seem to result in expected generalizations of system trade-offs, MOO can be advantageous when it is used to separate the specific areas of a system which could affect the decision making process as a system designer. For example, the trade-off in capital cost versus the operating cost could be beneficial to quantify when considering long term versus short term investments in a desalination plant.

### 1.7.2 Continuous Optimization Methods

In order to determine the optimal performance criteria for a given objective function and fixed system flowsheet, continuous optimization methods are employed by many authors. The common methods used are single parameter parametric studies or multi-variable nonlinear programming (NLP) techniques such as local gradient based methods, e.g., variants of Newton's method, non-gradient based methods, e.g., evolutionary algorithms, and deterministic global optimization methods. These methods are deemed continuous because they consider continuous variables, e.g., operating temperatures, pressures, flow rates, and PWR, in order to achieve an optimal solution.

Single parameter parametric studies are typically the easiest to implement since they require merely a system model and the ability to evaluate its mathematical functions. Single parameter parametric studies can identify an optimal value of the varied variable for fixed values of the other variables. However, single parameter parametric studies do not systematically and simultaneously provide a deterministic optimal solution, i.e., the absolute best objective value cannot be guaranteed, without cumbersome analysis which becomes computationally inefficient. In general, single parameter parametric studies best offer trade-offs between operating parameters in

trying to satisfy an objective function. Authors who have employed single parameter parametric studies within the context of hybrid and dual-purpose systems in order to quantify sensitivities among several performance criteria such as heat transfer areas, power plant extraction flow rates and temperatures, and costs of fuel or pre/post treatment chemicals, include [7, 8, 52, 79, 97, 114, 115].

Parametric studies have also been used to evaluate location-specific feasibility of hybrid system integration to improve performance of existing plants [24, 51] or to address a particular concern of the region's water demands [63, 149, 173]. For example, the result of [173] shows that a hybrid co-generating GT-MED-SWRO plant would most likely be cheaper than their currently installed freshwater transport scheme, given economic considerations specific to Spain. In these types of analyses, the optimal design of a system is not necessarily the most important consideration because the analysis need only show that an installation could be feasible, i.e., profitable given a set of location and/or plant-retrofit constraints. Once feasibility is shown, more detailed analysis for optimizing a system would be conducted. Therefore, single parameter parametric studies can be suitable for a relatively simple review of the feasibility of a proposed installation.

In the above examples of location specific feasibility, the capital costs of equipment, fuel prices, demand, etc. vary with location of installation. The implementation of single parameter parametric studies in these cases makes the proposed optimal solution very specific to a particular system installation. In contrast, parametric optimization could be employed in order to create a general framework assuming unknown prices or other values for parts of a design. Parametric optimization returns the optimal solution as a function of unknown parameters; however, it is assumed that these unknown parameters would be known at time of installation. For example, a hybrid MSF-SWRO plant could be generally optimized as a function of fuel price. Then, when the installation location is chosen, the fuel price would subsequently be known, and the particular optimal solution for the hybrid system would be calculated based on the solution of the general parametric optimization. Additionally, parametric optimization can be used to capture uncertainty associated with the technology

performance and identify optimal resource allocation for the advancement of the technology [129, 128]. For example, for a fixed investment in a hybrid desalination plant, parametric optimization could be employed to determine whether improvement in anti-fouling measures in MED or the permeability of SWRO would garner a greater performance gain for the overall plant.

Parametric studies seem to be most useful in identifying general trends in desalination systems but do not establish a systematic approach to finding an optimal solution for a general set of performance criteria. In contrast, continuous optimization methods involving NLP are more appropriate to systematically solve for optimal performance. However, these methods have not been employed as commonly as parametric studies within the context of hybrid or dual-purpose desalination systems. [121, 130, 156, 174] use NLP gradient based methods to solve hybrid or dual-purpose optimization problems. In these studies, a framework is developed to describe the operating constraints of the system. Common constraints include maximum brine salinities, maximum temperatures able to be seen by SWRO membranes, and temperature limitations in the thermal desalination section. This framework is more rigorous than a single parameter parametric study because all non-fixed variables within a system are simultaneously considered in order to find an optimal solution. Further, the framework more easily allows for flexibility among different design conditions which are common in desalination and co-generation applications, e.g., location-dependent fuel prices, availability of resources, and differences in water composition and temperatures.

It is important to note that the use of a local solver such as in [174] does not necessarily guarantee that the best solution has been found. In complex systems such as hybrid and dual-purpose desalination, introducing thermophysical property correlations and other non-convex functions within a system model means that many suboptimal local minima may exist.

Some authors use evolutionary algorithms, i.e., genetic algorithms (GA), to solve hybrid and dual-purpose NLP optimization problems. Ansari et al. [30] use a genetic algorithm within the context of thermoeconomic optimization of MED-TVC coupled

to a nuclear reactor. Abdulrahim and Alasfour [5] use a genetic algorithm to quantify differences in MOO objective values of a MSF-SWRO hybrid system. GA can provide solutions to an optimization problem without needing to evaluate the gradients of system model functions. However, like local gradient-based optimization methods, GA does not guarantee that a global solution has been found at finite termination due to an inherent lack of convergence criteria within this method. Therefore, deterministic global NLP methods, such as used in [81], which account for non-convexity are necessary to guarantee that the global optimal solution has been found. The use of deterministic global optimization approaches are likely intractable for optimization of the design and operation of the concepts discussed herein due to the large size of the models. In such case, the use of heuristic global optimization can be considered, such as is used in [82].

### 1.7.3 Fixed versus Flexible Hardware Configurations for Optimization

When minimizing the cost of a system or achieve another objective such as was described in Section 1.7.1, continuous operating variables are not the only consideration which could affect the optimal solution. The types of desalination or power technologies employed and their subsequent connections inform the possible range of optimal operating parameters. Further, the optimization of combinations of several different configurations could lead to novel system flowsheets and provide a substantially better optimal solution than if only one configuration had been optimized for optimal performance.

Authors weigh the connectivity and hardware trade-offs of hybrid and dual-purpose desalination systems using two main methods. The most common is to propose several fixed configurations, solve them to optimal performance via an NLP method, and then compare results. This method could identify the better configuration between two options, but when several different flowsheets are proposed, the analysis becomes extremely cumbersome and computationally inefficient. In addition, the method does

not guarantee that a better configuration does not exist and is limited to combinations conceived by the designer. This method will be referred to as manual configuration optimization. The second method is to create a superstructure and then use mixed integer nonlinear programming (MINLP) to solve the optimization problem. This method and its merits will be described in further detail in the latter half of this section.

A disadvantage of using manual configuration optimization is that when several possible flowsheets are considered, extensive comparisons of performance between each possibility must be calculated and the interdependence of possible configuration and hardware choices may not be immediately evident. For example, Helal et al. [96, 98, 97] present model development, optimization results, and sensitivity analysis of hybrid a MSF-SWRO system. The objective minimizes the specific cost of product water among nine different hardware integration schemes with fixed MSF and SWRO output. Two of the configurations consider standalone systems of which one is MSF with brine recirculation and the other is two-stage SWRO. The seven other hybridized schemes combine SWRO brine to MSF make-up and SWRO feed preheat through the heat rejection section in several different ways; these configurations were originally proposed in [18].

Helal et al. come to general conclusions regarding process economics and thermal performance, but questions arise as to the methodological effectiveness of comparing among the nine configurations considered. Of the hybrid MSF-SWRO configurations, another topology could possibly be devised which exhibits improved performance over those envisioned. Also the large extent of sensitivity parameters explored in [97] shows that the interactions among variables are highly complex and dependent on the hardware configuration.

While Helal et al. use the fixed-configurations comparisons among MSF-SWRO connectivity, Mussati et al. [131] uses a similar analysis for determining the best power plant integration for a dual-purpose system. Mussati et al. use five power plant configurations coupled to MSF: EST, BST, CC-BST, an EST, and GT-HRSG. Mussati et al. use the power plant configurations to compare PWR ratio against

water costs for the different configurations and finds that a lower power to water ratio generally means a lower specific cost of water.

The examples of manual configuration optimization described above provide substantial direction to hardware trade-offs for fixed operating conditions. However, the method does not provide a systematic and flexible framework for finding an optimal solution. Further, hybrid and dual-purpose systems are thermodynamically and subsequently economically complex with many interdependent interactions. Superstructure development and its application to solving an MINLP problem provides this framework.

A superstructure is a tool typically used by the chemical process industry which helps the system designer think about the ways that considered technologies could be connected on a flowsheet [42]. Essentially, it is the set of all possible flowsheets that could be envisioned. The superstructure provides a flexible framework and allows for a systematic consideration of hardware and connectivity possibilities. Subsequently, MINLP is used to mathematically represent a superstructure and to optimize the flowsheet. MINLP simultaneously optimizes integer and continuous variables. Integer variables are used to capture possible choices between hardware or flowhsheet routings, e.g., the choice of whether or not to include a second stage for reverse osmosis, the possibility of blending brine with thermal desalination inlet feed, the number of stages or effects within a thermal desalination system, the type of power plant extraction for providing heat to thermal desalination, or even at which time periods to shut-off the plant [81]. The level of detail of system representation within a superstructure can vary, and the complexity of the superstructure has a direct impact on the relative difficulty of solving the corresponding MINLP problem.

Within the context of hybrid and/or dual-purpose configurations, [77, 132, 134, 122, 175] use superstructures and subsequently MINLP for optimization. In the existing literature, integer variable choices are considered either within the water production section or the power block, but not as an overall system MINLP optimization of both power and water section configurations. Superstructures proposed by [134] and [77] treat the water production section as a black-box, but include integer choices for

the power plant hardware configuration. In the case of [134], the superstructure allows the selection of an air re-heater exchanger, heat recovery generators, burners, gas turbine, and a low-pressure turbine within the power plant but keeps the MSF plant configuration fixed with brine recirculation. Conversely, the superstructure proposed by [122] considers several possible permeate and brine blending strategies between MSF and SWRO, but does not provide integration options for the power plant. The superstructure proposed by [175] depicts a black-box version of a hybrid desalination system, where the separation between permeate and brine occurs as a "process unit". The optimizer then chooses between SWRO or MSF for each process unit.

The current literature does not provide the solution of a MINLP problem for desalination/power systems which simultaneously consider power and water production integer variables. Superstructures considering both should be developed to consider water and power configurations and choices of hardware which are strongly coupled to the performance and overall production. For example, when thermal desalination is integrated with power production, the type of extraction from the power production section informs a trade-off between potential electrical work and water production. In cases where power or water load will vary with a high frequency, an EST may be preferable to a BST since the quality of heat can be varied. However, if the water production section can include both thermal desalination and SWRO, SWRO could be used to provide an electrical demand when the nominal electricity demand is low and the water demand is high. Therefore, in this case, the optimal choice of both power and water production hardware for minimal TAC is not obvious since there are many possible trade-offs between configuration and operation, i.e., MINLP would be a favorable method to use for the solution of this problem.

## 1.8 Conclusion

Thermal desalination and seawater reverse osmosis suffer from thermodynamic, reliability, and economic challenges, e.g., scaling/fouling and high operational and capital costs. Further, most often these desalination systems are combined in co-

generation (dual-purpose) plants which produce both power and water and have additional concerns, e.g., power/water demand following. Hybrid desalination plants, which combine thermal and mechanical desalination technologies, have been utilized to help address these challenges. However, there are many opportunities to improve these complex hybrid systems so that they maximize benefits as compared to using thermal desalination or seawater reverse osmosis alone, e.g., improved hardware integration between thermal desalination and reverse osmosis, reduced operational/capital costs, and reduced pretreatment burdens (especially when nanofiltration is utilized).

Upon reviewing available literature on the design and optimization of hybrid desalination systems, it is concluded that numerical optimization should be employed in order to maximize the benefits possible by hybridized seawater desalination systems. Pilot scale experimental hybrid plants and parametric studies of plant performance provide some insight into operation improvements and limitations as compared to traditional dual-purpose plants alone, e.g., increased top brine temperatures of thermal desalination, and proof of hybrid concepts through feasibility studies. However, these analyses do not efficiently weigh the many design variables of hybrid systems, e.g., hardware configurations, feed/brine blending, and power-to-water ratios under varying loads. Numerical optimization more appropriately addresses these design decisions and could possibly elucidate new hybrid concepts. However, the choice of objective functions, detailed mathematical models, and continuous vs. structural optimization should be considered in order to optimally address the economic, reliability, and thermodynamic questions surrounding hybrid co-generation systems for the production of power and water.

# Chapter 2

# Integration of Thermal Desalination Methods with Membrane-Based Oxy-Combustion Power Cycles*

## 2.1 Introduction

The need for increased water production via seawater desalination is a growing problem worldwide. Water scarcity, especially in arid regions, has driven the widespread use of seawater desalination. Specifically, in the Middle East, thermal desalination is often employed over reverse osmosis due to water and environmental conditions, e.g., fouling potential and high seawater temperatures [67]. These thermal desalination plants are most often coupled with carbon dioxide emitting electrical power production, e.g., Rankine or Brayton cycles utilizing fossil fuels, as a dual-purpose plant. In this case, the thermal desalination plant utilizes steam from the power cycle which improves the thermodynamic performance of the overall plant as compared to thermal desalination with a stand alone boiler. Thermal desalination

*This chapter includes contributions by Nicholas D. Mancini and is based partially on the work of [116, 117, 118].

is energy intensive and thus is associated with high levels of carbon emissions [6]. Therefore, it is of interest to investigate the possibility of reduced or zero emissions dual-purpose plants, particularly of industrial scale ($\geq$ 100 $MW_e$ electricity production), so as to reduce the environmental impact associated with water production.

In order to achieve low or zero emissions dual-purpose plants, power production could be fueled by a source that does not produce $CO_2$, e.g., solar or nuclear. Solar power is a possible candidate for powering thermal desalination since arid areas requiring desalination typically have abundant solar resources [123]. Investigations into solar powered thermal desalination include solar stills [85] and humidification-dehumidification cycles [139], among others. These technologies have merit (especially for distribution in populations with low-income and drought), but large collector area requirements and low thermal efficiencies limit these technologies to small-scale applications. Multi-effect distillation (MED) with concentrated solar power for dual-purpose production has also been investigated [157, 25, 143, 82]. These types of systems offer larger system capacities, but are unable to achieve current industrial dual-purpose plant capacities without large solar collector areas. Further, in order to continuously produce water, back-up boilers (which emit $CO_2$) need to be utilized when sunlight is not present [25]. Nuclear fuel could also be utilized for zero emissions thermal desalination dual-purpose plants [30, 180]. While nuclear dual-purpose plants have high efficiency and appropriate system capacities, widespread use of nuclear power is currently not available.

Fossil fuel plants which utilize carbon capture and sequestration methods (CCS) are a reasonable alternative with the intention of the continued use of fossil fuels without the release of harmful greenhouse gases into the atmosphere. With CCS, zero or reduced emissions power production could be achieved while the economy transitions to renewable, zero-emissions sources [166, 177]. However, the addition of CCS to power cycles are cited as significantly reducing the First Law efficiency of a plant as compared to a power cycle without CCS [161]. One of the most promising CCS technologies is oxy-combustion.

Oxy-combustion involves the separation of oxygen from air and combustion in a nitrogen-free environment such that the flue gases consist of $CO_2$ and $H_2O$; the $H_2O$ can be easily separated by condensation. Cryogenic systems are currently the only technology commercially available for industrial-scale oxygen separation. However, ion transport membranes (ITM), which utilize high-temperature mixed ionic and electronic ceramic membranes to separate oxygen from air, are growing in popularity as a viable technology for use in large-scale power generation. Investigations of ITM via rigorous modeling techniques have increased the understanding of ITM performance and its technology readiness for implementation in CCS power generation applications [117, 118, 55].

Many power cycle concepts utilizing ITM technology exist [111, 80, 78, 144, 28, 167, 55, 116], and most are based on the AZEP (Advanced Zero Emissions Plant) cycle, which is typically presented as a zero or partial-emissions cycle [55, 111, 167, 28, 116] e.g., AZEP100 or AZEP72 (100% or 72% $CO_2$ separation, respectively [116]). The AZEP cycles feature a combined cycle with the ITM technology integrated in a Brayton-like topping cycle. Here, an advantage of the AZEP cycles over other membrane-based oxy-combustion processes is that they are able to utilize standard turbomachinery for power production, unlike other proposed power cycle concepts reported to achieve higher efficiencies [80]. Similar to conventional combined cycles, a bottoming cycle is utilized to increase the First Law efficiency of the overall cycle. The design of the bottoming cycle varies between publications, but is typically some realization of a Rankine steam cycle.

As with any combined cycle, the freedom of design of the AZEP bottoming cycle makes it attractive for combining thermal desalination. Specifically, the high exergy of the AZEP topping cycle product streams could be utilized to produce both power and water at zero or partial emissions. Further, since penalties are associated with CCS power cycles as compared to non-CCS power cycles, increased thermal integration through the addition of thermal desalination could, at least in principle, help offset these penalties. Along these lines, Bolea et al. [44] investigated the integration of multi-effect distillation (MED) with $CO_2$ compression systems for a post-combustion

CCS cycle. Bolea et al. find that MED can be powered by the heat rejected from the $CO_2$ compression system without substantial power plant modification. However, these integrations result in high power-to-water ratios.

The goal of this article is to explore the feasibility of an AZEP cycle with thermal desalination. In this work, the thermal desalination integration with the $CO_2$ compression system is explored initially. However, it is found this results in small water production, and instead, the bottoming cycle is adjusted to produce similar to industrial practice power-to-water ratios. Therefore, several bottoming cycle integrations which provide steam to MED and/or thermal vapor compression multi-effect distillation (MED-TVC) are developed. The performance of these bottoming cycles is measured both in terms of thermodynamic performance and capital costs.

## 2.2 Plant Descriptions and Simulation of Thermodynamic Performance

The following section offers an overview of the AZEP power cycle and the thermal desalination processes of interest. Specifically, the main aspects of each process which influence the potential integration of water and power production in the current work are presented.

Herein, both the AZEP power cycle and the thermal desalination processes are modeled in ASPEN Plus® [32] flowsheet simulation software and are based partially on the models developed for [116, 117]. In addition, the membrane reactor for oxygen separation is simulated in JACOBIAN differential algebraic equation solver [1]. ASPEN Plus® is typically utilized in the chemical process industry, but can also be applied to power cycle simulations and other applications. ASPEN Plus® contains unit energy and mass balance models for generic components, e.g., turbines, pumps, and heat exchangers, which makes process flowsheet analysis straightforward and is therefore ideal for simulation of the power cycles and desalination processes considered hereafter.

### 2.2.1 Advanced Zero Emissions Plant Description and Simulation

The AZEP oxy-combustion cycle is a power cycle which is intended to reduce or eliminate the carbon emissions typically associated with power production from fossil fuels. The following process summaries describe the AZEP cycle as utilized by [116], which in turn is based on [28, 111, 55, 53, 54].

The topping cycle is similar to a conventional Brayton cycle. However, an ITM is added to the cycle in order to separate oxygen from inlet air, as shown in Figure 2-1. The oxygen is used for the combustion of fuel in a separate stream than the high temperature gas which flows through gas turbines for electrical power production. The gas turbine exhaust thus consists of oxygen-depleted air. Oxygen separation in an ITM consists of complex kinetic and diffusive transport properties that depend on the local membrane temperature and oxygen partial pressure difference. The ITM imposes a temperature limitation on the gas entering the turbine; thus partial emission AZEP variants, e.g., AZEP72 (72% carbon separation), have been created to increase the cycle efficiency at the expense of some $CO_2$ emissions. The AZEP cycle herein is fueled by methane. For further information on the AZEP topping cycle and the ITM process and modeling herein, see [116, 117, 118].

The purpose of the bottoming cycle is to increase the First Law efficiency of the overall plant by producing electrical work from high grade thermal energy of the topping cycle exhaust streams. The bottoming cycle is a standard triple-pressure steam cycle (Figure 2-2) which extracts energy from the gas turbine exhaust, stream "GTEXH", and the flue gas stream "PRODBOTM" via a heat recovery steam generator (HRSG). The AZEP100 pressure levels are 100/20/5 bar, and the AZEP72 are 100/25/5 bar (pressure levels from [116]). Once the turbine exhaust stream exits the HRSG, it is released to the atmosphere; to avoid acid condensation in the partial emissions cycle, the outlet temperature is kept above approximately 100°C. The combustion products are directed to the $CO_2$ compression and purification unit (CPU), which separates $CO_2$ from the combustion products stream via condensation

of the water vapor and compresses the $CO_2$ for sequestration. In the CPU (Figure 2-3), the flue gas, stream "TOCPU", is cooled and compressed significantly in order to separate the $CO_2$ from the water present in the stream. The exergy of the inlet stream is low (100°C) and cannot be utilized economically for further electrical work production.

### Motivation of Thermal Desalination Integration Strategy

The main purpose of this article is to investigate the integration of thermal desalination to CCS power cycle technology, specifically the AZEP cycle. As aforementioned, in the baseline AZEP cycle, the CPU rejects relatively low grade heat to the environment; utilizing this heat for thermal desalination would not decrease the First Law efficiency of the plant (excluding the parasitic electrical work requirement for pumping in thermal desalination). Non-CCS dual-purpose plants sacrifice much electrical work production due to the diversion of steam from turbines to thermal desalination. Therefore, CPU coupling is seemingly attractive.

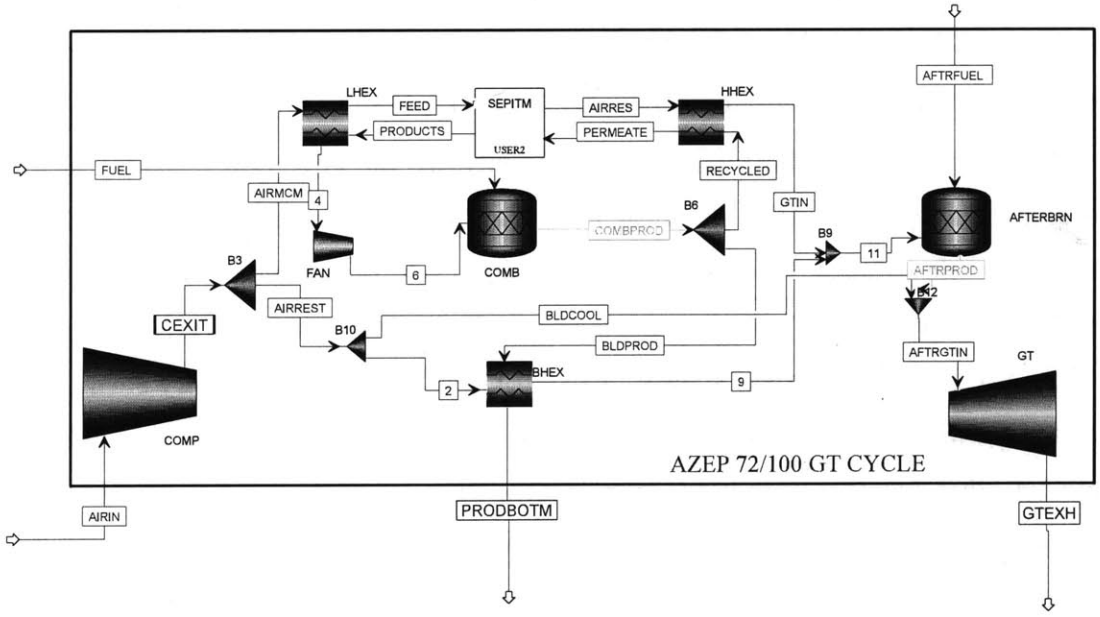


**Figure 2-1:** AZEP Topping Cycle; zero emission cycles do not include an afterburner (block "AFTERBRN").

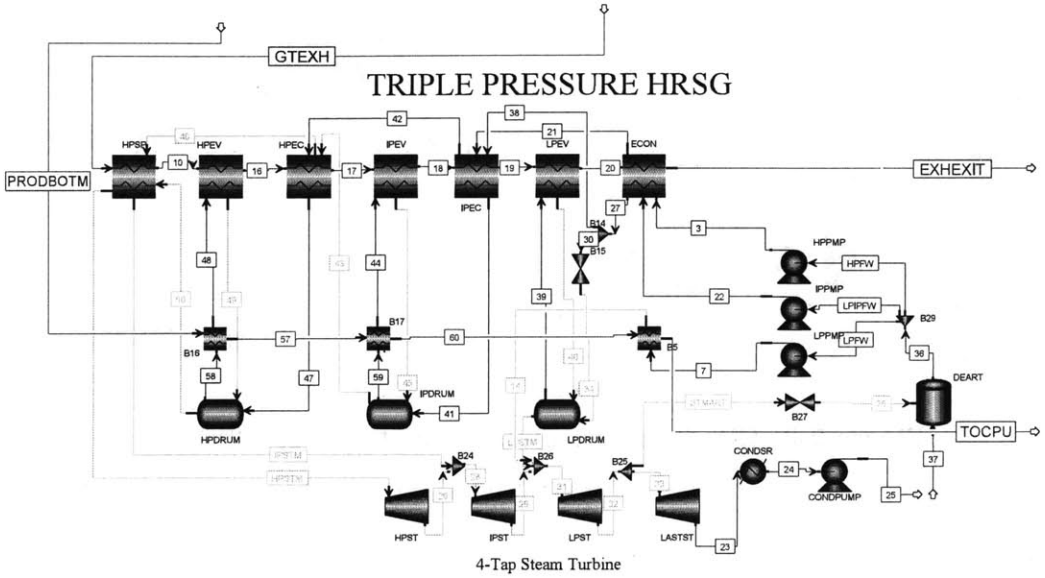


**Figure 2-2:** Triple pressure bottoming cycle for AZEP100/72: Pressure levels for AZEP100 are 100/20/5 bar and AZEP72 are 100/25/5 bar.

In order to estimate the amount of water which could be produced, the performance of MED powered by CPU rejected heat is simulated in the ASPEN Plus® model. The outlet temperatures of the units "HTSNK1", "HTSNK2", "HTSNK3", and "HTSNK4" in Figure 2-3, which model simple heat sinks to cool the $CO_2$ present in the stream, are modified such that they correspond to a typical steam supply temperature of a multi-effect distillation unit, i.e., approximately 70°C. Next, the thermal load of one MED unit is approximated.

For the MED, a performance ratio (PR, the ratio of mass flow of output water to input steam) of 12 is assumed; while for water/seawater, a constant enthalpy of vaporization of 2,330 kJ/kg and density of 1000 kg/m$^3$ is assumed. These values are typical in MED modeling literature [59, 67]. Given these assumptions, the specific heat demand for MED is 53.9 $\frac{\text{kWh}_\text{t}}{\text{m}^3}$. Consequently, the available heat in the CPU would produce 7,500 m$^3$/day of freshwater. This production corresponds to only one rather small MED unit; a typical industrial scale MED unit is on the order of 20,000 m$^3$/day [40], and industrial-scale dual-purpose plants usually have multiple MED units. The estimated production of 7,500 m$^3$/day corresponds to a very high PWR

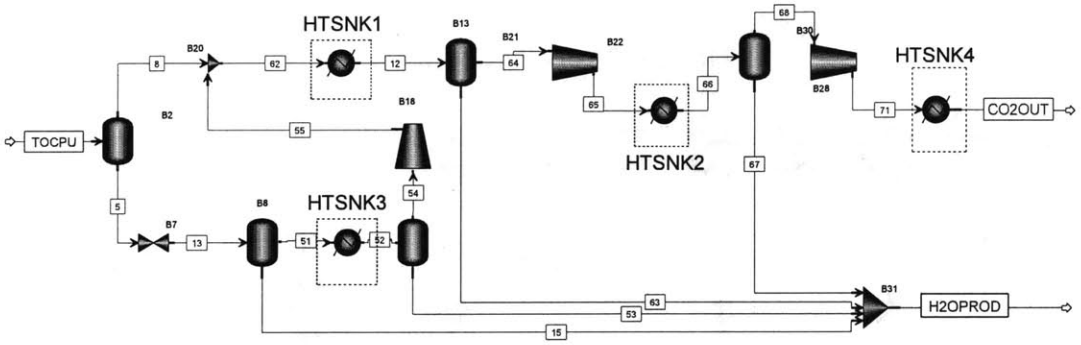


**Figure 2-3:** $CO_2$ Compression and Purification Unit (CPU).

of ≈1400 $kWh_e/m^3$, whereas typical combined cycle plants have a PWR of ≈ 50 – 60 $kWh_e/m^3$ [34]. Therefore, this integration would not provide enough water for typical demands and would most likely not be economical.

The CPU-coupling estimation shows that there is not enough available heat in the baseline AZEP cycle without modifying the flowsheet to provide more low grade heat to power thermal desalination. The most obvious possible modification is to utilize steam which is generated in the bottoming cycle. More specifically, the thermal energy of the topping cycle outlet streams can be employed to produce either electricity and/or water. Table 2.1 shows the AZEP zero and partial emissions results from [116] which are utilized hereafter as baseline cycles for performance comparison. Further, AZEP100 and AZEP72 thermal desalination integrations are developed utilizing fixed topping cycle exhaust streams, i.e., the gas turbine exhaust and flue gas streams, and will be discussed in more detail in following sections.

Proposed modifications require the quantification of both power cycle performance and water production through simulation since they are interdependent, i.e., as steam is taken from the power cycle to produce water, work production is decreased. As such, the bottoming cycle should be designed so that thermodynamic penalties, e.g., reduction of the First Law efficiency as compared to the baseline cycle, are appropriately weighed [107]. In this analysis, bottoming cycle steam will not be supplemented by heat from the CPU; in order to utilize CPU heat, substantial hardware addition

**Table 2.1:** Performance results of zero and partial emissions AZEP cycles from Mancini and Mitsos [116].

| | AZEP100 | AZEP72 |
|---|---|---|
| First Law Efficiency, $\eta_I$ (%) | 48.9 | 53.4 |
| Net work, $\dot{W}_{net}$ (MW) | 445 | 660 |
| Top cycle work, $\dot{W}_{top}$ (MW) | 239 | 372 |
| TIT (K) / TIP (bar) | 1415/18.8 | 1573/18.8 |
| Fuel input (kmol/s) | 1.14 | 1.55 |
| $CO_2$ Separated (%) | 97.4 | 71.6 |
| Air inlet flow, $\dot{m}_{air}$ (kg/s) | 1240 | 1298 |
| GT exhaust flow, $\dot{m}_{GTE}$ (kg/s) | 1168 | 1232 |
| GT exhaust temp., $T_{GTE}$ (°C) | 489 | 595 |
| GT exhaust pressure, $P_{GTE}$ (bar) | 1.2 | 1.2 |
| Flue gas flow, $\dot{m}_{FG}$ (kg/s) | 91 | 91 |
| Flue gas temp., $T_{FG}$ (°C) | 558 | 580 |
| Flue gas pressure, $P_{FG}$ (bar) | 19.4 | 19.4 |

and CPU redesign would be necessary for little gain in water production ($\lesssim$ 3% increase).

### 2.2.2 Thermal Desalination Method Descriptions and Simulations

Thermal desalination methods are established technologies for the industrial-scale production of water. These methods rely on the evaporation of water through boiling or flashing in order to separate pure water vapor from seawater. An external heat source is utilized to power the separation process, e.g., steam from an electrical power plant. Thermal desalination has reliable performance and produces high quality, virtually salt-free water with little performance dependence on the temperature or salinity of the inlet seawater. As such, thermal desalination plants are very popular in regions with high seawater temperatures and salinities, e.g., Saudi Arabia and the United Arab Emirates. It is important to note that reverse osmosis, which is frequently cited as requiring significantly less total energy input per unit of distillate

as compared to thermal desalination [155], suffers from high maintenance and operation costs when utilizing seawater with high seawater temperature and salinities due to current membrane limitations [64]. Therefore, reverse osmosis is most often not economically practical for installation in these environments.

Traditionally, the multi-stage flash (MSF) process, which generates salt-free water vapor through flashing seawater in a series of increasingly reduced pressure stages, has been the most common thermal desalination process. However, recent advances in anti-scaling technology, i.e., inhibitors which block the formation of $CaSO_4$ on heat transfer surfaces, improved heat transfer surfaces, and the ability to utilize lower pressure power plant steam as compared to MSF have made MED a rival to MSF in terms of reduced thermal and electrical consumption and capital costs [142]. In some cases thermal vapor compression (TVC) is added to MED in order to increase the performance ratio at the expense of increased motive steam pressure. For further information on advantages of MED and MED-TVC, see [56, 109, 43, 15] .

Due to the energetic and economic advantages of MED and MED-TVC over MSF, the integration of these technologies as a CCS dual-purpose scheme are most appropriate for investigation. Further, because the addition of CCS to a power cycle inherently imposes thermodynamic penalties on the power cycle, the most efficient thermal desalination technology available should be utilized to minimize further penalties. The simulation of MED and MED-TVC is performed in ASPEN Plus®. Representative values of common industrial performance are utilized for the choice of thermal desalination operating parameters. It is important to note that ASPEN Plus® does not explicitly include unit models for typical desalination components, e.g., horizontal tube evaporators. However, basic thermodynamic models for flashing and heat transfer are provided, e.g., the "FLASH2" and "HEATER" unit models, respectively. Therefore, MED and MED-TVC models are constructed from ASPEN Plus® unit operations.

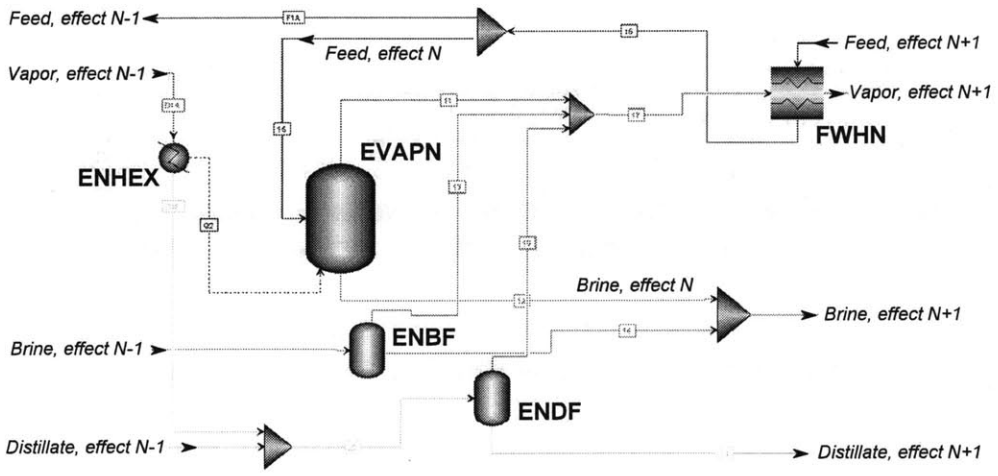


**Figure 2-4:** Unit Model of MED Effect "N" modeled in ASPEN Plus®.

### Simulation of Multi-Effect Distillation

The MED plant considered consists of a parallel-cross configuration with twelve effects and eleven feed water heaters. Many industrial MED plants are parallel-cross due to easy maintenance as compared to other MED configurations [67]. Feed water heaters are utilized to increase thermal integration. As a first step, a single MED effect is modeled in terms of ASPEN Plus® unit models, shown in Figure 2-4 as effect "N".

For the simulation of MED, ASPEN Plus® physical property model are utilized. For water vapor and distillate streams, steam tables are utilized, i.e., enthalpies of vaporization and specific heat values are not considered constant across effects. The seawater and brine streams are approximated as an electrolyte solution containing NaCl using the electrolyte-NRTL physical property model. The effects of boiling point elevation are taken into account through the utilized ASPEN Plus® thermal property method.

The evaporator, unit "EVAPN" in Figure 2-4, is represented via the "FLASH2" unit model, which uses vapor-liquid equilibrium calculations in order to calculate the flowrates of the separated distillate and brine. Although the primary mode of evaporation in an MED effect is by boiling and not flashing as the "FLASH2" model

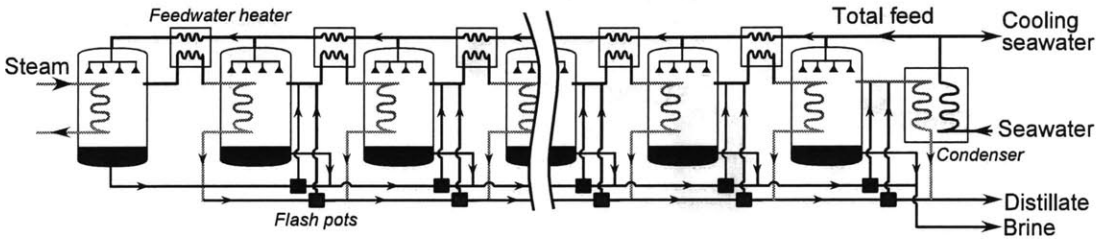


**Figure 2-5:** Parallel-cross MED with feedwater heaters.

suggests, from a black box perspective, it is valid to model the horizontal falling-film evaporator of MED in this way since only mass balance and First Law analysis are necessary herein. Here, the thermal energy input and the saturation pressure drop is fixed in each effect. The small effect of brine flashing from brine flowing to a pressure drop between effect in the parallel-cross configuration is taken into account in the "FLASH2" unit named "ENBF" in Figure 2-4. Similarly, the effect of condensate flashing is taken into account in unit "ENDF".

The vapor generated from "EVAPN", "ENBF", and "ENDF" flows to the feedwater heater "FWHN" and is partially condensed in order to increase the temperature of the feedwater. The remaining vapor is condensed in effect N+1 in order to power the evaporation process of the incoming feedwater. The condensation process is represented via the "HEATER" unit model, shown as "ENHEX" in Figure 2-4, in which remaining enthalpy of vaporization of the stream is directed to "EVAPN". For effect 1, the flow through "ENHEX" is heating steam from a power plant or boiler. For each effect, an equal amount of feedwater is provided to "EVAPN" from the total feedwater stream.

The unit model of effect "N" is repeated to build the full MED plant of twelve effects. A flow diagram of the full plant is shown in Figure 2-5. In addition to the effects, there is also a condenser after the last effect, which serves to condense the vapor generated in the last effect and raise the feedwater temperature. In order to fully condense the vapor to a saturated liquid, additional cooling seawater besides the feedwater flows through the condenser and is then rejected to the sea.

Several assumptions are made regarding the operating parameters of the plant and are summarized in Table 2.2. It is assumed that the temperature drop across each effect is constant, i.e., the difference between the top brine temperature and the brine discharge temperature divided by the number of effects. Further, it is assumed that the temperature rise in each feedwater heater is equal to the temperature drop across each effect. These assumptions correspond to the assumptions made by Darwish et al. [59] and Darwish and Abdulrahim [58].

The total feed flowrate is calculated via a design specification that the outlet brine salinity does not exceed 72 g/kg so that scaling is avoided. In other words, the recovery ratio (defined as the ratio of distillate flowrate to feed flowrate) is approximately 0.37. The steam flowrate requirement for a single MED unit is calculated via a design specification that the production rate is 20,000 $m^3$/day, which is a typical unit size for today's industrial scale MED units [40]. For this analysis, the production rate of one unit is held constant for all integration schemes, i.e., the total production rate of an AZEP integration scheme consists of multiple MED units and is determined by finding how many MED units could be installed. Finally, the cooling water flowrate is calculated by the amount of water, less the total feed, which is necessary to fully condense the vapor generated in the final effect.

**Table 2.2:** Thermal desalination operating parameters for integration with AZEP.

| | |
|---|---|
| Unit distillate flow, $D_{out}$ ($m^3$/day) | 20,000 |
| Number of effects | 12 |
| Seawater temp., $T_{sea}$ (°C) | 30 |
| Seawater salinity, $X_{sea}$ (g/kg) | 46 |
| Max brine salinity, $X_{brine,max}$ (g/kg) | 72 |
| Top brine temperature (°C) | 62 |
| Brine temp., $T_{brine}$ (°C) | 42.5 |
| Effect temp. drop, $\Delta T_{drop}$ (°C) | 1.81 |
| Electricity required, MED (kWh/$m^3$) | 2.2 |
| Electricity required, MED-TVC (kWh/$m^3$) | 1.5 |
| Compression ratio for MED-TVC, $\frac{P_{di}}{P_e}$ | 3.5 |

It is assumed that the specific electricity requirement is a constant 2.2 kWh/m$^3$; this value is chosen based on the average reported value among several sources [125, 15, 24, 29, 49, 52, 146, 59]. The range of the specific electricity requirements from the cited literature is 1.8-2.5 kWh/m$^3$. It should be noted that the commonly used approximation of constant electricity requirement is in general a significant approximation. However, since the capacity of one thermal desalination unit is fixed in this work and steady-state operation at industrial standard conditions is assumed, a constant specific electricity value is acceptable herein.

The resulting performance values from simulation are shown in Table 2.3. For some bottoming cycle simulations in later sections, the steam inlet conditions vary slightly due to turbine discharge conditions in the back-pressure configuration; these variations are taken into account for plant performance calculations, but the results shown in Table 2.3 provide a general performance estimation for the MED system considered.

### Simulation of Multi-Effect Distillation with Thermal Vapor Compression

The addition of thermal vapor compression to MED allows for a higher performance ratio for the same production capacity of a given plant. A TVC unit utilizes high pressure motive steam to entrain a low pressure vapor. A mixture of the high and low pressure steams is discharged at some intermediate pressure. TVC units are attractive from an economic viewpoint because they have no moving parts and are relatively inexpensive and easy to maintain [65].

The same basic ASPEN Plus® MED model developed in the previous section is utilized and expanded upon in order to simulate the performance of MED-TVC, i.e., the MED-TVC is also a twelve effect parallel-cross configuration. A TVC unit is added to the conventional MED plant which draws part of the vapor generated in the last effect and compresses the vapor to power the first effect, as shown in Figure 3-4. In addition to the TVC, a desuperheater is added so that the compressed vapor entering the tubes of the first effect is saturated (superheated steam entering heat exchanger tubes have a substantially lower heat transfer coefficient and can damage

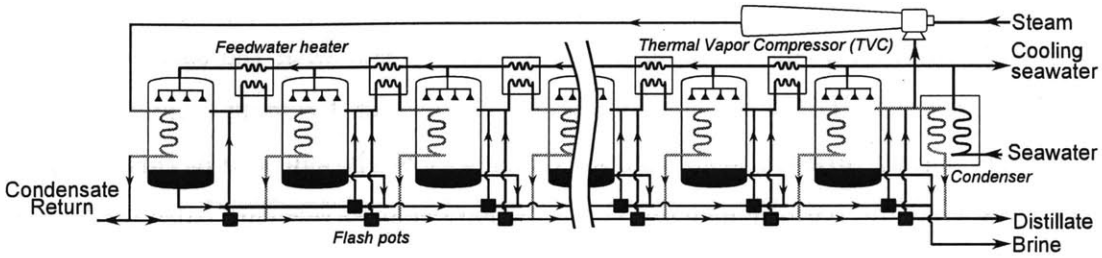


**Figure 2-6:** Parallel-cross MED-TVC with feedwater heaters.

equipment [152]). For the purpose of this analysis, it is assumed that an external ancillary cooling loop cools the vapor to a saturated vapor, and a small (negligible) amount of energy is lost from the MED-TVC system.

The performance of the TVC unit is simulated using correlations developed by El-Dessouky and Ettouney [69]. These correlations calculate the entrainment ratio, i.e., the ratio of mass flowrates of motive steam to entrained vapor, as follows:

$$ER = 0.296 \frac{(P_{di})^{1.19}}{(P_e)^{1.04}} \left(\frac{P_m}{P_e}\right)^{0.015} \left(\frac{3 \times 10^{-7} (P_m)^2 - 0.0009 (P_m) + 1.6101}{2 \times 10^{-8} (T_e)^2 - 0.0006 (T_e) + 1.0047}\right)$$

where $P_m$ is in kPa and $T_e$ is in °C. According to El-Dessouky and Ettouney, this correlation agrees to within 10% of manufacturer's data over the following ranges: $ER \leq 4.5$, $10 < T_e \leq 500$°C, $100 \leq P_m \leq 3500$kPa, and $\frac{P_{di}}{P_e} \geq 1.81$. Recently McGovern et al. [124] developed a second-law analysis of TVC and concluded that an isentropic efficiency could be utilized to model their performance. These results could have equivalently been used in this analysis.

**Table 2.3:** ASPEN Plus® Simulation Results of MED and MED-TVC.

| | MED | MED-TVC | | | |
|---|---|---|---|---|---|
| Steam pressure (bar) | 0.312 | 35 | 25 | 20 | 5 |
| Steam flow (kg/s) | 18.75 | 15.5 | 13.6 | 12.5 | 13.5 |
| Performance ratio, PR | 12.4 | 15 | 17 | 18.5 | 17.2 |
| Entrainment ratio, ER | N/A | 4.31 | 2.48 | 2.02 | 2.42 |

The MED-TVC plant is simulated in ASPEN Plus® with the same operating parameters as the MED plant shown in Table 2.2. However, the main difference is that the steam supply pressure is substantially higher. For the purpose of this analysis, the steam flowrate, performance ratio, and the entrainment ratio are calculated using 35, 25, 15, and 5 bar steam; see Table 2.3. The steam operating pressures are chosen for bottoming cycle heat exchanger balancing and will be discussed in upcoming sections. For all simulations, it is assumed that the compression ratio, i.e., the ratio of discharge pressure to entrained pressure, is 3.5. Again, a constant specific electricity requirement is utilized; a value of 1.5 kWh/m$^3$ is assumed based on averaged values reported by [30, 63, 61].

## 2.3 Estimation of Capital Expenditures

Economic considerations play an important role in the feasibility of a proposed thermal plant concept. Therefore, herein the capital expenditures associated with each proposed bottoming cycle are calculated. The economic results presented in the following sections are meant for comparison of relative magnitude to aid in the determination of favorable bottoming cycle integrations. In this analysis, the topping cycle is held fixed as compared to the base case (without thermal desalination integration). In the economic reporting of AZEP72 and AZEP100, only the bottoming cycle power cycle and thermal desalination capital expenditures will be considered as a relative measure of economic feasibility of an integration.

The CAPEX associated with the bottoming power cycle include the component costs of HRSG units, pumps, turbines, and condensers. In order to estimate these costs, the turbine, condenser, and pump correlations are taken from Silveira and Tuna [160] and are as follows

$$C_{ST} = 6000\dot{W}_{ST}^{0.7} \quad C_{CD} = 177\dot{m}_{in} \quad C_P = 3540\dot{W}_P^{0.71}$$

**Table 2.4:** HRSG economic parameters [50].

| | k [\$US/m$^2$] | U [W/(m$^2$K)] |
|---|---|---|
| Economizer | 45.7 | 42.6 |
| Evaporator | 34.9 | 43.7 |
| Superheater | 96.2 | 50 |

where C is the capital expenditure (\$US), $\dot{W}$ is the shaft work (kW), and $\dot{m}$ is the component flowrate (kg/s).

These correlations account for component installation, electrical equipment, control systems, piping and assembly. Silveira and Tuna provide a correlation for HRSGs, but this only applies to single pressure HRSGs. Therefore, overall heat transfer coefficients and the cost per unit area for economizers, evaporators, and superheaters by Casarosa et al. [50] are utilized for HRSG CAPEX estimations, as shown in Table 2.4.

The thermal desalination units considered in this study are of fixed capacity despite the type of bottoming integration. Therefore, it is sufficient to estimate the CAPEX of MED and MED-TVC installations on a unit capacity basis, as opposed to accounting for each effect or pump in a unit. The CAPEX values of MED and MED-TVC used in this study are 875 \$/ (m$^3$/day) which is an average between two reported CAPEX values for MED and MED-TVC [141, 126].

## 2.4 Bottoming Cycle Integrations

Three bottoming cycle flowsheets are developed and studied in order to investigate the feasibility of AZEP dual-purpose plants. Specifically, feasibility is measured with respect to thermodynamic considerations, i.e., thermal balancing and high First Law efficiency, economic considerations, i.e., low capital costs for equipment, and appropriate power-to-water ratios, which is both a thermodynamic and economic consideration. Since the AZEP topping cycle is of fixed design in this study, multiple

bottoming cycle flowsheets are utilized in order to estimate the range of possibilities of water and power production for an AZEP dual-purpose cycle.

The operating conditions of the proposed integrations are chosen such that a reasonable performance estimate is achieved. Optimization is outside the scope of this article. In the following sections, each flowsheet is simulated with the operating conditions of the zero emissions topping cycle (AZEP100) and the partial emissions topping cycle (AZEP72).

### 2.4.1 MED Back-Pressure Bottoming Cycle

The first integration studied is similar to the baseline AZEP bottoming cycle. However, MED is coupled in a back-pressure arrangement and replaces the condenser of the steam cycle, as shown in Figure 2-7. Hereafter, this cycle is referred to as AZEPXX-BST-MED, i.e., AZEP72-BST-MED or AZEP100-BST-MED. As compared to the baseline operating conditions, the discharge pressure of the low pressure turbine, unit "LASTST" in Figure 2-7 is adjusted such that steam is provided to MED at a saturation pressure of 0.312 bar, i.e., the steam operating pressure of MED as specified in Table 2.3. The coupling of MED to the power cycle is modeled by the ASPEN Plus® unit model "HEATER" and is shown in Figure 2-7 as "MEDHEX".

In order to estimate the amount of water which could be produced from this integration, the flowrate through unit "MEDHEX" is calculated. The flowrate is set given the following design specifications: the outlet temperature of the gas turbine exhaust (stream "EXHEXIT") is 105 °C, the minimum temperature approach of the HRSG is 5°C, and the pinch between steam and the combustion products is 10°C. The pressure levels of the HRSG remain at 100/20/5 bar for AZEP100 and 100/25/5 bar for AZEP72.

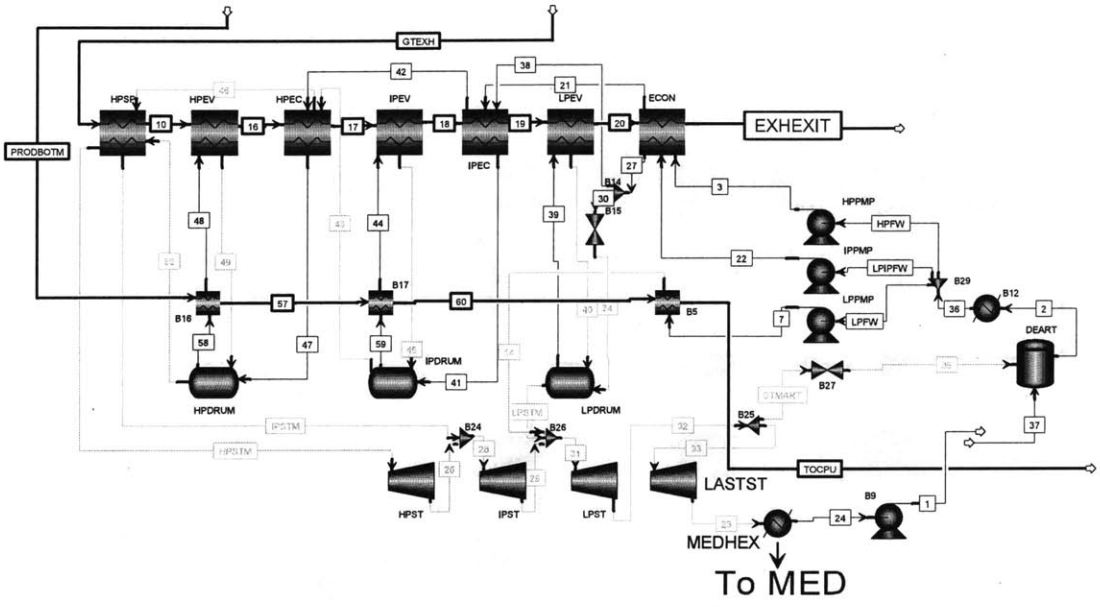


**Figure 2-7:** MED Back-pressure bottoming cycle, AZEPXX-BST-MED, flowsheet.

### 2.4.2 MED-TVC Extraction Bottoming Cycle

The second integration studied couples MED-TVC in an extraction arrangement. Hereafter, this cycle is referred to as AZEPXX-EST-TVC. This integration is considered in order to see if MED-TVC, which typically has a much high performance ratio than MED alone, will outperform AZEPXX-BST-MED in water production, First Law efficiency, and/or capital expenditures. However, in this integration, it is not immediately clear if the higher performance ratio of MED-TVC outweighs the lost work of the bottoming cycle due to higher extraction pressures as compared to MED.

The steam generated in the intermediate pressure steam drum, "IPDRUM" in Figure 2-8, is directed to MED-TVC. The steam generated in the high and low pressure drums, "HPDRUM" and "LPDRUM", is directed through steam turbines and condensed at 0.03 bar (the same condensing pressure of the baseline cycle). The flowrate to MED-TVC is chosen such that the pinches across the HRSG are reasonable, i.e., not less than 5°C. The overall flowrate of the cycle is found through the same design specifications as AZEPXX-BST-MED.

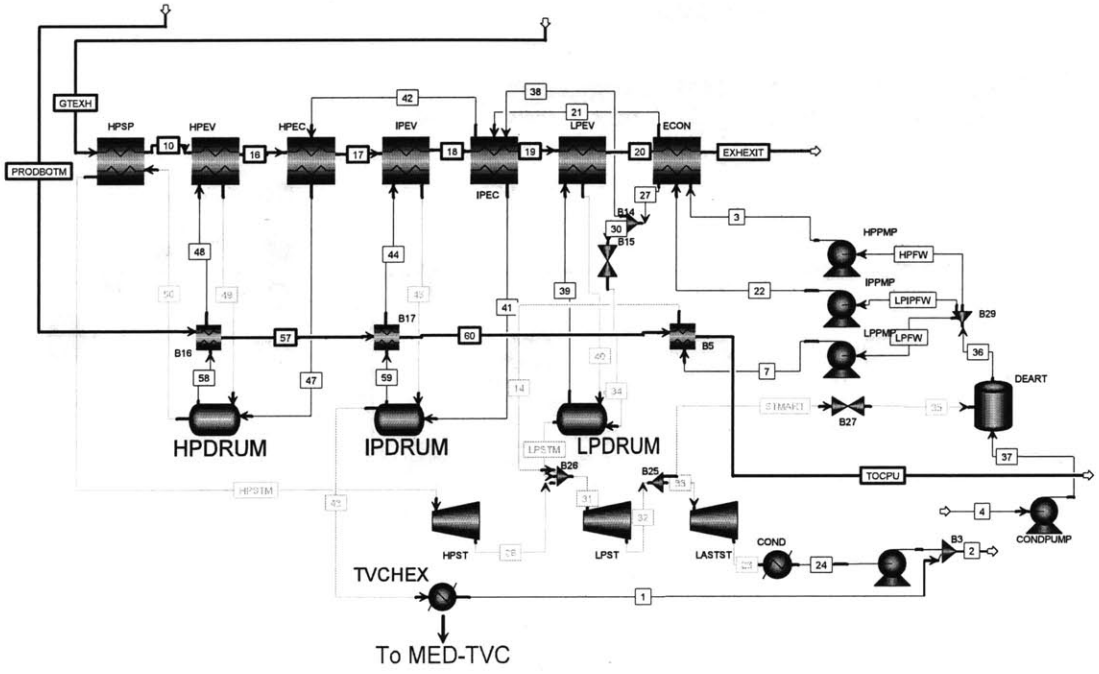


**Figure 2-8:** MED-TVC extraction bottoming cycle, AZEPXX-EST-TVC, flowsheet.

### 2.4.3 Water-Only Bottoming Cycle

The two previous integrations are designed to produce both power and water in the bottoming cycle. Consequently, these integrations require hardware installation for both power and water production. Therefore, a water-only bottoming cycle is considered in order to evaluate if for the AZEP operating conditions, it could be cheaper from a CAPEX perspective to remove power cycle machinery from the bottoming cycle.

For a water-only bottoming integration, the production of water could be estimated by directing the topping cycle exhaust gases directly to thermal desalination. Such an arrangement could reduce the total heat transfer area necessary for energy transfer to thermal desalination (as opposed to a secondary steam loop to thermal desalination). However, this arrangement would result in high thermal stresses in the thermal desalination plant material since the temperature of the exhaust gas is on the order of 800 K, i.e., a temperature difference of greater than 700 K would

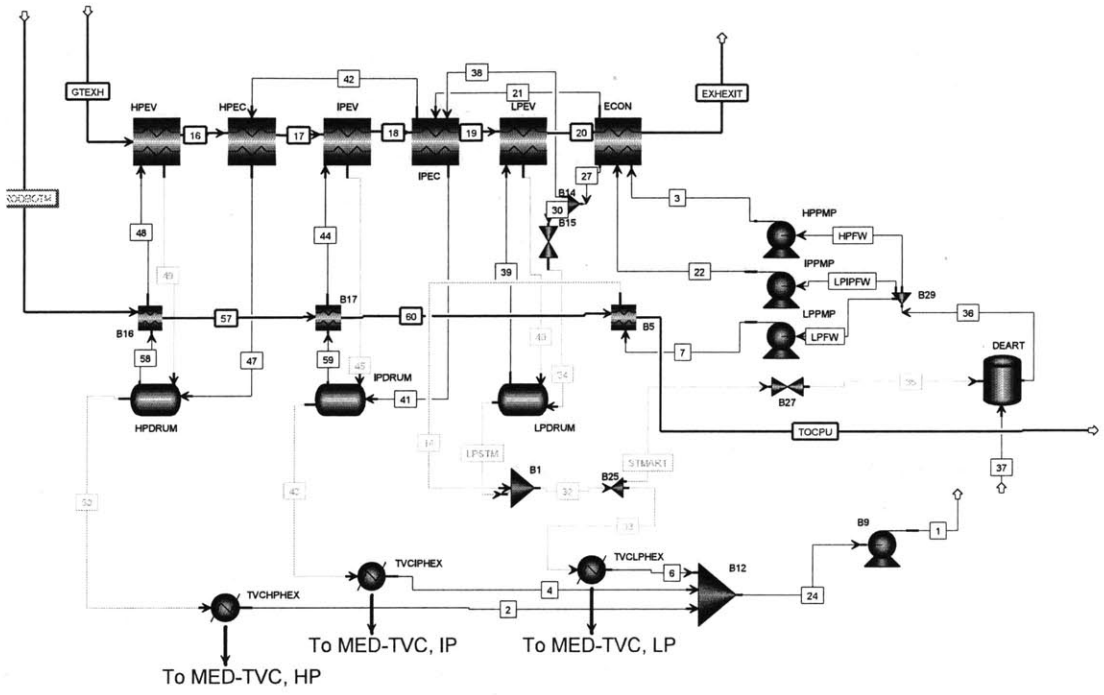


**Figure 2-9:** Triple pressure TVC water-only bottoming cycle, AZEPXX-3TVC, flowsheet.

occur on the hot end of the heat exchanger. Besides the material problems, such an arrangement would generate large amounts of entropy due to the large temperature difference. Thus, this arrangement seems neither practical nor thermodynamically sound. Rather, a water-only bottoming cycle should follow the temperature profile of the cooling exhaust gases, both from a material limitation perspective and a thermal balancing perspective.

Given these two considerations, the use of a HRSG unit is utilized for a water-only bottoming integration. In order to approximately follow the temperature profile of the topping cycle exhaust streams, a triple pressure HRSG is utilized (similar to the baseline cycle). For each pressure level, it is proposed that the evaporators provide saturated steam directly to MED-TVC operating at the corresponding pressure level, as shown in Figure 2-9. That is, the turbines of the original bottoming cycle are replaced with steam supply to TVCs. Hereafter, this integration is referred to as AZEPXX-3TVC. For AZEP100, the pressure levels are taken as 35/20/5 bar, and

for AZEP72, the pressure levels are taken as 35/25/5 bar. In these configurations, a superheater is not utilized in the HRSG since superheated steam is not desired for the MED-TVC units. The overall flowrate of the cycle is determined via the same design specifications as AZEPXX-BST-MED and AZEPXX-EST-TVC. Also, the flow to each pressure level is adjusted such that pinch in each evaporator is reasonable ($\geq 5°C$).

## 2.5 Results and Discussion

The thermodynamic performance and capital costs for each bottoming integration are estimated via simulation of the flowsheets developed in ASPEN Plus®. These estimations serve to give a level of relative performance as compared to the baseline bottoming cycle, between each integration, and to dual-purpose cycles with no carbon capture technology.

### 2.5.1 Thermodynamic Performance and Water Production

Table 2.5 shows the water and power results of each integration scheme for both AZEP100 and AZEP72. The net work of each cycle includes the work of the respective topping cycle and the bottoming cycle minus the electricity required for pumping to thermal desalination, which is dependent on the amount of water produced. The total amount of water produced is calculated by the water flowing through each "HEATER" unit model that provides steam to MED or MED-TVC. Note that the negative bottoming cycle net work of the 3TVC schemes is due to the triple pressure pumps for the HRSG and is considered a parasitic load on the topping cycle since there is no bottoming cycle work production.

Figure 2-10 shows the water production and corresponding cycle efficiency of the investigated cycles. For both the zero and partial emissions cycles, the BST-MED integrations result in the least lost efficiency points as compared to the corresponding baseline cycle. Conversely, the water-only integration corresponds to the greatest

**Table 2.5:** Power and water production performance results of bottoming integrations; the negative bottoming work of 3TVC is due to HRSG pumping requirements.

| | AZEP72 | | | AZEP100 | | |
|---|---|---|---|---|---|---|
| | BST-MED | EST-TVC | 3TVC | BST-MED | EST-TVC | 3TVC |
| Water prod. ($\times 10^5$ m$^3$/day) | 2.53 | 1.83 | 4.58 | 2.16 | 1.51 | 3.66 |
| Net work, bottom (MW) | 254.8 | 127.0 | -1.0 | 166.8 | 108.8 | -0.6 |
| Desal. parasitic work (MW) | 23.2 | 11.4 | 28.7 | 19.8 | 9.5 | 22.9 |
| Net work, overall (MW) | 603.9 | 487.9 | 342.7 | 386.2 | 338.5 | 215.7 |

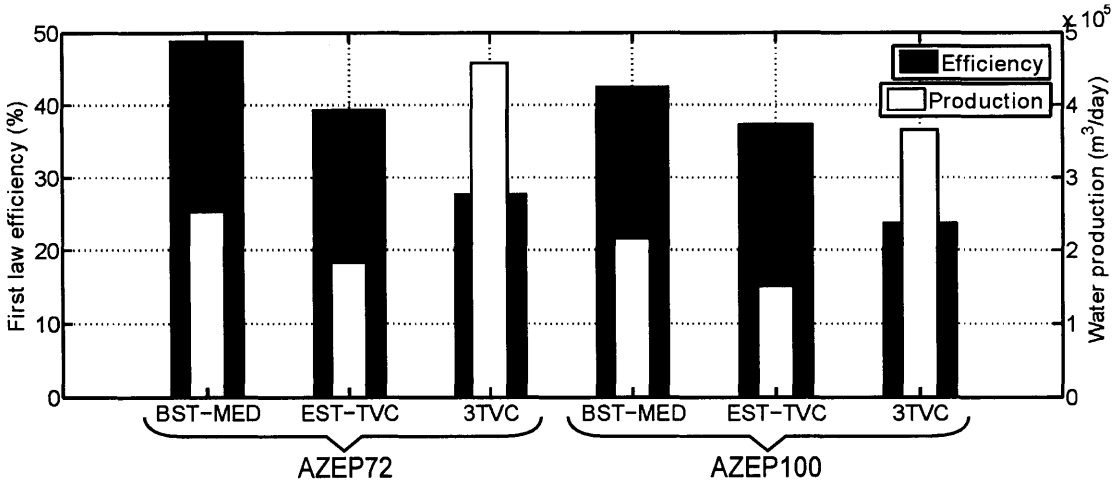


**Figure 2-10:** First Law efficiency and water production results for proposed bottoming cycle integrations. The baseline efficiencies of AZEP100 and AZEP72 are 48.9% and 53.4%, respectively.

loss of efficiency points. As expected, for BST-MED and 3TVC, water production corresponds with the decrease in efficiency, i.e., 3TVC loses the most efficiency, but is able to produce the most water.

However, EST-TVC is less efficient as compared to BST-MED and produces less water. This trend is explained by the high exergy which is associated with the steam provided to EST-TVC as compared to BST-MED. Further, due to pinch constraints in the HRSG, the flow to the intermediate pressure drum in the EST-TVC arrangement is quite low as compared to the flow to thermal desalination in BST-MED. There are many design possibilities for the EST-TVC arrangement, and it is possible that lower TVC extraction pressure could result in favorable performance as compared to the

back-pressure arrangement. The extraction arrangement allows for some flexibility in water production to follow changing demands, which is a potential advantage over the back-pressure arrangement.

### 2.5.2 Capital Expenditures

The capital expenditures of each bottoming integration are considered in order to measure the relative investment of each case. Table 2.6 shows the CAPEX values of bottoming cycle components and thermal desalination for each integration. The difference in HRSG CAPEX values between BST-MED and EST-TVC/3TVC is mainly due to the removal of the superheater in the case of EST-TVC and 3TVC. Also, in BST-MED and 3TVC, it is assumed that the main power plant condenser is replaced with hardware for steam supply to thermal desalination and is accounted for in the cost of desalination. On the other hand, the condenser CAPEX in EST-TVC is accounting for the sub-atmospheric power plant condenser still necessary in the cycle with extraction.

Figure 2-11 shows the total CAPEX of the bottoming components compared to the thermal desalination CAPEX of each cycle investigated. It is clear from the CAPEX values for thermal desalination that the CAPEX of a dual-purpose AZEP cycle would be significantly higher than a power-only AZEP cycle. However, the same is true of comparing dual and single purpose cycles without CCS.

The CAPEX estimations shown in Figure 2-11 indicate that the total CAPEX of a given bottoming cycle is dominated by the cost of thermal desalination. One

**Table 2.6:** Capital expenditures of bottoming cycle components (million $US).

| | AZEP72 | | | AZEP100 | | |
|---|---|---|---|---|---|---|
| | BST-MED | EST-TVC | 3TVC | BST-MED | EST-TVC | 3TVC |
| HRSG | 23.64 | 15.59 | 15.91 | 19.77 | 12.92 | 14.86 |
| Pumps | 0.98 | 0.80 | 0.62 | 0.67 | 0.60 | 0.46 |
| Steam turbine | 55.23 | 30.92 | 0 | 41.06 | 29.05 | 0 |
| Condenser | 0 | 0.51 | 0 | 0 | 0.40 | 0 |
| Thermal desal. | 221.13 | 160.15 | 401.04 | 189.12 | 132.44 | 320.39 |

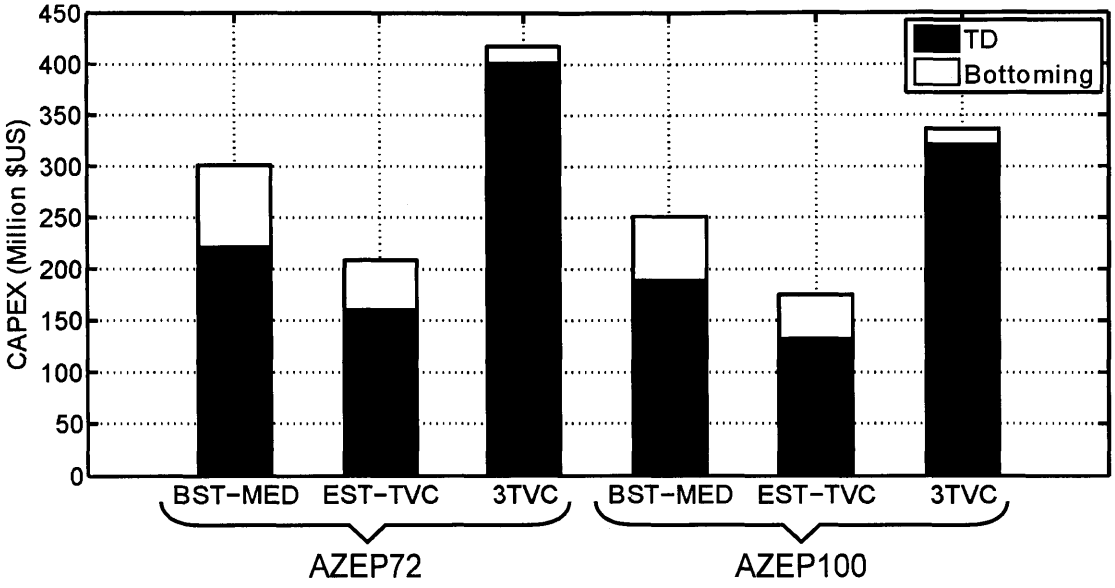


**Figure 2-11:** Capital expenditures of proposed bottoming cycle integrations.

motivation for investigating the water-only integration was to possibly reduce capital costs by elimination of turbomachinery. Indeed, when comparing the CAPEX of bottoming hardware in 3TVC to BST-MED, the CAPEX is significantly less for the zero and partial emissions cycles. However, significantly more water is produced in 3TVC than the other integrations. Subsequently, the total CAPEX of 3TVC is much greater than the other integration on the order of hundreds of millions of dollars. In choosing between the BST-MED or 3TVC integration, further analysis into the water and power demands of a given installation would be necessary. Although the 3TVC integration has a higher CAPEX, this integration could be favorable for a population with a low average power-to-water ratio.

It is important to note that although the total CAPEX of the AZEP100 bottoming integrations is less than the AZEP72, their values should not be directly compared since their topping cycles differ in power production scale. Determining whether a full or partial emissions dual-purpose cycle should be employed requires further analysis also taking into account environmental aspects as well as power and water demand as compared to a non-CCS dual-purpose cycle.

### 2.5.3 Specific Lost Work and Power-to-Water Ratios

Table 2.7 shows the specific lost work and PWR results of the considered integrations. The specific lost work is the difference of the net work (both the bottoming and topping cycle) to the baseline cycle normalized by the total water production. As such, it includes both the loss of electricity production due to supplying steam to thermal desalination and the parasitic electricity requirement for thermal desalination.

The specific lost work values indicate that the BST-MED integrations require the least amount of energy from the power cycle in order to produce one unit of water. This result is expected, given the First Law efficiencies for BST-MED as compared to the other bottoming integrations. The specific lost work of the AZEP100-BST-MED cycle is approximately 16% greater than the AZEP72 cycle. This difference can be explained bye the greater $CO_2$ separation in the AZEP100 cycle. The AZEP100 cycle has a greater efficiency penalty for greater separation and also has lower temperature and flow streams to the bottoming cycle as compared to AZEP72. However, this difference elucidates that a rather small increase in energy investment is needed achieve emissions-free water production as compared to partial emissions.

The PWR values shown in Table 2.7 give a measure of the power and water demand which could be met with the investigated bottoming cycle integrations. For example, although the 3TVC cycles have a large drop in First Law efficiency, large quantities of water can be created. As with a non-CCS dual-purpose cycle, the penalty in efficiency may be acceptable if the water demand in the region of installation is very high. It is also important to note that the resulting PWR values herein are reasonable in comparison to typical PWR values of non-CCS dual-purpose plants [34]; Awerbuch cites the typical PWR of a combined-cycle with back-pressure MED as 52.7. These PWR values indicate that the AZEP zero and partial emissions plants can produce quantities of water which are typical for industrial-scale seawater desalination.

Although ITM membrane separation is not a market-ready technology, the results produced herein indicate that once the ITM technology is market-ready, the

**Table 2.7:** Specific lost work and PWR results of proposed bottoming cycle integrations ($kWh/m^3$).

| | AZEP72 | | | AZEP100 | | |
|---|---|---|---|---|---|---|
| | BST-MED | EST-TVC | 3TVC | BST-MED | EST-TVC | 3TVC |
| Specific lost work | 5.5 | 22.8 | 16.7 | 6.4 | 16.7 | 15.0 |
| PWR | 57.3 | 64.0 | 17.9 | 42.9 | 53.7 | 14.1 |

AZEP cycle can be easily modified to produce emissions-free water at an industrial scale, i.e., economically-feasible AZEP power-only production is necessary for economically-feasible dual-purpose production. The back-pressure and extraction integration schemes shown herein are standard technologies for non-CCS dual-purpose plants which could almost directly be applied to the AZEP combined cycle.

However, sufficiently determining economic feasibility of the AZEP dual-purpose plant in comparison to a non-CCS dual-purpose plant requires an analysis weighing capital costs, operating costs, power-to-water production, $CO_2$ savings, and $CO_2$ tax. These analyses depend heavily on plant installation conditions and is outside the scope of this study. Such an analysis should answer from a fleet perspective whether it would be better to build AZEP power production and non-CCS dual purpose plants separately or build them integrated, as is explored in this study. Further, this analysis should explore whether the additional performance penalty to achieve a zero emissions dual-purpose cycle outweighs the benefit. Capital/operating costs and $CO_2$ emissions versus plant power and water production is a possible metric for determining these answers.

## 2.6 Conclusion

In this study, dual-purpose oxy-combustion cycles for power and water production are investigated. In particular, the AZEP cycle which utilizes ITM oxygen separation technology is integrated with thermal desalination. Two cycles which produce power and water in the bottoming cycle are developed: back-pressure turbine with MED and steam extraction with MED-TVC. Also, a water-only bottoming cycle with

MED-TVC is developed for populations with low average power-to-water ratios and as a measure of the maximum water which could be produced. The thermodynamic performance and capital expenditures for zero and partial emissions plants are estimated.

The thermodynamic performance results of the zero and partial emissions AZEP dual-purpose plant show feasibility for industrial-scale water production. Specific lost work analysis shows that a zero-emissions dual-purpose plant does not require significantly more thermodynamic investment ($\approx$ 16% greater) for dual-purpose as compared to a partial emissions plant. The bottoming cycle integrations which are explored produce water at a power-to-water ratio which is reasonable for industrial-scale dual-purpose plants. Assuming market-readiness of the ITM separation technology, standard (without CCS) dual-purpose water production technology could almost directly be applied to the AZEP concept in order to produce zero or low emissions water by thermal desalination. Future work should include detailed economic and environmental studies and numerical optimization in order to determine whether zero or partial emissions AZEP dual-purpose cycles achieve the most gains as compared to non-CCS dual-purpose cycles.

# Chapter 3

# Structural Optimization of Thermal Desalination

## 3.1 Introduction

Industrial-scale thermal desalination technologies involve evaporative processes and in general, are highly energy intensive with high capital and operating costs. As such, since their development in the early and mid-twentieth century, many different technologies have been developed in order to reduce the energy and economic investment associated with thermal desalination.

The main types of industrial-scale thermal desalination, multi-stage flash (MSF) and multi-effect distillation (MED), each have several configurations. For MSF, the most common configurations are once-through (OT), brine mixing, or brine-recirculation (BR) [66]. For MED, the most common configurations are parallel feed, forward-feed (FF), parallel-cross (PC), and backward-feed with or without thermal vapor compression (TVC) [58, 43]. Each of these technologies have performance trade-offs in thermal efficiency, capital costs, operating costs, and reliability. Currently, the most commonly installed technology is the MSF-BR system because of its proven reliability and large capacity [2]. However, MED and MED-TVC are gaining

attention due to higher thermal efficiency and the potential for lower steam supply temperatures [142, 110, 15].

Despite the many existing thermal desalination configurations, alternative configurations could prove to exhibit better performance. Authors have investigated the gain in thermal efficiency, reduction in heat transfer areas, gain in reliability, or reduction in costs, with alternative routings of feed, brine, or distillate and combinations of hardware.

Nafey et al. [138] utilize exergetic and thermoeconomic analyses to develop a hybrid MED-MSF system where brine of an MSF stage is utilized as feed to an MED effect. Nafey et al. cite a reduction in specific cost of water as compared to MSF-BR, FF-MED with feedwater heaters, and PC-MED without feedwater heaters. However, El-Dessouky and Ettouney [67] show that PC-MED with feedwater heaters exhibits a higher performance ratio (PR, ratio of distillate flow rate to input steam flow) for fixed number of effects and operating conditions as compared to FF-MED with feedwater heaters. Therefore, this configuration should have also been considered by Nafey et al. [138] in order to measure the hybrid MED-MSF system against existing configurations.

Sommariva et al. investigate the routing of distillate in MSF systems [164, 162, 163]. Sommariva et al. thermodynamically model and experimentally confirm that extracting distillate from MSF stages leads to higher distillate production. Further, according to Sommariva et al., the extracted distillate can be utilized for secondary processes which informed the addition of a distillate to brine heat exchanger [164] and the possibility of a hybrid MSF-MED scheme where the extracted distillate is utilized to power MED effects [162].

Although Nafey et al. and Sommariva et al. propose alternative configurations than the standard MED or MSF, other alternative configurations could exhibit better performance than their proposed systems. Utilizing systematic methods could aid in finding optimal thermal desalination structures. Numerical optimization methods provide a systematic framework for weighing structural possibilities and can elucidate non-obvious configurations as an optimal structure. A superstructure is a tool which

is primarily utilized in the chemical process industry to aid in the development of this systematic framework. A superstructure depicts hardware and connectivity possibilities and is essentially the set of all possible flowsheets that could be envisioned [42]. The superstructure can then be implemented as a disjunctive or mixed-integer nonlinear program (MINLP) which considers both continuous (operational) and integer (structural) variables for optimization [181]. Integer variables are used to capture possible choices between hardware or flowsheet routings, e.g., the choice of whether or not to include feedwater heaters, the possibility of blending brine with inlet feed, the number of stages or effects, or the type of power plant extraction for providing heat to thermal desalination.

Mussati et al. utilize a numerical approach to the structural optimization of MSF systems [133, 135, 136]. This work is based partially on the work by Scenna [153, 154] who approached the numerical optimization of MSF and MED structures as a heat exchanger network problem. In [133], Mussati et al. present a superstructure (expanded in [135, 136]) for MSF configurations which allows routing possibilities for distillate extraction and feed and recycle streams. A heuristic solving method is utilized for optimization where a simplified, non-rigorous model is solved before solving the full optimization problem. Mussati et al. do not consider the possibility of utilizing other evaporation methods, e.g., boiling, to construct an optimal thermal desalination configuration.

Herein, a superstructure is developed to explore alternative thermal desalination configurations. This superstructure encompasses existing configurations, i.e., MSF and MED standard configurations, and the possibility for new connectivity with the goal to achieve to better performance than standard configurations. Better performance is measured by the objective that the ideal thermal desalination configuration would exhibit a minimum steam supply flow and temperature for a given distillate output, a minimum specific heat transfer area, a maximum seawater recovery, and a low risk for scaling. The superstructure herein can also be employed in conjunction with structural optimization of hybrid or dual-purpose facilities.

The superstructure developed herein is generated manually, as opposed to an automatic method which generates connectivity possibilities during optimization [176]. The connectivity of the thermal desalination configuration is governed by several Boolean constraints for mostly fixed basic components with many stream connectivity possibilities. Therefore, it should be noted that the structural optimization of thermal desalination lends itself to being expressed as a non-linear generalized disjunctive program (GDP). A GDP utilizes Boolean constraints as well as continuous and integer variable constraints [84]. Non-linear GDP problems can be reformulated as MINLPs. However, it has been shown that global optimization of non-convex, non-linear GDP problems can be better solved by specialized algorithms as opposed to global solvers for their non-convex MINLP reformulations [112].

In the following discussion, a general framework for the superstructure is developed under the pretense that industrial-scale thermal desalination systems share similar physical processes. The proposed superstructure depicts the possible connections between these processes, as well as extraction or mixing of feedwater, brine, and distillate. The connectivity possibilities of the resulting superstructure are demonstrated in terms of the standard configurations which can be expressed by the superstructure. Further, case studies of non-standard thermal desalination configurations are given as an exploration of viable configuration alternatives and as a precursor to numerical optimization.

## 3.2 Thermal Desalination by Physical Processes

The following section describes existing industrial-scale thermal desalination processes in terms of their physical processes (neglecting losses). Thermodynamic models are then presented for these physical processes. Simple First Law models are shown; however, more detailed models could be utilized for greater accuracy, e.g., considering pressure drops (to calculate pumping requirements), non-constant heat transfer coefficients, or non-constant physical properties. However, more detailed models would likely increase difficulty of numerical optimization.

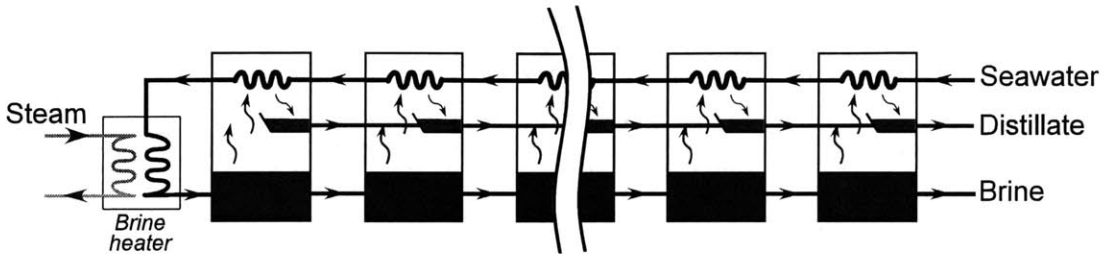


**Figure 3-1:** Once-through multi-stage flash (MSF).

This discussion motivates a framework for thermodynamically modeling thermal desalination from a systematic, structural viewpoint. The general approach to identifying these physical processes is to view a single stage/effect of thermal desalination as a collection of control volumes, e.g., a flashing process or preheating. This control volume perspective has been utilized by authors to develop thermal desalination models [23, 164, 136]. Herein, this approach elucidates the processes which are common between existing thermal desalination technologies; further, it is shown that the connectivity of these physical processes, i.e., material and energy streams, define a particular thermal desalination technology and will be utilized to develop the thermal desalination superstructure.

### 3.2.1 Multi-Stage Flash by Physical Processes

Multi-stage flash (MSF) involves flashing of seawater in order to generate water vapor. The once-through (OT) MSF configuration is shown in Figure 3-1. In the first stage, the feed seawater is heated and then flashed. The remaining brine is flashed in subsequent stages at progressively lower pressures. The vapor generated in each stage is condensed, and its enthalpy of vaporization is used to preheat incoming feedwater. The distillate is directed from stage to stage along trays; when the distillate reaches a lower pressure, part of the distillate flashes again and generates more vapor. Heating steam from a power plant or stand-alone boiler is used to raise the feedwater in the first stage to the top brine temperature (TBT, typically 90-120°C, which is limited by $CaSO_4$ solubility [89]).

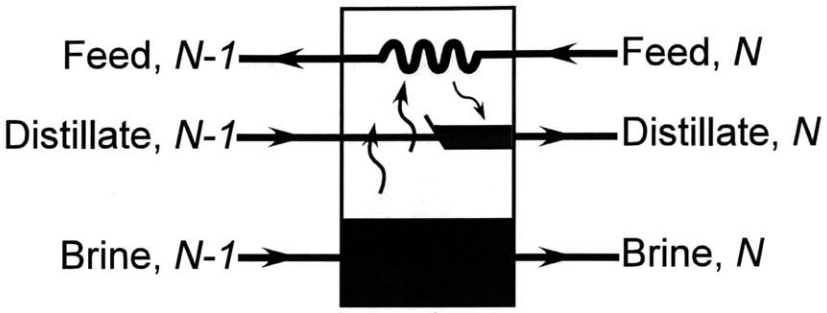


(a) Mechanical construct of MSF Stage $N$

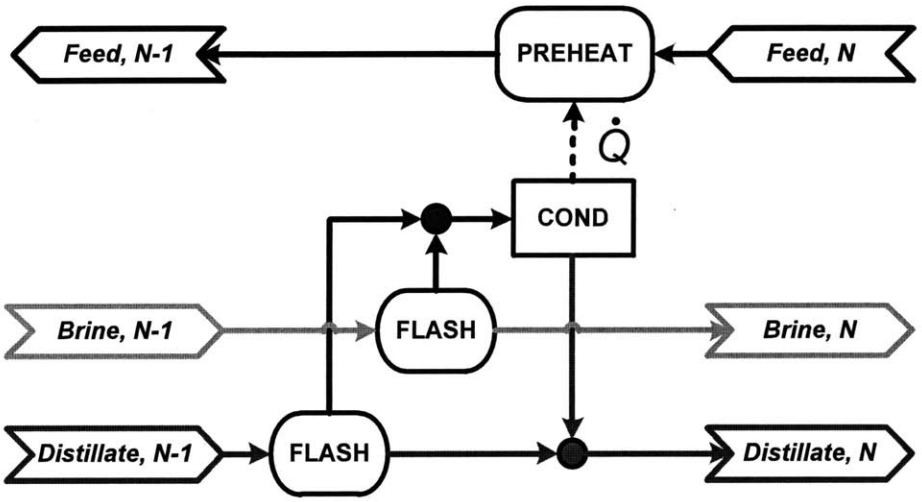


(b) Physical processes and connectivity of MSF Stage $N$

**Figure 3-2:** Single stage of MSF with depiction of physical processes.

Alternate configurations of MSF include brine-mixing and brine-recirculating (BR) [135, 75]. These configurations are meant to increase the feed recovery of the system as compared to once-through MSF for fixed distillate output. Increasing the recovery of the system decreases the operating costs associated with seawater pretreatment [67]. The recirculation flow rates of brine-mixing and brine-recirculating MSF are chosen based on a maximum brine salinity to avoid scaling. The performance of MSF-BR is less sensitive to changes in seawater temperature as compared to MSF-OT or MSF-mixing due to the presence of a cooling water stream [95].

As its name suggests, MSF consists of multiple stages; the same process configuration is repeated, but at different operating conditions. Figure 3-2(a) shows a general stage $N$ of MSF. Figure 3-2(b) shows stage $N$ by its physical processes with respect

to energy and mass balance. Brine and distillate are directed from the previous stage (stage *N-1*); part of each stream flashes due to reduced pressure upon entering the stage. The generated vapor condenses (block "COND", referring to condensation, in Figure 3-2(b)), and its enthalpy of vaporization raises the temperature of the inlet feed. The condensed distillate is mixed with distillate from the previous stage. In the case of the first stage, there is no incoming distillate. The incoming brine of the first stage is its outlet feed which has been further heated by an external steam source. Therefore, the main physical processes in MSF are evaporation by flashing, preheat, condensation, and mixing [23].

### 3.2.2 Multi-Effect Distillation by Physical Processes

Multi-effect distillation (MED) involves the boiling, specifically film boiling, of seawater in order to generate water vapor. The parallel feed MED configuration is shown in Figure 3-3. In the first effect, steam from an external source is condensed inside of tubes. Feedwater is sprayed on the tubes and vapor is generated. The vapor is then condensed inside the tubes of the next effect and more vapor is generated at a lower pressure. The TBT of MED is typically limited to $\approx 65-70°C$ in order to avoid scaling in the evaporators [110] and the steam temperature is $\approx 5-10°C$ higher.

In the parallel feed configuration (PF-MED), the total feed is split almost equally among the effects based on a maximum allowable salinity. An alternate form of this feed routing is the parallel-cross (PC) MED configuration. In PC-MED, the brine from an effect is allowed to flash to the operating conditions of the next effect, thereby generating more vapor. Other MED configurations exist which route the feed differently. The forward-feed (FF) MED configuration directs the total feed to the first effect. Then, the brine from each effect is directed as feed to the subsequent effect. In FF-MED, the maximum salinity occurs in the last effect. Another configuration is the backward-feed MED, where the brine from an effect is used as feed for the previous effect. In this configuration, the maximum salinity occurs in the first effect.

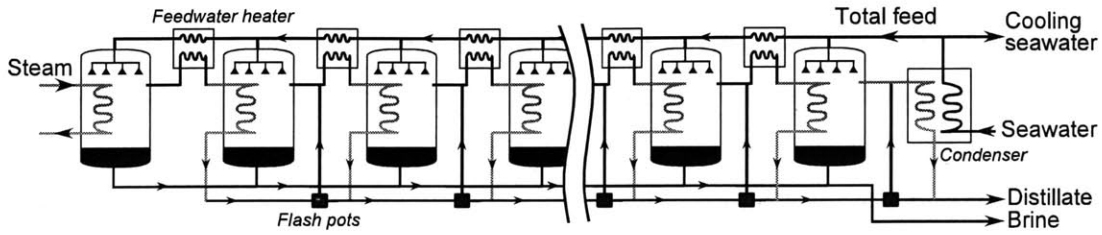


**Figure 3-3:** Parallel feed multi-effect distillation (PF-MED).

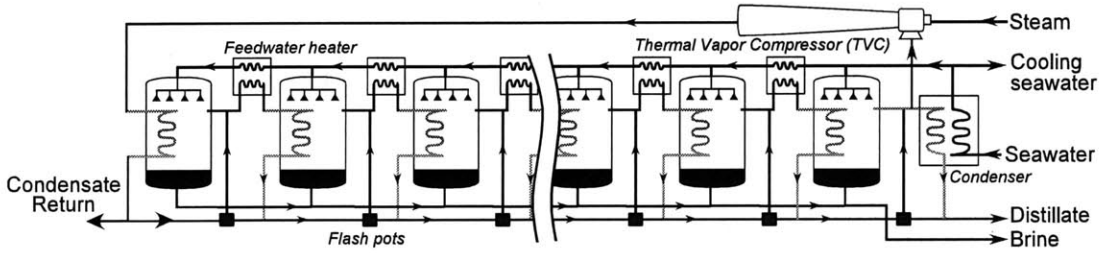


**Figure 3-4:** Parallel feed multi-effect distillation with thermal vapor compression (PF-MED-TVC).

Sometimes thermal vapor compression (TVC) is used with MED. The addition of TVC to MED allows for a higher performance ratio for approximately the same heat transfer surface area. However, a significantly higher steam supply temperature (and pressure) is utilized ($\gtrsim$ 100°C) as compared to MED alone ($\approx$ 75 - 80°C). This difference results in higher lost electricity (per unit mass of steam provided) with an integrated power cycle as compared to MED alone. In MED-TVC, part of the vapor generated in the last effect is compressed and used to power the first effect, as shown in Figure 3-4. TVC can be utilized with any of the MED feed configurations (FF, PF, PC, and BF).

As with MSF, MED consists of a repeating process configuration operating at lower pressures. Figure 3-5(a) shows a general effect $N$ of MED. Figure 3-5(b) shows effect $N$ by its physical processes with respect to energy and mass balance. The main physical processes in MED are evaporation by film boiling, evaporation by flashing, preheat, condensation, and mixing. Water vapor, brine, and distillate are directed from effect *N-1*. The incoming distillate is flashed in a flash pot to meet

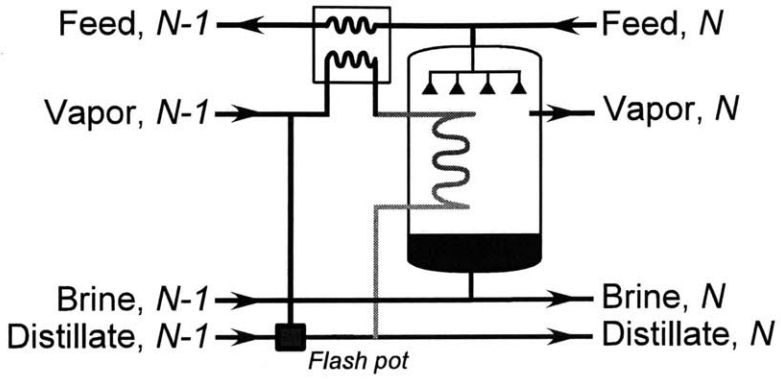


(a) Mechanical construct of PF-MED effect $N$

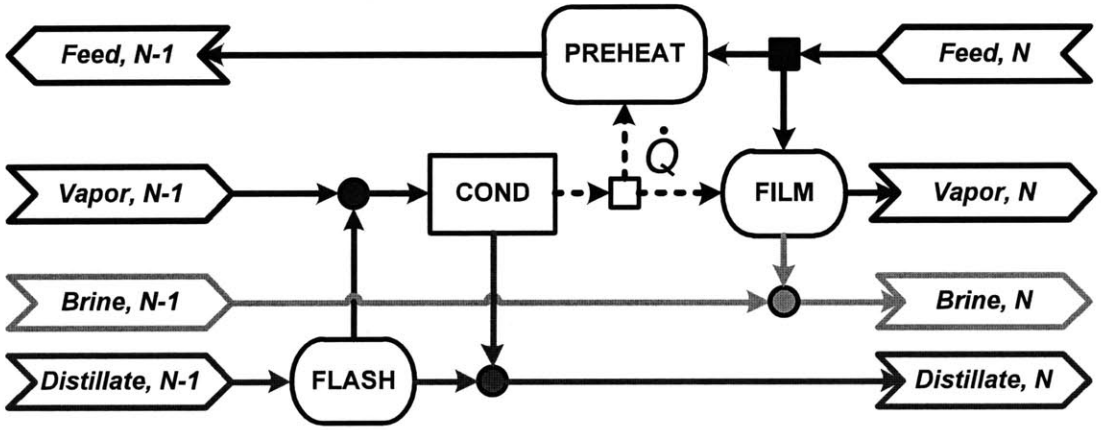


(b) Physical processes and connectivity of PF-MED effect $N$

**Figure 3-5:** Single effect of PF-MED with depiction of physical processes.

the lower pressure of effect *N*. A small amount of vapor is generated and mixed with the incoming vapor from effect *N-1*. The vapor is condensed; part of its enthalpy of vaporization is used to raise the temperature of the feedwater going to effect *N-1* and the rest is used to boil more vapor from the feedwater. It is important to note that flashing the distillate indirectly generates more vapor from brine by utilizing the distillate's enthalpy of vaporization which otherwise would have been extracted from the series of evaporation processes. The resulting brine is mixed with the brine from effect *N-1*.

The first effect of MED is powered by steam condensing from an external source such as a power plant. However, when MED-TVC is used, a mixture of external steam and vapor generated by the last effect is condensed. As such, the MED-TVC

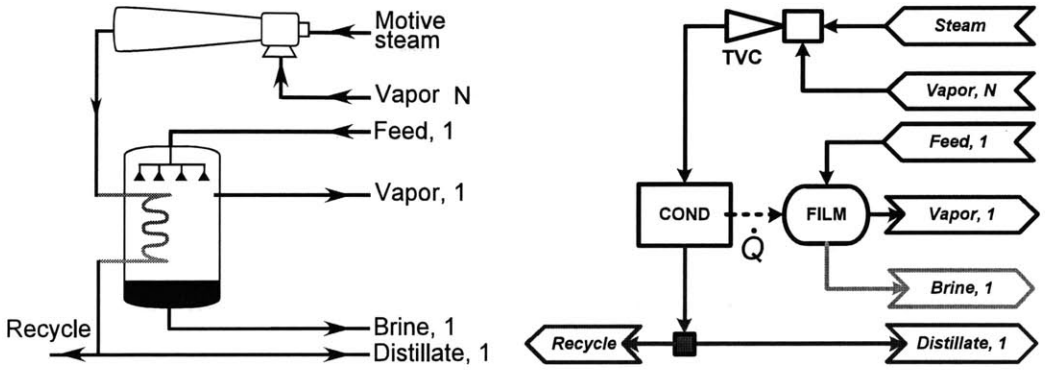


(a) Mechanical construct of first effect of MED-TVC

(b) Physical processes and connectivity of first effect of MED-TVC

**Figure 3-6:** First effect of MED-TVC with depiction of physical processes.

first effect configuration, i.e., the interface with the power plant, differs as compared to MED alone (which is simply direct condensation of the supplied steam in the tubes of the first effect). Figure 3-6(a) shows the first effect of MED-TVC.

### 3.2.3 Thermodynamic Modeling of Physical Processes

As shown in Figures 3-2(b), 3-5(b) and 3-6(b), thermal desalination plants can be decomposed into physical processes; in order to represent a specific technology, material and energy streams can be connected in various ways. In this section, First Law models of evaporation by flashing, evaporation by film boiling, condensation, preheat, mixing, and thermal vapor compression are presented. These are common processes considered in literature [31, 59, 58, 127, 70, 169]. Additional considerations could include the effect of demisters, non-condensable gases, de-superheaters, fouling resistances, and/or non-equilibrium allowances [76, 65, 151, 152, 26]. However, their calculation requires detailed knowledge of process configuration and geometry. These considerations could be included in conjunction with the analysis herein, but would require iteration with regards to numerical computation.

Simplified physical properties are utilized in these models. The purpose of these models is to estimate the dependence of thermal desalination plant performance based on its structure, therefore extremely accurate physical properties are not necessary.

However, more accurate models could be utilized within this framework. Constant enthalpy of vaporization and specific heat capacity are assumed as 2300 kJ/kg and 4 kJ/(kg K), respectively. The effect of pressure is neglected in the calculation of enthalpy; therefore, $\Delta h = c_p \Delta T$. These assumptions are common in thermal desalination modeling literature [59, 67, 165]. A common assumption in literature is a constant temperature loss to account for boiling point elevation (BPE). However, herein, the BPE is accounted for by empirical correlations (discussed later) of sensitivity of heat transfer area calculations with respect to the accuracy of BPE calculation [127]. In process models which interface with external steam supply (first effect condenser and TVC), the 1997 IAPWS Industrial Formulation for pure water [103] is utilized to capture the effect of steam supply pressure. The purpose of utilizing this formulation is to coincide with typical power production modeling where the use of IAPWS properties is customary (though it is not essential for the purposes herein). Physical property formulations which are less exact (and less computationally expensive) than the IAPWS formulation could be utilized, e.g., steam as an ideal gas and liquid water as an incompressible liquid, without substantial loss of accuracy. The working fluids involved in thermal desalination include pure water (distillate), water vapor, and water containing dissolved salts (brine and feedwater). It is assumed that water vapor, and hence, distillate is also salt-free. The effect of non-condensable gases are neglected herein.

Evaporation of water is the main goal of thermal desalination and can occur by flashing or film boiling. In the case of flashing, there is no heat input; the change in enthalpy of the feed is equal to the enthalpy of vaporization gained by the vapor. In the case of film boiling, evaporation is mainly due to heat input. Therefore, based on the physical property assumptions made herein, the energy balance of evaporation is given by

$$\dot{Q} = \dot{m}_i c_p (T_b - T_i) + \dot{m}_v \Delta h_{fg} \tag{3.1}$$

where $\dot{m}_i$ is the inlet mass flow rate, $T_i$ is the inlet temperature, $\dot{m}_v$ is the mass flow rate of the produced vapor, $T_b$ is the temperature of the brine, $\Delta h_{fg}$ is the enthalpy

of vaporization of the seawater, and $c_p$ is the specific heat capacity. In the case of flashing, $\dot{Q} = 0$. The mass balance is given by $\dot{m}_i = \dot{m}_b + \dot{m}_v$. It should be noted that in the case of film boiling, if $T_i > T_b$, or more precisely $P_{i,sat} > P_{b,sat}$, then part of the formed vapor is generated by flashing [59].

The heat transfer area required for film boiling is given by

$$A = \frac{\dot{Q}}{U(T_q - T_b)} \tag{3.2}$$

where $T_q$ is the temperature of the heat input, U is the overall heat transfer coefficient, and A is the heat transfer area. In this work, the overall heat transfer coefficient is taken as a constant 3 kW/(m$^2$K) [59]. Taking the overall heat transfer coefficient as constant limits the accuracy of heat transfer area calculations. However, since the overall structure is the main consideration herein (which influences the possible operating temperatures of the plant and thus, the $T_q - T_{b,ev}$ term of equation (3.2)), this loss of accuracy is acceptable for a gain in computational simplicity. Considering the possible tube geometries and flow velocities associated with the boiling process would be needed in order to accurately model a non-constant overall heat transfer coefficient.

The temperature of the vapor in both flashing and film boiling is

$$T_v = T_b - BPE(T, X) \tag{3.3}$$

where BPE is the boiling point elevation of the brine. The BPE is calculated by correlations provided by [158] as a function of temperature and salinity:

$$BPE = A\left(X \times 10^{-3}\right)^2 + B\left(X \times 10^{-3}\right)$$

$$A = \left(-4.585 \times 10^{-4}\right) T^2 + \left(2.823 \times 10^{-1}\right) T + 17.65$$

$$B = \left(1.536 \times 10^{-4}\right) T^2 + \left(5.267 \times 10^{-2}\right) T + 6.56$$

The BPE calculations are valid for $0 < T < 200°C$ and $0 < X < 120$ $g/kg_{seawater}$ to an accuracy of $\pm 0.018°C$.

Since the generated vapor of the evaporation processes is considered salt-free, species balance for both flash and film boiling is simply given by

$$\dot{m}_b X_b = \dot{m}_i X_i$$

where $X_b$ and $X_i$ are the salinities of the brine and feed, respectively.

Condensation of water vapor is associated with a heat output which is related to its enthalpy of vaporization. It is assumed that inlet water vapor is a saturated vapor and outlet distillate is a saturated liquid. Further, it is assumed that there is no pressure drop and the condensation process occurs at the saturation temperature of the inlet water vapor. Therefore, energy balance of the condensation process is simply given by

$$\dot{Q} = \dot{m}\Delta h_{fg}$$

Preheat of feedwater is modeled herein as a one-sided heat exchanger with a heat input. Assuming that the inlet seawater is always increasing in temperature, the energy balance of preheating based on the physical property assumptions is given by

$$\dot{Q} = \dot{m}c_p (T_o - T_i)$$

In order to estimate the heat transfer area, the $\epsilon$-NTU method is utilized [102] where a constant overall heat transfer coefficient of 2.4 $kW/(m^2K)$ is assumed [58]. Also, it is assumed that the heat input is produced by a two-phase process (condensation) which is a constant temperature.

The mass, energy (based on physical property assumptions), and species balance of mixing are as follows

$$\dot{m}_o = \sum_{j=1}^{n} \dot{m}_j \tag{3.4a}$$

$$\dot{m}_o T_o = \sum_{j=1}^{n} \dot{m}_j T_j \tag{3.4b}$$

$$\dot{m}_o X_o = \sum_{j=1}^{n} \dot{m}_j X_j \tag{3.4c}$$

where n is the number of inlet streams. This combination of equations is referred to hereafter as "MIX" where its arguments are the input streams to be mixed.

Thermal vapor compression uses high pressure steam to entrain a low pressure vapor. TVC involves a nozzle, mixer, and diffuser with supersonic flows [100]. The mass balance of the TVC is given by

$$\dot{m}_e + \dot{m}_m = \dot{m}_{di} \tag{3.5}$$

where subscript "e" is the entrained stream, subscript "m" is the motive stream, and subscript "di" is the discharged stream. The ratio of mass flowrate of motive steam to entrained vapor, i.e., the entrainment ratio, is dependent on the design of the TVC. In order to estimate the TVC performance, the following correlation is utilized [69]:

$$ER = \frac{\dot{m}_m}{\dot{m}_e} = 0.296 \frac{(P_{di})^{1.19}}{(P_e)^{1.04}} \left(\frac{P_m}{P_e}\right)^{0.015} \left(\frac{3 \times 10^{-7} (P_m)^2 - 0.0009 (P_m) + 1.6101}{2 \times 10^{-8} (T_e)^2 - 0.0006 (T_e) + 1.0047}\right) \tag{3.6}$$

The discharged stream is at a intermediate pressure as compared to the motive and entrained streams which is typically chosen by the compression ratio (CR), i.e., the ratio of discharge pressure to entrained pressure. Finally, assuming an adiabatic process, the energy balance is given by

$$\dot{m}_{di} h_{di} = \dot{m}_e h_e + \dot{m}_m h_m \tag{3.7}$$

As noted earlier, the TVC process interfaces with power plant steam supply and therefore, non-simplified physical properties are used.

## 3.3 Thermal Desalination Superstructure

This section presents a thermal desalination superstructure and its mathematical formulation. The flexible structure can be used for thermal desalination plant simulation and structural optimization. The superstructure consists of three main components: the evaporation unit, the steam supply interface, and the down condensing unit. The steam supply interface serves to condense steam from a power plant or other steam source in order to power evaporation. The evaporation units direct incoming seawater to evaporate by film boiling or flashing through various connectivity possibilities. The down condensing unit is necessary based on the structural development of the evaporation unit.

The concept of an MED effect or MSF stage is generalized herein as an evaporation unit. More specifically, the evaporation unit of the superstructure encompasses the physical construct of an MED effect and MSF stage, but also other possibilities, some of which will be highlighted.

### 3.3.1 Evaporation Unit and Down Condensing Unit

The evaporation unit, referred to hereafter as "Unit N", is shown in Figure 3-7. This structure depicts the flow and process possibilities which comprise the generation of vapor for arbitrary operation conditions. A set of binary variables specifies the flow configuration of Unit N. Unit N captures the choice of evaporation method and feed configuration. In addition, vapor, feed, brine, and distillate extraction as well as feed, brine, and distillate mixing are possibilities. This structure allows the flexibility to use different configurations for different units, unlike traditional MED or MSF plants, which typically repeat the same effect or stage configuration at different operating conditions.

**Table 3.1:** Superstructure stream types, associated variables, and figure keys.

| Stream type | Flow type | Variables | Key |
|---|---|---|---|
| Feed | Mass | T, X | |
| Brine | Mass | T, X | |
| Water vapor | Mass | T | |
| Distillate | Mass | T | |
| Heat | Energy | T | |

Unit N consists of feed seawater, brine, distillate, water vapor, and heat streams. The associated variables of each stream type are shown in Table 3.1. Unit N is comprised of inlet and outlet streams which are meant for units to be connected in series and are denoted by subscript "i" for inlet and subscript "o" for outlet. For example, the inlet brine, distillate, and heat streams to unit N are the outlet brine, distillate and heat streams from unit (N-1). Feed extraction ("*FE*"), feed mixing ("*FM*"), brine extraction ("*BE*"), brine mixing ("*BM*"), distillate extraction ("*DE*"), distillate mixing ("*DM*"), and vapor extraction ("*V*") streams are not necessarily connected between effects in series and will be described in more detail later.

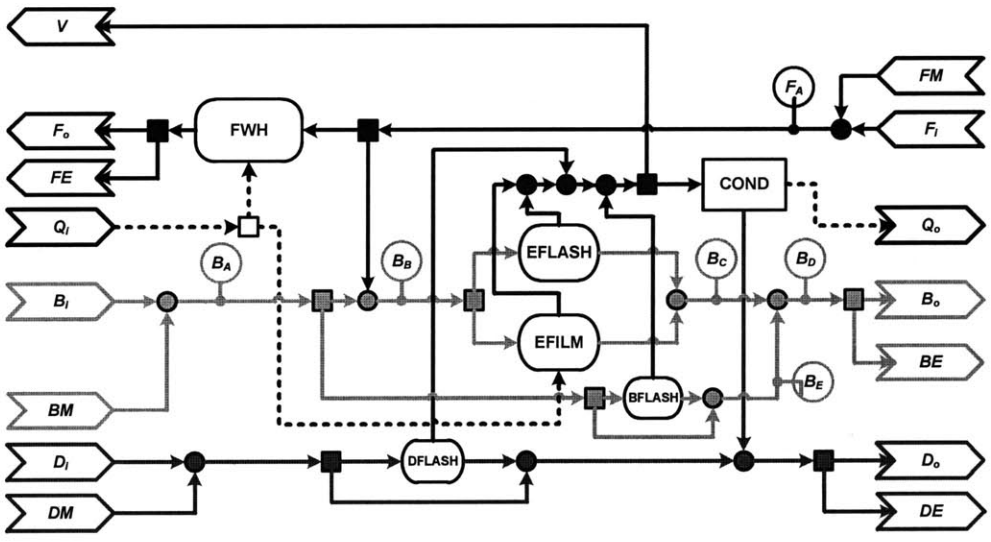


**Figure 3-7:** Thermal desalination structure: Evaporation unit, Unit N.

Physical processes include feedwater preheating (block "FWH" in Figure 3-7), condensation (block "COND"), evaporation from brine/seawater by flashing (block "EFLASH") or film boiling (block "EFILM"), evaporation from distillate (block "DFLASH"), and additional brine flashing (block "BFLASH"), as described in Section 3.2.3.

The choice of evaporation process is given by the binary variable $\xi_{ev}$ where $\xi_{ev} = 1$ denotes the use of film boiling evaporation and $\xi_{ev} = 0$ denotes the use of flash evaporation. The subscript "ev" denotes a variable associated with the evaporation process, whether it by flashing or film boiling. The material flow to and from evaporation process is stream $B_B$ and $B_C$ in Figure 3-7, respectively, where

$$\dot{m}_{i,ev} = \dot{m}_{B_B}, \quad T_{i,ev} = T_{B_B}, \quad X_{i,ev} = X_{B_B}$$
$$\dot{m}_{b,ev} = \dot{m}_{B_C}, \quad T_{b,ev} = T_{B_C}, \quad X_{b,ev} = X_{B_C}$$

The value of $\xi_{ev}$ describes the following cases:

$$\text{IF} \quad \xi_{ev} = 1 \quad \text{THEN} \quad \begin{cases} \dot{Q}_{ev} = \lambda_q \dot{Q}_i \\ A_{ev} = \dot{Q}_{ev} \,/\, (U\,(T_q - T_{b,ev})) \end{cases} \quad \textit{(Eqn 3.2)}$$

$$\text{ELSE} \quad \begin{cases} \dot{Q}_{ev} = 0 \\ A_{ev} = 0 \end{cases}$$

where $\lambda_q$ is a fraction from 0 to 1 and is a design variable, and the energy balance of the evaporation process is given by Equation (3.1).

The vapor produced by evaporation is condensed and its enthalpy of vaporization is directed to the next unit. Formulating the superstructure in this way allows for greater flexibility of configurations. For traditional MED effects, the vapor is condensed on the inside of tubes, but in traditional MSF stages, the vapor is condensed on the outside of tubes. These processes result in different heat transfer coefficients, but energetically, they are equivalent under the assumption of neglecting losses. Therefore, representing the enthalpy of condensation as a heat stream which can be split

between either feedwater preheating or film boiling in the next unit decouples the processes from its common physical construct of an MED effect or MSF stage and creates new configuration possibilities. For example, a flash process whose resulting heat stream is input directly to film boiling implies a different physical construct than a traditional MSF stage, i.e., its vapor would be condensed on the inside of tubes as opposed to the outside. More detailed models could capture the difference in heat transfer coefficient but is not considered herein.

Considering these possibilities, the choice of evaporation process in a given unit does constrain how incoming heat stream $Q_i$ can be utilized. If flash evaporation is chosen ($\xi_{ev} = 0$) then all of $Q_i$ must be utilized in the feedwater heater (block "FWH") since flash evaporation is adiabatic. If film boiling is chosen ($\xi_{ev} = 1$), then part or none of stream $Q_i$ can be used in the feedwater heater, e.g., none of $Q_i$ would go to the feedwater heater ($\lambda_q$=1) if the change in feedwater temperature is set to zero.

The choice of feed configuration is given by the binary variable $\xi_f$ where $\xi_f = 1$ denotes directing the brine from the previous unit as the input to evaporation and $\xi_f = 0$ denotes using a portion of the feed stream as input to evaporation. The feed configuration is described by the following cases:

$$\text{IF} \quad \xi_f = 1 \quad \text{THEN} \quad \begin{cases} B_B = B_A \\ B_D = B_C \end{cases}$$

$$\text{ELSE} \quad \begin{cases} \dot{m}_{B_B} = \lambda_f \dot{m}_{F_A}, \; T_{B_B} = T_{F_A}, \; X_{B_B} = X_{F_A} \\ B_D = \text{MIX}(B_C, \; B_E) \end{cases} \quad \textit{(Eqn 3.4)}$$

where $\lambda_f$ is a fraction from 0 to 1 and is a design variable.

When $\xi_f = 0$ and the saturation temperature of stream $B_A$ is greater than the saturation temperature of $B_C$, additional vapor can be generated by letting stream $B_A$ flash to the operating pressure of the main evaporation process. However, it could be desired that this stream is not allowed to flash in order to reduce pumping requirements. These options constitute the difference between the MED parallel-cross

and parallel configurations [67]. This choice of brine flashing is given by the binary variable $\xi_{\text{BFL}}$ where $\xi_{\text{BFL}} = 1$ denotes brine flashing when $\xi_{\text{f}} = 0$. The vapor formed by brine flashing is given by Equation 3.1 where the temperature of the flashed brine is equal to the temperature of stream $B_C$ and $\dot{Q} = 0$. If $\xi_{\text{BFL}} = 0$, then stream $B_E$ is equal to stream $B_A$.

Additional flashing of distillate typically occurs in both MED and MSF due to decreasing saturation pressures along the effects. However, in some cases, not allowing this flashing to occur could reduce heat transfer areas and decrease pretreatment costs [135, 162, 163]. This possibility is captured by the design variable $\lambda_d$ which indicates the fraction of mass flow $D_i$ which is to be routed around block "DFLASH", i.e., $\lambda_d = 1$ indicates no distillate is allowed to flash. The amount of vapor produced in "DFLASH" is given by Equation 3.1 where $\dot{Q} = 0$ and the temperature of the outlet streams (salt-free saturated liquid and vapor) is equal to the vapor temperature of the evaporation process given by Equation 3.3.

The remaining evaporation unit configuration choices involve the extraction and mixing of brine, feed, and distillate streams between units. The mixing or extraction of brine, feed, or distillate could improve performance, e.g., reduce heat transfer surface areas or increased recovery. These streams are meant to be connected across the thermal desalination plant, e.g., stream $BE$ in unit 2 could be set equal to stream $FM$ in unit 8. For a given unit, the extraction and mixing connectivity is given by the binary variables $\xi_{\text{FM}}$, $\xi_{\text{BM}}$, $\xi_{\text{DM}}$, $\xi_{\text{FE}}$, $\xi_{\text{BE}}$, and $\xi_{\text{DE}}$. If set equal to zero, these denote the presence of feed mixing, brine mixing, distillate mixing, feed extraction, brine extraction, and distillate extraction, respectively. For the extraction streams, the fraction of the incoming stream to extract is a design variable given by $\lambda_{\text{FE}}$, $\lambda_{\text{BE}}$, and $\lambda_{\text{DE}}$. The extraction of vapor, stream $V$, is associated with the presence of TVC and will be explained in the next section.

The down condensing unit is shown in Figure 3-8. This unit is used when the enthalpy of vaporization of the previous unit is not used to continue more evaporation, i.e., all of the enthalpy of vaporization from condensation is directed to increasing the temperature of feedwater with no additional vapor generation. For example, the

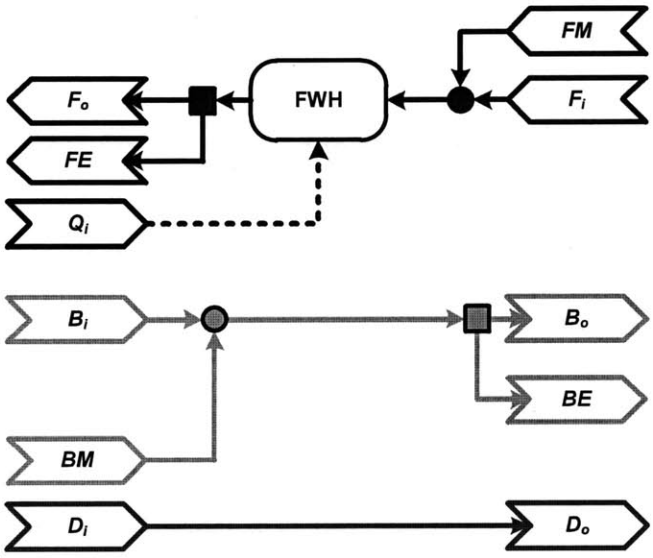


**Figure 3-8:** Thermal desalination structure: down condensing unit.

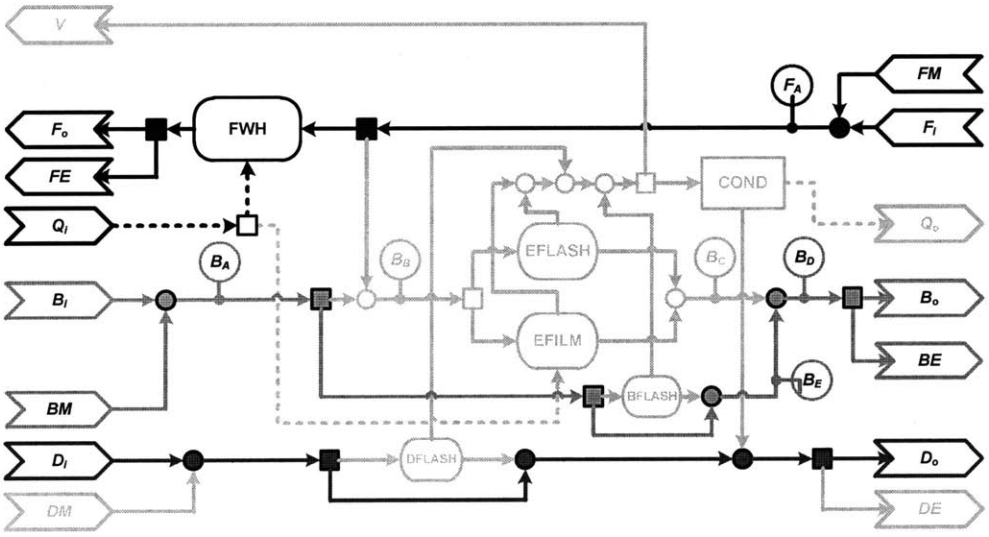


**Figure 3-9:** Down condensing unit as a subset of evaporation unit.

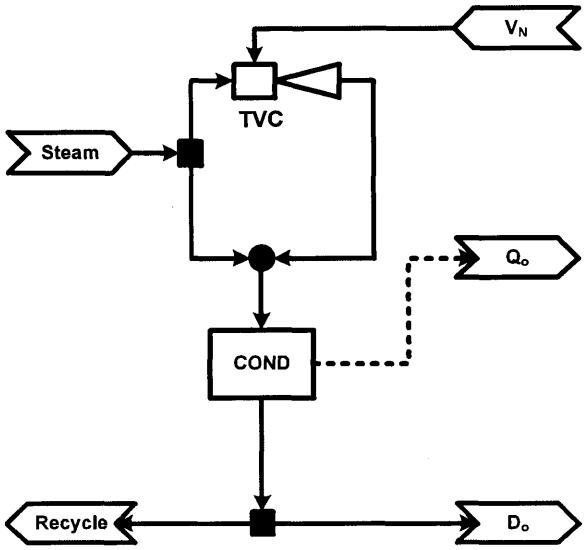


**Figure 3-10:** Thermal desalination structure: Steam supply interface, Unit 0.

vapor generated in the last effect of MED is condensed in an additional condenser where the cold side flow rate is the total feed and cooling flow. The down condensing unit captures this example and also allows for additional configuration possibilities, such as the brine mixing of MSF-BR (discussed in more detail later).

The down condensing unit is in fact a subset of the evaporation unit (shown in Figure 3-9), but is shown herein for simplified representation; in terms of the evaporation unit, the down condenser is represented by diverting brine around the evaporation process ($\xi_f = 0$) and additional brine flashing ($\xi_{BFL} = 0$). Further, the portion of stream $F_A$ to evaporation is set to zero ($\lambda_f = 0$) and distillate is not allowed to flash ($\lambda_d = 1$).

### 3.3.2 Steam Supply Interface

Figure 3-10 shows the steam supply interface, referred to hereafter as "Unit 0". This structure allows the choice of using steam (typically from a power plant in extraction or back-pressure turbine) to directly condense in block "COND" or to serve as motive steam in block "TVC". Multiple Unit 0 blocks can be utilized in parallel to supply steam to different sections of units in series. The total steam from

a coupled power plant could be split among several steam supply interfaces, thereby creating the possibility for parallel operation of units and/or multiple TVCs. Unit 0 is meant to connect to a unit in series.

The configuration of unit 0 is given by the binary variable $\xi_s$ where $\xi_s = 1$ denotes that the power plant steam is directly condensed in block "COND" and $\xi_s = 0$ denotes the use of TVC. As mentioned in Section 3.2.3, IAPWS steam properties are utilized in unit 0. The configuration of unit 0 is described by the following cases:

$$\text{IF} \quad \xi_s = 1 \quad \text{THEN} \quad \begin{cases} \dot{m}_s = \dot{m}_{i,c} \\ T_s = T_{i,c}, \; h_s = h_{i,c} \\ \dot{m}_e = 0 \end{cases}$$

$$\text{ELSE} \quad \begin{cases} \dot{m}_s = \dot{m}_m, \; \dot{m}_{di} = \dot{m}_{i,c} & \textit{(Eqn 3.5)} \\ T_s = T_m, \; h_s = h_m, \; T_{di} = T_{i,c}, \; h_{di} = h_{i,c} & \textit{(Eqn 3.7)} \\ \dot{m}_e = f(\dot{m}_m, \; P_m, \; P_{di}, \; P_e, \; T_e) & \textit{(Eqn 3.6)} \end{cases}$$

where subscript "s" denotes the steam from the power plant, subscript "i,c" denotes the inlet of the block "COND", subscript "e" denotes the entrained vapor to TVC or stream $V_N$, subscript "m" denotes the motive steam to TVC, and subscript "di" denotes the discharged stream of TVC.

The entrained vapor of TVC, stream $V_N$, is directed from a chosen unit, i.e., stream $V$. Therefore, if TVC is active ($\xi_s = 0$) then the flow of $V$ is given by the entrainment ratio (Equation 3.6) and the state of the stream is given by that effect's vapor saturation temperature. Otherwise, the flow of $V$ within that effect is zero. The flow of stream $D_N$ is simply equal to the flow rate of entrained vapor and the flow of "Recycle" is equal to the flow of power plant steam.

### 3.3.3 Configuration Examples

The following gives examples of existing thermal desalination configurations and shows their configuration as a subset of the thermal desalination superstructure. Examples of once-through MSF, brine-recirculating MSF, parallel-feed MED, backward-feed MED, and a hybrid MED-MSF configuration by [138] are given for comparison to the process configurations shown in Sections 3.2.1 and 3.2.2 and to demonstrate the structural flexibility provided by the proposed thermal desalination superstructure.

Figure 3-11 shows a stage of once-through MSF as depicted within unit N. Here, evaporation by flashing is active ($\xi_{ev} = 0$) with brine from the previous stage routed as feed ($\xi_f = 1$). Note that all $Q_i$ from unit (N-1) is directed to preheating the feedwater. No feed or brine extraction/mixing is utilized.

However, in the case of MSF with brine recirculation, the same unit configuration is used, but feed extraction and brine mixing is active in some stages. Figure 3-12 shows the heat recovery section of a twenty-four stage plant where the heat rejection section comprises the last three stages. The configuration within each stage is the same as in Figure 3-11.

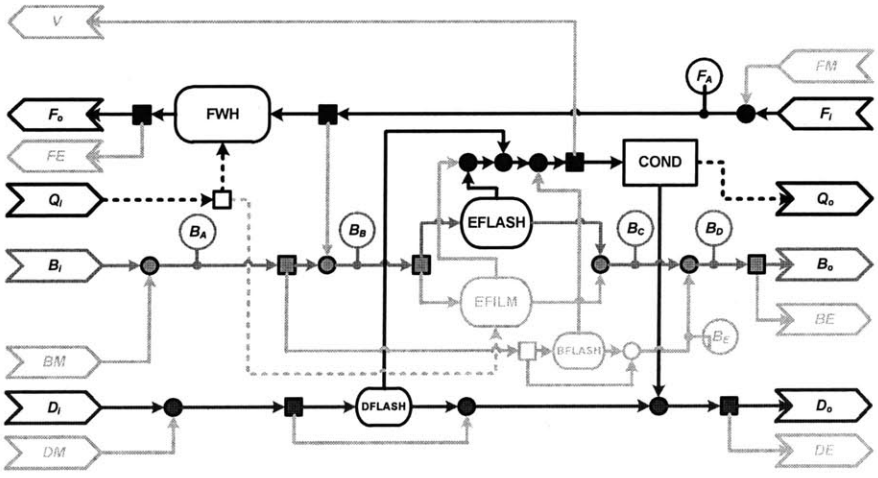


**Figure 3-11:** Example connectivity of unit N: a stage of once-through MSF.

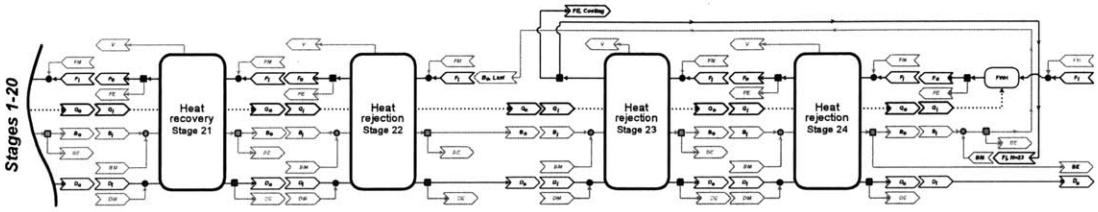


**Figure 3-12:** Example connectivity: Heat rejection section of brine-recirculating MSF.

In the last stage, part of the stream $F_o$ from Stage 23 is mixed with Stream $B_M$. Part of the resulting stream $B_o$ is then connected to stream $F_i$ in Stage 22. The enthlapy of vaporization from condensation in Stage 21 preheats the new feed of Stage 22.

Figure 3-13 shows effects 1 and 2 of parallel-feed MED. Unit 0 is connected in series with unit 1 and 2. For unit 1 and 2, evaporation by film boiling is active ($\xi_{ev} = 1$), the feed is a part of the total feed stream ($\xi_f = 0$), and brine flashing is not allowed ($\xi_{BFL} = 0$). No mixing or extraction is utilized. In unit 0, steam from the power plant is used for direct condensation ($\xi_s = 1$). In unit 1, $\lambda_f = 1$ and no flow goes through the feedwater heater and subsequently, all of $Q_o$ of unit 0 is directed to unit 1 evaporation. In the other units, the value of $\lambda_f$ can vary; typically, the flow to each effect is set to nearly equal and $\lambda_{f,i} \approx 1/i$ where i is the effect number. $\lambda_f$ can also be set such that the brine salinity of stream $B_C$ is at the maximum salinity which avoids scaling [58].

For comparison to the parallel feed MED case, the backward-feed MED configuration is shown in Figure 3-14. The brine of a given effect is directed as feed to the

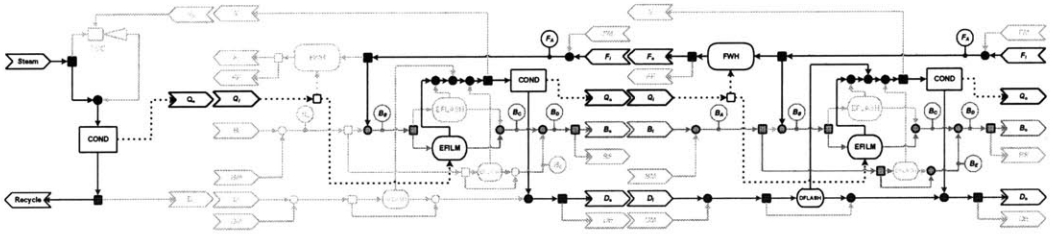


**Figure 3-13:** Example connectivity of unit N and unit 0: Effect 1 and 2 of MED parallel configuration.

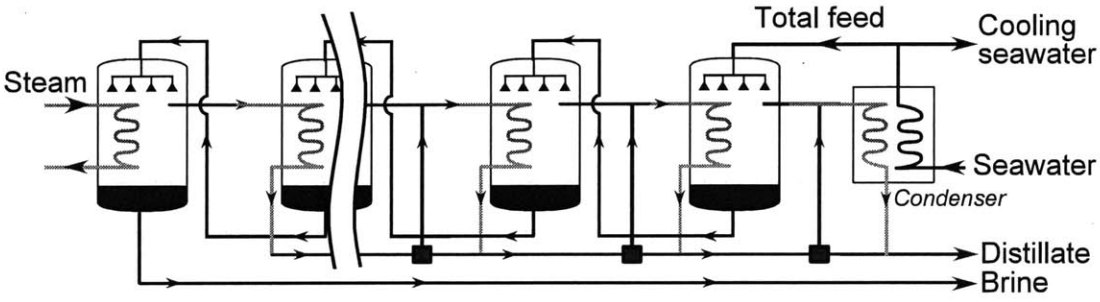


**Figure 3-14:** Backward-feed MED configuration.

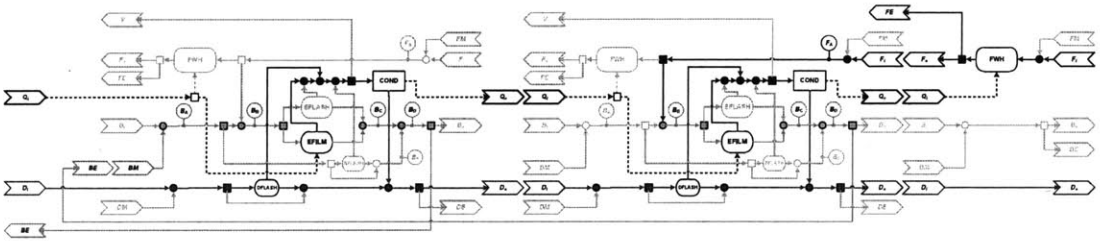

**Figure 3-15:** Example connectivity: Last two effects of backward MED configuration.

previous effect. Figure 3-15 shows the last two effects of the backward-feed MED configuration in terms of the thermal desalination superstructure. In order to represent this configuration, the brine mixing and extraction streams are utilized. In the last effect, the seawater from the down condenser is directed as feed to the film boiling process ($\xi_f = 0$ with $\lambda_f = 1$). Then, all of the brine from the last effect is extracted ($\xi_{BE} = 0$ with $\lambda_{BE} = 1$) and directed to the brine mixing stream, steam $BM$, of the previous effect.

Figure 3-16 shows the hybrid MED-MSF configuration which is discussed by Nafey et al [138]. The configuration features MSF and MED operating in parallel. Specifically, part of the brine from an MSF stage is used as feed for an MED effect. The resulting brine and distillate from the MED effect is then mixed with the inlet streams to the next MSF stage. Each MED effect is powered by the vapor from the previous MED effect. The motive steam for this configuration is split between a brine heater for the MSF section and the first effect of the MED section.

Figure 3-17 shows the hybrid MED-MSF configuration expressed by superstructure repeating units. This example demonstrates the use of the extraction and mixing possibilities given by the superstructure. It is important to note that the physical construct of the MED effects are described by a combination of two repeating units. In addition to the repeating units shown in Figure 3-17, this configuration utilizes two unit 0 steam supply interfaces operating in parallel in order to provide steam to the MSF and MED sections.

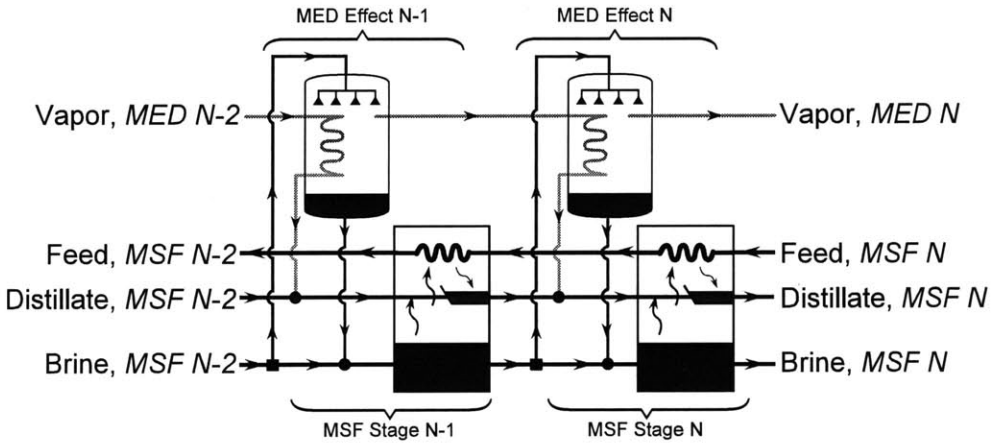


**Figure 3-16:** Evaporation section of hybrid MED-MSF configuration discussed by Nafey et al. [138].

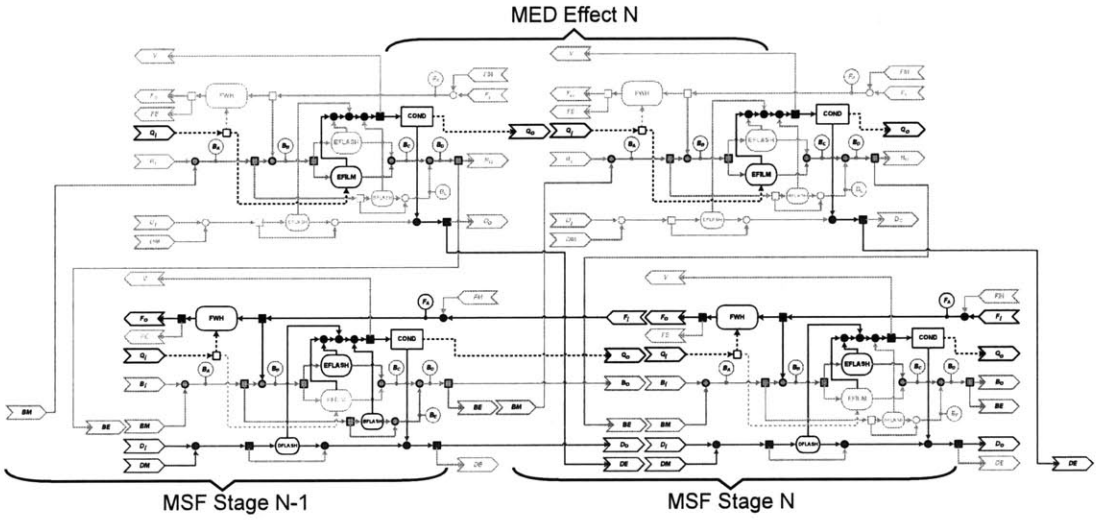


**Figure 3-17:** Hybrid MED-MSF configuration [138] expressed by repeating superstructure units.

## 3.4 Case Studies of Non-Standard Configurations

The following sections highlight some structural configurations that are possible given the superstructure presented in the previous chapter. Case studies of these configurations are given in order to explore feasible alternatives to standard industrial thermal desalination configurations and serve as a precursor to numerical optimization.

In these case studies, the performance of these alternatives is measured in terms of performance ratio, feedwater recovery, and specific surface area under operating conditions which can be compared to standard thermal desalination configurations. As such, it is desired that performance ratio is maximized, recovery ratio is maximized (RR, the percentage of distillate produced versus the total feed flowrate), and specific surface area is minimized. Weighing the performance of different configurations constitutes trade-offs between these competing objectives. The performance ratio is a measure of operating cost, recovery is a measurement of operating costs, and specific surface area is a measure of capital costs [69].

The steam supply conditions also impact the performance of the overall co-generation system, i.e., greater steam supply temperatures results in greater loss of electrical work per unit of steam extracted from the power cycle as compared lower steam supply temperatures. Since most industrial-scale thermal desalination plants are integrated with power cycles, it is important to consider this trade-off in electricity production with varying steam supply conditions. However, for these case studies, alternative configurations are compared against standard configurations with the same steam supply conditions, e.g., a non-standard configuration compared against MSF will use a steam supply temperature of $\approx 110 - 120°C$, and a non-standard configuration compared against MED will use a steam supply temperature of $\approx 70 - 80°C$. Therefore, the objective of maximizing performance ratio also minimizes its impact to a coupled power cycle, and only the thermal desalination plant performance is discussed hereafter and is for illustrative purposes.

Three non-standard configuration case studies are presented herein. The first explores the performance trade-offs between forward and parallel-cross MED by investigating a concept which transitions from the forward-feed to parallel-cross configuration within a given number of effects. The second combines MSF with forward-feed MED in order to demonstrate alternate vapor routing from an MSF stage which is possible with the presented superstructure. The last structural study combines MSF and forward-feed MED-TVC and features parallel steam supplies.

### 3.4.1 Forward to Parallel-Cross MED

The first configuration considered is a hybrid between forward-feed and parallel-cross MED (FF-PC-MED). For a given number of total effects, $N_t$, the feed switches from forward to parallel-cross at effect $N_s$. Figure 3-18 shows the configuration transition in terms of the thermal desalination superstructure, the first $N_s - 1$ effects are forward-feed ($\xi_{\text{f}} = 1$) and effects $N_s$ through $N_t$ are parallel-cross ($\xi_{\text{f}} = 0$ and $\xi_{\text{BFL}} = 1$). The mechanical construction representation is shown in Figure 3-19.

The forward-feed effects have higher brine temperature than the parallel-cross effects since they are closest to the steam supply. This choice is motivated by the gradual increase in brine salinity along effects which is characteristic of FF-MED. With the forward-feed effects first, the lowest brine salinities are at the highest temperatures, which is an operational advantage as compared to a pure parallel-cross configuration. In the parallel-cross configuration, the maximum brine salinity is reached at the highest temperatures, thereby introducing a greater risk for scaling [58].

The primary motivation for exploring the forward to parallel-cross configuration is the trade-off in performance ratio and specific surface area that exists between FF-MED and PC-MED. In particular, for fixed operating temperatures, maximum brine salinity, and number of effects, PC-MED has a higher performance ratio but also a higher specific surface area as compared to FF-MED (shown in more detail later). It is expected that the FF-PC-MED configuration exhibits intermediate performance ratio and specific surface area as compared to FF-MED and PC-MED under the same

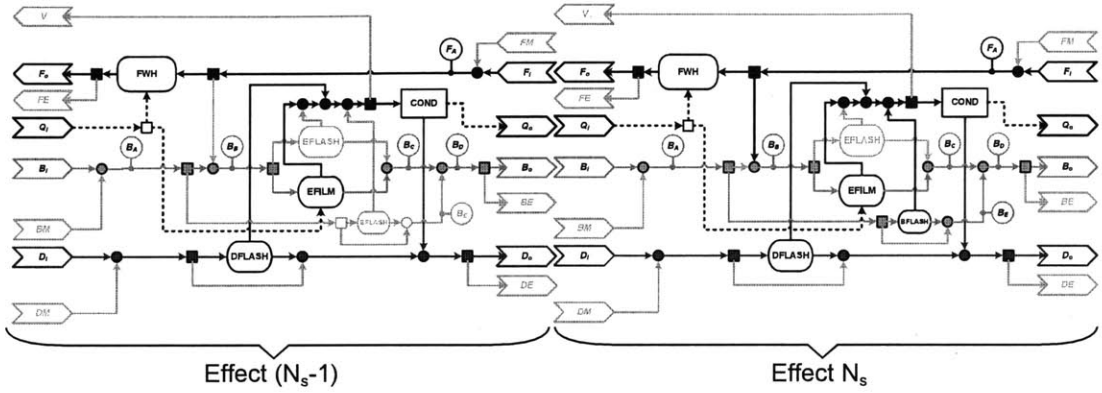


**Figure 3-18:** Transition from forward to parallel-cross configuration of FF-PC-MED concept depicted by thermal desalination superstructure.

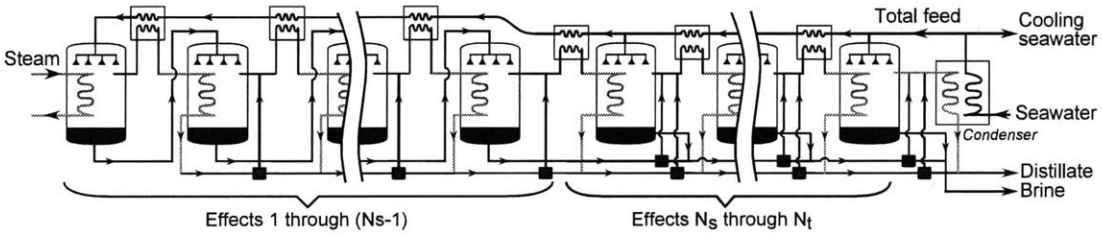


**Figure 3-19:** Forward to parallel-cross MED concept

operating conditions and number of effects. However, the goal of this case study is to show that for a given performance ratio, the FF-PC-MED has a lower specific surface area than a linear combination of forward and parallel-cross MED alone.

The linear combination is a performance measure for a hybrid system as compared to the standalone systems [116, 159]. A hybrid system of two existing technologies must be able to exhibit better performance than a combination of plants which could be built by the existing technologies alone. Otherwise, the hybrid concept is not competitive on the fleet level. In this context, both the performance ratio and specific surface area are independent of total distillate mass flowrate for fixed temperatures, recovery, and number of effects. Therefore, a linear combination of FF-MED and PC-MED plants can be used to achieve an intermediate overall performance ratio and specific surface area for fixed number of effects and operating conditions as compared to either FF-MED or PC-MED alone.

As a first step in this comparison, the performance of forward-feed and parallel-cross MED with feedwater heaters is simulated utilizing the physical process models and thermal superstructure. Each system is operated under the conditions shown in Table 3.2. The number of effects is variable, and it is assumed that the brine temperature drop between effects is constant. Therefore, the brine temperature profile is linear and described by:

$$\Delta T = \frac{(TBT - T_{bd})}{N_t - 1}$$

where TBT is the top brine temperature (brine temperature of the first effect) and $T_{bd}$ is the brine blowdown temperature (brine temperature of the last effect). A linear temperature profile is a common assumption in literature [30, 59, 26]. It is also assumed that the temperature rise in the feedwater heaters is equal to the drop temperature drop between effects ($\Delta T$).

The total feed flowrate of each case is determined based on the required distillate flow (100 kg/s) and the maximum allowed brine salinity (72 g/kg). In the case of forward-feed, where the total feed is directed to the first effect, the total feed is determined such that the brine salinity exiting the last effect is the maximum brine salinity given the required distillate flow. In the case of parallel-cross, the total feed is split among the effects, and therefore, the feed to each effect is determined by setting the brine salinity exiting each effect to the maximum brine salinity. Since the feed is chosen such that the maximum brine salinity is achieved for both forward and parallel-cross, the feed recovery of each system is the same (RR=41.7%) and the maximum allowed.

Tables 3.3 and 3.4 show simulation results for twelve effect forward-feed and parallel-cross MED, respectively. The parameter $\dot{m}_{vap}$ is the total vapor generated by the effect (including brine and distillate flashing). The vapor temperatures after evaporation, $T_{v,ev}$, are different between forward-feed and parallel-cross MED despite setting the same brine temperatures. This difference is due to the variation in brine salinity which affects the BPE and thus the vapor temperature. The specific surface

**Table 3.2:** Operating parameters for PC-MED, FF-MED, and FF-PC-MED (Figure 3-19) configurations.

| | |
|---|---|
| Unit distillate flow (kg/s) | 100 |
| Seawater temperature (°C) | 25 |
| Seawater salinity (g/kg) | 42 |
| Max. brine salinity (g/kg) | 72 |
| Steam supply temperature, saturated (°C) | 70 |
| Top brine temperature, TBT (°C) | 65 |
| Brine blowdown temperature, $T_{bd}$ (°C) | 40 |
| Condenser temp. (°C) | 35 |

area is the sum of evaporator, feedwater heater, and down condenser heat transfer surface areas versus the total mass flow rate of distillate produced.

The forward-feed configuration achieves a performance ratio of 9.47 with a specific surface area of 439 $m^2/(kg/s)$. The parallel-cross configuration achieves a performance ratio of 10.32 with a specific surface area of 525 $m^2/(kg/s)$. These results show the trade-off in performance ratio and specific surface area between forward-feed and parallel-cross MED configurations.

Next, the operating conditions shown in Table 3.2 are utilized to simulate FF-PC-MED system. The total number of effects, $N_t$, and the effect where the configuration switches from forward to parallel-cross, $N_s$, are variable. As with the forward-feed and parallel-cross cases, the temperature drop across effects and temperature rise in the feedwater heaters is assumed constant. The feed of the system is determined by setting the outlet brine salinity of the parallel-cross section (effects $N_s$ to $N_t$) to the maximum brine salinity. In addition, the feed that is directed to the forward-feed section (effects 1 to $N_s - 1$) is determined such that the outlet brine salinity in effect $(N_s - 1)$ is equal to the maximum brine salinity. Therefore, the recovery is the same as the forward-feed and parallel-cross system.

Table 3.5 shows simulation results of the FF-PC-MED configuration with twelve effects. The configuration transitions to parallel-cross at the sixth effect. The performance ratio is 10.19 and the specific surface area is 491 $m^2/(kg/s)$. As expected, the performance ratio and the specific area are intermediate values to that of the

**Table 3.3:** Forward-feed MED results. 12 effects, PR=9.47, SA=439 $m^2/(kg/s)$, Area of down condenser=1009 $m^2$.

| Effect | $T_{b,ev}$ | $T_{v,ev}$ | $T_{i,ev}$ | $T_{i,FWH}$ | $\dot{m}_{i,ev}$ | $\dot{m}_{vap}$ | $\dot{m}_{b,ev}$ | $\dot{m}_{D_o}$ | $X_{b,ev}$ | $A_{ev}$ | $A_{FWH}$ |
|---|---|---|---|---|---|---|---|---|---|---|---|
| 1 | 65.0 | 64.5 | 60.0 | 60.0 | 240.0 | 8.5 | 231.5 | 8.5 | 44 | 1643 | 0 |
| 2 | 62.7 | 62.2 | 65.0 | 57.7 | 231.5 | 8.5 | 223.0 | 17.0 | 45 | 3375 | 164 |
| 3 | 60.45 | 59.9 | 62.7 | 55.5 | 223.0 | 8.5 | 214.6 | 25.4 | 47 | 3403 | 165 |
| 4 | 58.2 | 57.6 | 60.5 | 53.2 | 214.6 | 8.5 | 206.2 | 33.8 | 49 | 3434 | 165 |
| 5 | 55.9 | 55.3 | 58.2 | 50.9 | 206.2 | 8.5 | 197.8 | 42.2 | 51 | 3468 | 166 |
| 6 | 53.6 | 53.0 | 55.9 | 48.6 | 197.8 | 8.5 | 189.5 | 50.6 | 53 | 3506 | 166 |
| 7 | 51.4 | 50.7 | 53.6 | 46.4 | 189.5 | 8.5 | 181.1 | 58.9 | 56 | 3550 | 167 |
| 8 | 49.1 | 48.4 | 51.4 | 44.1 | 181.1 | 8.5 | 172.9 | 67.2 | 58 | 3598 | 168 |
| 9 | 46.8 | 46.1 | 49.1 | 41.8 | 172.9 | 8.5 | 164.6 | 75.4 | 61 | 3654 | 168 |
| 10 | 44.6 | 43.8 | 46.8 | 39.5 | 164.6 | 8.5 | 156.4 | 83.6 | 64 | 3718 | 169 |
| 11 | 42.3 | 41.5 | 44.6 | 37.3 | 156.4 | 8.5 | 148.2 | 91.8 | 68 | 3793 | 170 |
| 12 | 40.0 | 39.2 | 42.3 | 35.0 | 148.2 | 8.5 | 140.0 | 100.0 | 72 | 3880 | 171 |

**Table 3.4:** Parallel-cross MED results. 12 effects, PR=10.32, SA=525 $m^2/(kg/s)$, Area of down condenser=895 $m^2$.

| Effect | $T_{b,ev}$ | $T_{v,ev}$ | $T_{i,ev}$ | $T_{i,FWH}$ | $\dot{m}_{i,ev}$ | $\dot{m}_{vap}$ | $\dot{m}_{b,ev}$ | $\dot{m}_{D_o}$ | $X_{b,ev}$ | $A_{ev}$ | $A_{FWH}$ |
|---|---|---|---|---|---|---|---|---|---|---|---|
| 1 | 65.0 | 64.1 | 60.0 | 60.0 | 22.8 | 9.5 | 13.3 | 9.5 | 72 | 1507 | 0 |
| 2 | 62.7 | 61.8 | 57.7 | 57.7 | 22.2 | 9.3 | 13.0 | 18.8 | 72 | 5504 | 17 |
| 3 | 60.5 | 59.6 | 55.5 | 55.5 | 21.7 | 9.1 | 12.8 | 27.8 | 72 | 5267 | 33 |
| 4 | 58.2 | 57.3 | 53.2 | 53.2 | 21.2 | 8.9 | 12.5 | 36.6 | 72 | 5041 | 49 |
| 5 | 55.9 | 55.0 | 50.9 | 50.9 | 20.7 | 8.8 | 12.3 | 45.3 | 72 | 4824 | 64 |
| 6 | 53.6 | 52.8 | 48.6 | 48.6 | 20.2 | 8.6 | 12.0 | 53.7 | 72 | 4618 | 79 |
| 7 | 51.4 | 50.5 | 46.4 | 46.4 | 19.7 | 8.4 | 11.8 | 61.9 | 72 | 4420 | 94 |
| 8 | 49.1 | 48.3 | 44.1 | 44.1 | 19.2 | 8.3 | 11.5 | 69.9 | 72 | 4231 | 108 |
| 9 | 46.8 | 46.0 | 41.8 | 41.8 | 18.8 | 8.1 | 11.3 | 77.7 | 72 | 4050 | 121 |
| 10 | 44.6 | 43.8 | 39.6 | 39.6 | 18.3 | 7.9 | 11.1 | 85.3 | 72 | 3878 | 134 |
| 11 | 42.3 | 41.5 | 37.3 | 37.3 | 17.9 | 7.8 | 10.9 | 92.7 | 72 | 3712 | 147 |
| 12 | 40.0 | 39.3 | 35.0 | 35.0 | 17.4 | 7.6 | 10.7 | 100 | 72 | 3553 | 159 |

**Table 3.5:** Forward to parallel-cross MED results, 12 effects with transition at effect 6. PR=10.19, SA=491 $m^2/(kg/s)$, Area of down condenser = 912 $m^2$.

| Effect | $T_{b,ev}$ | $T_{v,ev}$ | $T_{i,ev}$ | $T_{i,FWH}$ | $\dot{m}_{i,ev}$ | $\dot{m}_{vap}$ | $\dot{m}_{b,ev}$ | $\dot{m}_{D_o}$ | $X_{b,ev}$ | $A_{ev}$ | $A_{FWH}$ |
|---|---|---|---|---|---|---|---|---|---|---|---|
| 1 | 65.0 | 64.4 | 60.0 | 60.0 | 106.1 | 8.9 | 97.2 | 8.9 | 46 | 1527 | 0 |
| 2 | 62.7 | 62.1 | 65.0 | 57.7 | 97.2 | 8.9 | 88.3 | 17.8 | 50 | 3855 | 73 |
| 3 | 60.5 | 59.8 | 62.7 | 55.5 | 88.3 | 8.9 | 79.5 | 26.6 | 56 | 3983 | 74 |
| 4 | 58.2 | 57.4 | 60.5 | 53.2 | 79.5 | 8.9 | 70.6 | 35.4 | 63 | 4155 | 75 |
| 5 | 55.9 | 55.0 | 58.1 | 50.9 | 70.6 | 8.9 | 61.9 | 44.2 | 72 | 4399 | 76 |
| 6 | 53.6 | 52.8 | 48.6 | 48.6 | 20.6 | 8.7 | 12.2 | 52.8 | 72 | 4772 | 78 |
| 7 | 51.4 | 50.5 | 46.4 | 46.4 | 20.1 | 8.6 | 12.0 | 61.1 | 72 | 4514 | 92 |
| 8 | 49.1 | 48.3 | 44.1 | 44.1 | 19.6 | 8.4 | 11.8 | 69.3 | 72 | 4321 | 106 |
| 9 | 46.8 | 46.0 | 41.8 | 41.8 | 19.1 | 8.2 | 11.5 | 77.23 | 72 | 4137 | 120 |
| 10 | 44.6 | 43.8 | 39.6 | 39.6 | 18.7 | 8.1 | 11.3 | 85.0 | 72 | 3960 | 134 |
| 11 | 42.3 | 41.5 | 37.3 | 37.3 | 18.2 | 7.9 | 11.1 | 92.6 | 72 | 3791 | 147 |
| 12 | 40.0 | 39.3 | 35.00 | 35.00 | 17.8 | 7.8 | 10.9 | 100.0 | 72 | 3630 | 159 |

forward-feed and parallel-cross MED. Comparing against the linear combination of forward-feed or parallel-cross alone is necessary; for a fixed performance ratio, the FF-PC-MED configuration should have a lower specific surface area than the linear combination of FF-MED and PC-MED surface areas. Given that the FF-PC-MED performance ratio is 84.7% of the difference between the forward-feed and parallel-cross systems, the specific surface area of the linear combination is 512 $m^2/(kg/s)$ for a performance ratio of 10.19. The specific surface area of the FF-PC-MED simulation is less than the linear combination specific surface area by 4.1%. Therefore, a performance advantage exists for the FF-PC-MED configuration as compared to the forward-feed or parallel-cross MED alone for fixed operation.

Figure 3-20 shows the change in performance of FF-PC-MED with varying number of effects, $N_t$, and transition effect, $N_s$. Figure 3-20(a) shows the variation in number of effects from eight to thirteen with fixed operating conditions. For a fixed number of effects, Figure 3-20(a) shows forward-feed alone at the lowest performance ratio and specific surface area and parallel-cross alone at the highest performance ratio and specific area with FF-PC-MED performance in between. For a fixed number of effects, all FF-PC-MED results are better than the linear combination of the forward-feed and parallel-cross alone results.

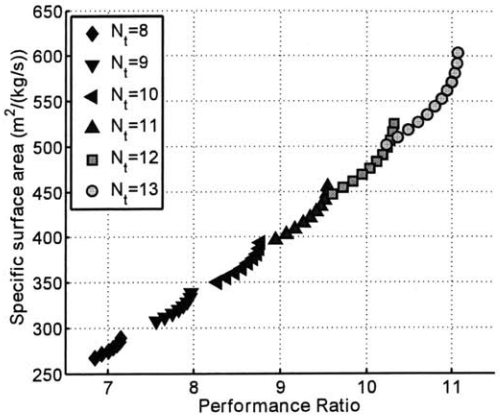


(a) Varying number of effects $N_t$ and transition effect $N_s$.

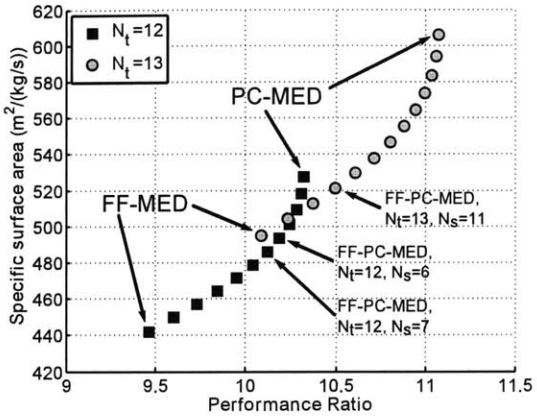


(b) Twelve and thirteen total effects emphasizing performance ratio and specific surface area trade-off.

**Figure 3-20:** Performance of FF-PC-MED (Figure 3-19) configuration with varying number of effects and transition effects.

The performance shows a strong dependence on number of effects, as expected. However, an interesting result occurs at higher number of effects; the performance between two effects overlaps. Figure 3-20(b) shows this outcome between twelve and thirteen effects. This overlap shows an advantage in performance for the FF-PC-MED configuration. Although the parallel-cross alone exhibits the highest performance among twelve effect options, the thirteen effect FF-PC-MED with transition at effect ten has a higher performance ratio ($\approx 0.18$ points higher) with a lower specific surface area ($\approx 7$ m$^2$/(kg/s) lower). Similarly, the twelve effect FF-PC-MED with transitions at six and seven effects exhibit greater performance ratio and lower specific surface area than the thirteen effect forward-feed MED.

The FF-PC-MED configuration is a promising alternative to either forward or parallel-cross MED alone. However, the analysis performed herein does not imply optimality since operating conditions are held fixed. Further, the heat transfer coefficients are held constant. The calculation of heat transfer surface areas is also sensitive to accuracy of vapor temperature calculations, i.e., BPE and other thermal losses; greater accuracy in these calculations could prove a smaller increase in performance for the FF-PC-MED as compared to the forward and parallel-cross configurations.

The pumping requirements should also be compared, a measure of operating costs, among the configurations. Despite the limitations of the analysis performed herein, the demonstrated performance of the FF-PC-MED configuration shows that there is merit in further examination through numerical optimization.

### 3.4.2 MSF to FF-MED

The second structural case study involves the combination of MSF and FF-MED in series, referred to hereafter as MSF-MED. The configuration involves a section of MSF stages in series with a section of MED effects. The brine of the last MSF stage is directed as feed of the first MED effect. In addition, the vapor produced in the last MSF stage is used to power the first MED effect. Figure 3-21 shows the transition from MSF stages to MED effects in terms of the thermal desalination superstructure. At unit $N_s$, the evaporation process transitions to film boiling ($\xi_{ev} = 1$). Since none of the enthalpy of vaporization from unit $N_s - 1$ is used for preheating feedwater, unit $N_s - 1$ constitutes a mechanical construct other than an MSF stage or MED effect, i.e., this corresponds flashed vapors of the main evaporation process condensing inside of tubes. The motivation for investigating the MSF-MED configuration is to determine if there is merit in utilizing this alternate unit type. Figure 3-22 shows the overall MSF-MED configuration. The total feed is preheated along both the MED and MSF sections.

The performance of the MSF-MED concept is simulated with fixed operating conditions and total number of units (24 stages/effects). Table 3.6 shows the operating parameters considered; a linear temperature profile is assumed. In this configuration, the TBT is the temperature at the outlet of the brine heater (typical of MSF configurations). Therefore, the temperature difference between each unit is given by

$$\Delta T = \frac{(TBT - T_{bd})}{N_t}$$

The transition unit, $N_s$, where the configuration switches from MSF to MED is considered variable given the constraint that the MED effects should not be operated

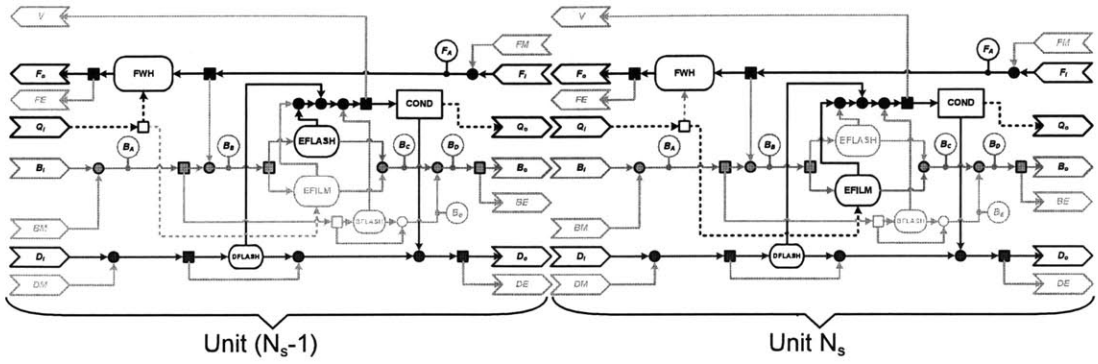


**Figure 3-21:** Transition from MSF configuration to MED configuration in MSF-MED concept.

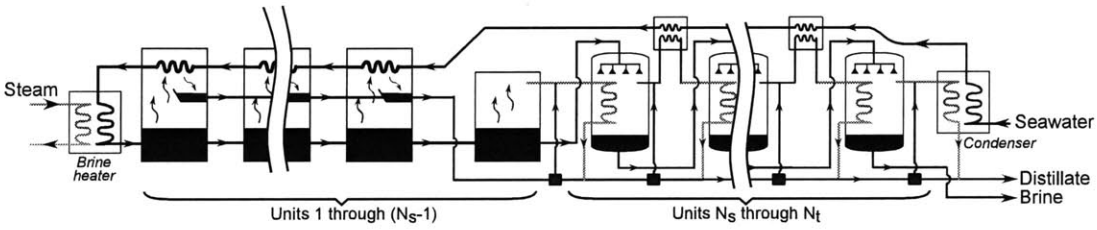


**Figure 3-22:** MSF to FF-MED concept with alternative vapor routing of MSF for unit ($N_s$-1).

at a brine temperature above $\approx$ 70°C in order to avoid scaling. Therefore, given a linear temperature profile with twenty-four units, the transition unit must be greater or equal to unit twelve ($N_s \geq 12$). It should be noted that in this configuration the feed flowrate is not a degree of freedom which can be used to set the brine blowdown salinity to a maximum allowed salinity. Therefore, the the recovery of this system is rather low.

Table 3.7 shows the performance of the MSF-MED concept for 24 total units with a transition unit of 12. The system achieves a performance ratio of 9.75 with a specific surface area of 238 $m^2/(kg/s)$ and a recovery ratio of 17.6%. The amount of vapor produced in unit 11 (powering the MED section) is approximately 30% of the steam necessary to power the twelve effect forward-feed system investigated in Section 3.4.1. Therefore, a significant amount of distillate can be generated by utilizing the enthalpy of vaporization of flashed vapors to power film boiling as opposed to feedwater heating. From the values of $\dot{m}_{D_o}$, the total flow of distillate leaving each unit, it can be seen

**Table 3.6:** Operating parameters for MSF-MED (Figure 3-22) and MSF-OT configuration.

| | |
|---|---|
| Unit distillate flow (kg/s) | 100 |
| Seawater temperature (°C) | 25 |
| Seawater salinity (g/kg) | 42 |
| Steam supply temperature, saturated (°C) | 116 |
| Top brine temperature, $TBT_{MSF}$ (°C) | 105 |
| Brine blowdown temperature, $T_{bd}$ (°C) | 35 |
| Total number of units, $N_t$ | 24 |

that the MED section produces about 70% of the total distillate generated. The performance ratio of the MED section alone is significantly higher than the FF-MED system because of gained enthalpy of the incoming MSF brine. In addition, this system is operated at a lower brine blowdown temperature without cooling seawater for fair comparison to the typical operating conditions of once-through MSF.

Figure 3-23 shows performance ratio versus specific surface area results of the MSF-MED system with fixed operating conditions and total number of units for varying transition unit $N_s$. The simulated performance of MSF-OT for twenty-four stages is also shown; the recovery of the MSF-OT system is 11.3%. Figure 3-23 shows that the transition to MED effects increases the performance ratio and the specific surface area. As compared to the FF-MED system in Section 3.4.1, the specific surface area is significantly less for a similar PR. However, the steam supply temperature is much higher in the MSF-MED case, the recovery ratio is less, and there is no cooling water stream to buffer against changes in seawater temperature [75].

Despite the limitations of the concept shown herein, feed/brine extraction or mixing could possibly be utilized in order to increase recovery. Utilizing a variation of the MSF-MED concept could result in a higher performance ratio versus specific surface area as compared to FF-MED or MSF-BR (not compared herein due to differences in operation conditions). In addition, the alternate unit configuration of condensing flashed vapors inside of tubes should be further investigated through detailed heat transfer models to account for changes in heat transfer coefficient as compared to a typical MSF stage or MED effect.

**Table 3.7:** MSF-MED results for $N_t$=24 with transition unit $N_s$=12. PR=9.75, SA=238 $m^2/(kg/s)$, RR=17.6%.

| Unit | $T_{b,ev}$ | $T_{v,ev}$ | $T_{i,ev}$ | $T_{i,FWH}$ | $T_{o,FWH}$ | $\dot{m}_{i,ev}$ | $\dot{m}_v$ | $\dot{m}_{b,ev}$ | $\dot{m}_{D_o}$ | $X_{b,ev}$ | $A_{ev}$ | $A_{FWH}$ |
|---|---|---|---|---|---|---|---|---|---|---|---|---|
| 1 | 102.1 | 101.4 | 105.0 | 95.0 | 105.0 | 566.9 | 2.8 | 564.1 | 2.8 | 42 | 0 | 610 |
| 2 | 99.2 | 98.5 | 102.1 | 92.1 | 95.0 | 564.1 | 2.8 | 561.3 | 5.7 | 42 | 0 | 353 |
| 3 | 96.3 | 95.6 | 99.2 | 89.2 | 92.1 | 561.3 | 2.8 | 558.4 | 8.5 | 43 | 0 | 352 |
| 4 | 93.3 | 92.7 | 96.3 | 86.2 | 89.2 | 558.4 | 2.8 | 555.7 | 11.3 | 43 | 0 | 352 |
| 5 | 90.4 | 89.8 | 93.3 | 83.3 | 86.2 | 555.7 | 2.8 | 552.9 | 14.0 | 43 | 0 | 352 |
| 6 | 87.5 | 86.9 | 90.4 | 80.4 | 83.3 | 552.9 | 2.8 | 550.1 | 16.8 | 43 | 0 | 351 |
| 7 | 84.6 | 84.0 | 87.5 | 77.5 | 80.4 | 550.1 | 2.8 | 547.4 | 19.5 | 44 | 0 | 351 |
| 8 | 81.7 | 81.1 | 84.6 | 74.6 | 77.5 | 547.4 | 2.8 | 544.6 | 22.3 | 44 | 0 | 351 |
| 9 | 78.8 | 78.2 | 81.7 | 71.7 | 74.6 | 544.6 | 2.8 | 541.9 | 25.0 | 44 | 0 | 350 |
| 10 | 75.8 | 75.3 | 78.8 | 68.7 | 71.7 | 541.9 | 2.8 | 539.2 | 27.7 | 44 | 0 | 350 |
| 11 | 72.9 | 72.3 | 75.8 | 65.8 | 68.7 | 539.2 | 2.8 | 536.5 | 30.4 | 44 | 0 | 350 |
| 12 | 70.0 | 69.4 | 72.9 | 65.8 | 65.8 | 536.5 | 5.7 | 531.0 | 35.9 | 45 | 939 | 0 |
| 13 | 67.1 | 66.5 | 70.0 | 62.9 | 65.8 | 531.0 | 5.7 | 525.5 | 41.4 | 45 | 937 | 560 |
| 14 | 64.2 | 63.6 | 67.1 | 60.0 | 62.9 | 525.5 | 5.7 | 520.0 | 46.9 | 46 | 935 | 559 |
| 15 | 61.2 | 60.7 | 64.2 | 57.1 | 60.0 | 520.0 | 5.7 | 514.6 | 52.3 | 46 | 933 | 559 |
| 16 | 58.3 | 57.8 | 61.3 | 54.2 | 57.1 | 514.6 | 5.7 | 509.2 | 57.7 | 47 | 932 | 558 |
| 17 | 55.4 | 54.9 | 58.3 | 51.2 | 54.2 | 509.2 | 5.7 | 503.8 | 63.1 | 47 | 930 | 558 |
| 18 | 52.5 | 52.0 | 55.4 | 48.3 | 51.2 | 503.8 | 5.7 | 498.5 | 68.5 | 48 | 928 | 557 |
| 19 | 49.6 | 49.1 | 52.5 | 45.4 | 48.3 | 498.5 | 5.7 | 493.1 | 73.8 | 48 | 926 | 556 |
| 20 | 46.7 | 46.1 | 49.6 | 42.5 | 45.4 | 493.1 | 5.7 | 487.8 | 79.1 | 49 | 924 | 556 |
| 21 | 43.8 | 43.2 | 46.7 | 39.6 | 42.5 | 487.8 | 5.7 | 482.6 | 84.4 | 49 | 922 | 555 |
| 22 | 40.8 | 40.3 | 43.8 | 36.7 | 39.6 | 482.6 | 5.7 | 477.3 | 89.6 | 50 | 920 | 555 |
| 23 | 37.9 | 37.4 | 40.8 | 33.7 | 36.7 | 477.3 | 5.7 | 472.1 | 94.8 | 50 | 918 | 554 |
| 24 | 35.0 | 34.5 | 37.9 | 30.8 | 33.7 | 472.1 | 5.7 | 466.9 | 100.0 | 51 | 916 | 554 |

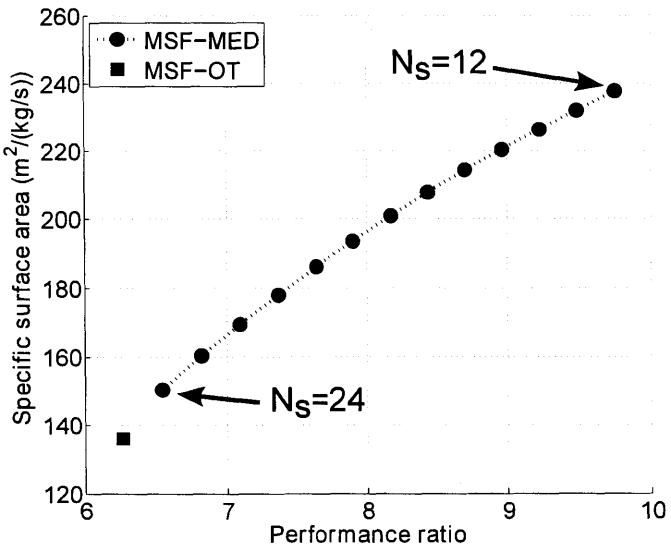


**Figure 3-23:** Performance of MSF-MED concept as compared to MSF-OT for fixed operating conditions and total number of units ($N_t$=24) with varying transition unit from $N_s$=12 to $N_s$=24.

### 3.4.3 MSF to FF-MED-TVC

The final structural case study combines MSF with FF-MED-TVC, referred to hereafter as MSF-MED-TVC. This configuration is similar to the previous case, but TVC is used to power the first MED effect. Further, a motivation for investigating this configuration is the common steam supply temperature that is possible for TVC motive steam and MSF brine heaters. Since the MED TBT is limited to not more than $\approx 70°C$ to avoid scaling [110], the higher operating range of MSF stages could improve performance as compared to MED-TVC alone.

Figure 3-24 shows the transition from the MSF section to the MED section in terms of the thermal desalination superstructure. Two steam supplies are utilized where the steam supply connected to the MSF section is directly condensed ($\xi_s = 1$) and the steam supply to the MED section utilizes TVC ($\xi_s = 0$). The MED steam

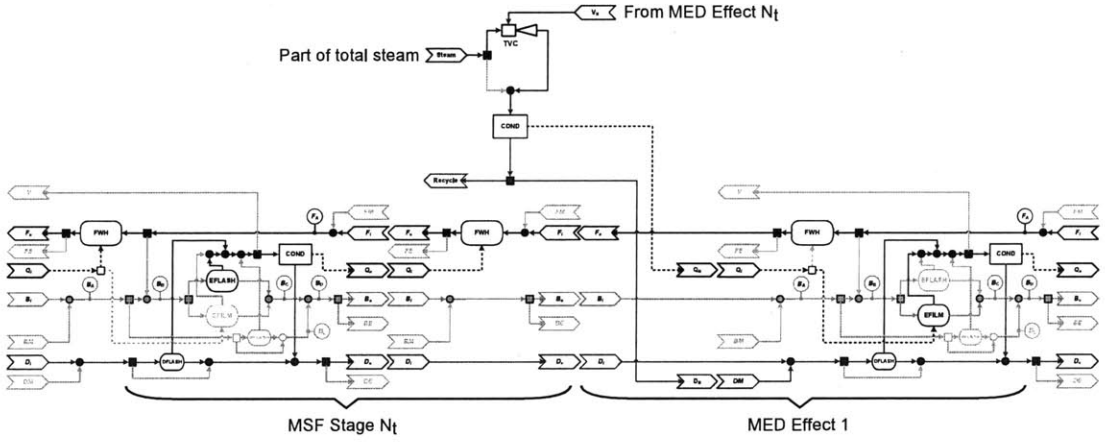


**Figure 3-24:** Transition from MSF configuration to MED configuration in MSF-MED-TVC concept, shown with MED steam supply configuration.

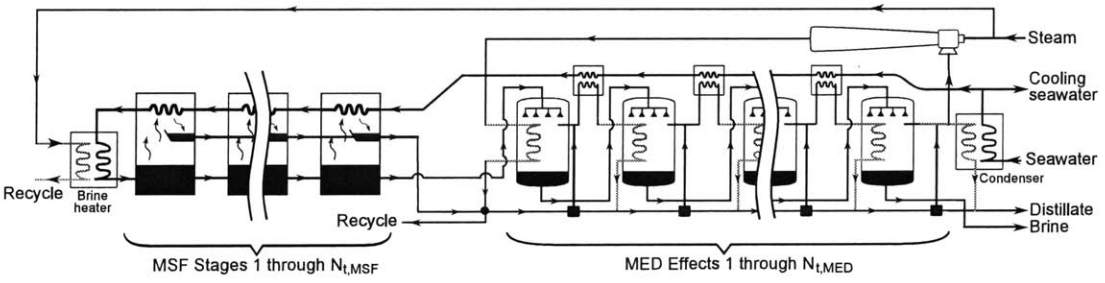


**Figure 3-25:** MSF to MED-TVC concept

**Table 3.8:** Operating parameters for FF-MED-TVC, PC-MED-TVC, and MSF-MED-TVC (Figure 3-25) configurations.

| | |
|---|---|
| Unit distillate flow (kg/s) | 100 |
| Seawater temperature (°C) | 25 |
| Seawater salinity (g/kg) | 42 |
| Max. brine salinity (g/kg) | 72 |
| Steam supply temperature, saturated (°C) | 116 |
| MSF top brine temperature, $TBT_{MSF}$ (°C) | 105 |
| Brine blowdown temperature, $T_{bd}$ (°C) | 40 |
| Condenser temp. (°C) | 35 |
| Number of MSF stages, $N_{t,MSF}$ | 15 |
| Number of MED effects, $N_{t,MED}$ | 12 |

supply interface $V_N$ stream is connected to the $V$ stream of the last MED effect. Figure 3-25 depicts the overall configuration of MSF-MED-TVC considered herein. The total feed is preheated along both the MED and MSF effects and directed to the first MSF stage.

To simulate the performance of the MSF-MED-TVC system, the steam supply conditions, blowdown conditions, and number of stages/effects are held fixed. Table 3.8 shows the operating parameters considered herein. The TVC compression ratio, MSF last stage brine temperature, and MED TBT are considered variable. Since the motive steam and blowdown temperatures are held fixed, varying the compression ratio of the TVC changes the discharge saturation temperature of the TVC. The MED TBT and MSF last stage brine temperature are fixed with respect to the discharge conditions. The difference in temperature between the TVC discharge temperature and the MED TBT is set as 4°C, and the difference in temperature between the MSF last stage brine temperature and MED TBT is set as 1°C. These values ensure that reasonable pinches exist in the feedwater heaters and MED effects.

Table 3.9 shows the considered compression ratios and the resulting entrainment ratio and operating temperatures given the steam supply and blowdown conditions that are assumed herein. A linear brine temperature profile is assumed between the MSF TBT and MSF last stage brine temperature; similarly, a linear brine temperature

**Table 3.9:** Variation of TVC compression ratio for $P_{m,sat}$ = 0.175 MPa ($T_{m,sat}$ = 116°C), $P_{e,sat}$ = 0.00732 MPa ($T_{e,sat}$ = 40°C), with resulting entrainment ratio, discharge temperature, MED TBT, and MSF last effect brine temperature.

| CR | ER | $T_{sat,di}$ (°C) | $TBT_{MED}$ (°C) | MSF $T_{b,N_t}$ (°C) |
|---|---|---|---|---|
| 3 | 2.31 | 62.3 | 58.3 | 59.3 |
| 3.5 | 2.77 | 65.7 | 61.7 | 62.7 |
| 4 | 3.25 | 68.7 | 64.7 | 65.7 |
| 4.5 | 3.74 | 71.5 | 67.5 | 68.5 |
| 5 | 4.23 | 73.9 | 69.9 | 70.9 |

profile is assumed (not-necessarily equal to the MSF section) between the MED TBT and MED last stage brine temperature ($T_{bd}$). The total feed flowrate is chosen such that the MED last effect blowdown salinity is the maximum allowable salinity (72 g/kg). Table 3.10 shows the resulting performance of the MSF-MED-TVC concept for TVC CR=4. The system achieves a performance ratio of 13.0 and specific surface area of 418 $m^2/(kg/s)$.

It is necessary to compare this configuration's performance versus standard configurations. Specifically, FF-MED-TVC and PC-MED-TVC are considered. The motivation behind comparing to FF-MED-TVC is to determine if the addition of the MSF section (with the same MED section configuration as FF-MED-TVC) constitutes a gain in performance with respect to performance ratio or specific heat transfer area. Based on the results of Section 3.4.1, the PC-MED-TVC configuration exhibits higher performance ratio and specific heat transfer area for fixed operating conditions as compared to FF-MED-TVC. Therefore, if the MSF-MED-TVC concept exhibits a gain in performance as compared to FF-MED-TVC, it is important to weigh this difference with respect to the PC-MED-TVC configuration.

The performance of FF-MED-TVC and PC-MED-TVC is simulated with the same MED section operating conditions shown in Table 3.6. For fixed number of effects ($N_t$ = 12), the TBT is varied by the TVC compression ratio (based on Table 3.9). Figure 3-26 shows the resulting MSF-MED-TVC, FF-MED-TVC, and PC-MED-TVC performance for varying CR and fixed number of stages/effects. For MSF-MED-

**Table 3.10:** MSF-MED-TVC results for MSF $N_t$=15, MED $N_t$ = 12, and CR=4. PR=13.0, SA=418.1 $m^2/(kg/s)$.

| Effect/stage | $T_{b,ev}$ | $T_{v,ev}$ | $T_{i,ev}$ | $T_{i,FWH}$ | $T_{o,FWH}$ | $\dot{m}_{i,ev}$ | $\dot{m}_v$ | $\dot{m}_{b,ev}$ | $\dot{m}_{D_o}$ | $X_{b,ev}$ | $A_{ev}$ | $A_{FWH}$ |
|---|---|---|---|---|---|---|---|---|---|---|---|---|
| MSF 1 | 102.4 | 101.7 | 105.0 | 99.0 | 105.0 | 240.0 | 1.08 | 238.9 | 1.1 | 42.2 | 0 | 174 |
| MSF 2 | 99.8 | 99.1 | 102.4 | 96.4 | 99.0 | 238.9 | 1.08 | 237.9 | 2.1 | 42.4 | 0 | 268 |
| MSF 3 | 97.1 | 96.5 | 99.8 | 93.8 | 96.4 | 237.9 | 1.08 | 236.8 | 3.2 | 42.6 | 0 | 268 |
| MSF 4 | 94.5 | 93.9 | 97.1 | 91.1 | 93.8 | 236.8 | 1.08 | 235.7 | 4.3 | 42.8 | 0 | 267 |
| MSF 5 | 91.9 | 91.3 | 94.5 | 88.5 | 91.1 | 235.7 | 1.08 | 234.7 | 5.3 | 43.0 | 0 | 267 |
| MSF 6 | 89.3 | 88.7 | 91.9 | 85.9 | 88.5 | 234.7 | 1.08 | 233.6 | 6.4 | 43.1 | 0 | 266 |
| MSF 7 | 86.7 | 86.1 | 89.3 | 83.3 | 85.9 | 233.6 | 1.08 | 232.6 | 7.4 | 43.3 | 0 | 266 |
| MSF 8 | 84.1 | 83.5 | 86.7 | 80.7 | 83.3 | 232.6 | 1.08 | 231.5 | 8.5 | 43.5 | 0 | 265 |
| MSF 9 | 81.4 | 80.9 | 84.1 | 78.1 | 80.7 | 231.5 | 1.08 | 230.5 | 9.5 | 43.7 | 0 | 265 |
| MSF 10 | 78.8 | 78.2 | 81.4 | 75.4 | 78.1 | 230.5 | 1.08 | 229.4 | 10.6 | 43.9 | 0 | 264 |
| MSF 11 | 76.2 | 75.6 | 78.8 | 72.8 | 75.4 | 229.4 | 1.08 | 228.4 | 11.6 | 44.1 | 0 | 264 |
| MSF 12 | 73.6 | 73.0 | 76.2 | 70.2 | 72.8 | 228.4 | 1.08 | 227.4 | 12.6 | 44.3 | 0 | 264 |
| MSF 13 | 71.0 | 70.4 | 73.6 | 67.6 | 70.2 | 227.4 | 1.08 | 226.4 | 13.6 | 44.5 | 0 | 263 |
| MSF 14 | 68.4 | 67.8 | 71.0 | 65.0 | 67.6 | 226.4 | 1.08 | 225.4 | 14.6 | 44.7 | 0 | 263 |
| MSF 15 | 65.7 | 65.2 | 68.4 | 62.4 | 65.0 | 225.4 | 1.08 | 224.3 | 15.7 | 44.9 | 0 | 262 |
| MED 1 | 64.7 | 64.2 | 65.7 | 59.7 | 59.7 | 224.3 | 7.20 | 217.2 | 24.4 | 46.4 | 1318 | 0 |
| MED 2 | 62.5 | 61.9 | 64.7 | 57.5 | 59.7 | 217.2 | 7.21 | 210.1 | 31.5 | 48.0 | 2902 | 164 |
| MED 3 | 60.2 | 59.6 | 62.5 | 55.2 | 57.5 | 210.1 | 7.22 | 203.0 | 38.6 | 49.7 | 2927 | 165 |
| MED 4 | 58.0 | 57.4 | 60.2 | 53.0 | 55.2 | 203.0 | 7.22 | 195.9 | 45.7 | 51.5 | 2955 | 165 |
| MED 5 | 55.7 | 55.1 | 58.0 | 50.7 | 53.0 | 195.9 | 7.23 | 188.8 | 52.7 | 53.4 | 2985 | 165 |
| MED 6 | 53.5 | 52.9 | 55.7 | 48.5 | 50.7 | 188.8 | 7.24 | 181.8 | 59.8 | 55.4 | 3018 | 166 |
| MED 7 | 51.2 | 50.6 | 53.5 | 46.2 | 48.5 | 181.8 | 7.25 | 174.8 | 66.8 | 57.7 | 3055 | 166 |
| MED 8 | 49.0 | 48.3 | 51.2 | 44.0 | 46.2 | 174.8 | 7.25 | 167.8 | 73.8 | 60.1 | 3095 | 167 |
| MED 9 | 46.7 | 46.0 | 49.0 | 41.7 | 44.0 | 167.8 | 7.26 | 160.8 | 80.7 | 62.7 | 3141 | 168 |
| MED 10 | 44.5 | 43.8 | 46.7 | 39.5 | 41.7 | 160.8 | 7.27 | 153.9 | 87.7 | 65.5 | 3192 | 168 |
| MED 11 | 42.2 | 41.5 | 44.5 | 37.2 | 39.5 | 153.9 | 7.28 | 146.9 | 94.6 | 68.6 | 3250 | 169 |
| MED 12 | 40.0 | 39.2 | 42.2 | 35.0 | 37.2 | 146.9 | 7.29 | 140.0 | 100.0 | 72.0 | 3317 | 170 |

TVC, the number of MSF stages is 15, and the number of MED effects is 12. The specific surface area for each configuration increases with decreasing CR, i.e., MED TBT, because the number of effects is fixed and therefore the feedwater heater and effect pinches decreases. However, the performance ratio increases for decreasing CR, mostly due to the decrease in entrainment ratio, i.e., less motive steam is needed for the same vapor drawn from the last effect of MED.

Figure 3-26 demonstrates that the MSF-MED-TVC concept exhibits a higher performance ratio and lower specific surface area as compared to FF-MED-TVC for all compression ratios tested. However, the MSF-MED-TVC shows a lower performance ratio and lower specific as compared to PC-MED-TVC for a given compression ratio. On the other hand, for all compression ratios considered, the MSF-MED-TVC follows a similar performance trend as PC-MED-TVC. The performance of the MSF-MED-TVC concept as compared to the FF-MED-TVC configuration indicates that there

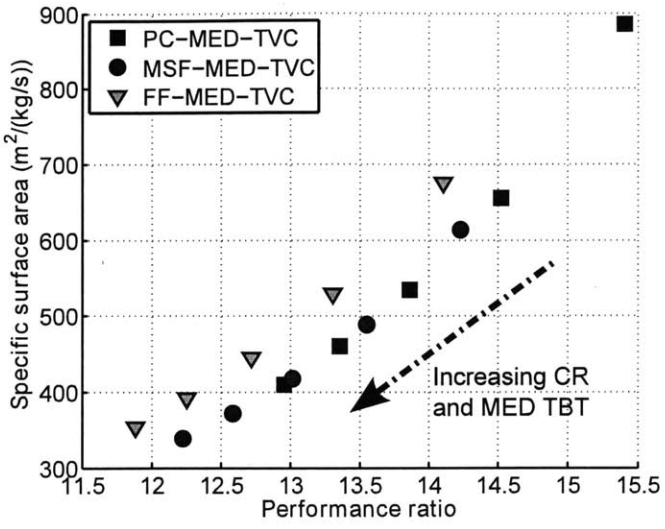


**Figure 3-26:** Performance of MSF-MED-TVC concept as compared to FF-MED-TVC and PC-MED-TVC with varying TVC compression ratio and fixed number of stages/effects.

is merit in the addition of high temperature MSF stages in combination with MED-TVC. Further, a scheme which integrates a parallel-cross MED section as oppose to a forward-feed MED section could perhaps exhibit better performance in comparison to PC-MED-TVC alone. Again, as with the other concepts studied, numerical optimization is necessary in order to determine an optimal structure.

## 3.5 Conclusion

In this study, standard thermal desalination technologies, i.e., multi-stage flash and multi-effect distillation, are decomposed by their physical processes with regards to energy, material, and species balance. The physical processes are then utilized to formulate a superstructure which describes existing thermal desalination configurations and allows for the exploration of alternative configurations.

The performance of three non-standard thermal desalination configurations are presented as a demonstration of the developed superstructure. The studied configurations are the following *i*) FF-PC-MED: a configuration which transitions from forward-feed MED effects to parallel-cross MED effects; *ii*) MSF-MED: a configura-

tion which transitions from MSF stages to forward-feed MED effects and features an alternative MSF stage type; *iii)* MSF-MED-TVC: a configuration which uses parallel steam supplies to power an MSF section and MED-TVC section operating in series. Each of these configurations are evaluated in terms of their performance ratio, specific surface area, and recovery and are promising alternatives to standard thermal desalination configurations.

However, the case studies do not utilize rigorous modeling or numerical optimization. Future work should include the use of non-constant physical properties and heat transfer coefficients. In addition, the possibility of distillate to brine or feed preheating can be easily added to the superstructure in order to consider the work of Sommariva et al. [164]. Numerical optimization will be performed in order to determine the optimal structure of thermal desalination systems integrated with hybrid and/or dual-purpose plants.

# Nomenclature

## Latin Letters

| | | |
|---|---|---|
| A | Area | $m^2$ |
| C | Capital expenditure | $US |
| $\dot{m}$ | Flowrate | kg/s |
| $\Delta h_{fg}$ | Enthalpy of vaporization | kJ/kg |
| P | Pressure | kPa |
| $\dot{Q}$ | Thermal power | kW |
| SA | Specific area | $m^2/(kg/s)$ |
| T | Temperature | °C |
| U | Overall heat transfer coefficient | $W/(m^2K)$ |
| $\dot{W}$ | Shaft work | kW |
| X | Salinity | g/kg |

| | |
|---|---|
| AC | Air compressor |
| AZEP | Advanced zero emissions plant |
| B | Brine stream |
| BE | Brine extraction |
| BF | Backward-feed (MED) |
| BFL | Brine flashing |
| BM | Brine mixing |
| BPE | Boiling point elevation |
| BR | Brine-recirculating (MSF) |
| BST | Back-pressure steam turbine |
| CAPEX | Capital expenditures |
| CC | Combined cycle |
| CCS | Carbon capture and sequestration |
| CD | Condenser |
| COND | Condensation |

| | |
|---|---|
| CR | Compression ratio |
| D | Distillate stream |
| DE | Distillate extraction |
| DM | Distillate mixing |
| ER | Entrainment ratio |
| EST | Extraction/condensing steam turbine |
| F | Feed stream |
| FE | Feed extraction |
| FF | Forward-feed (MED) |
| FG | Flue gas |
| FM | Feed mixing |
| FWH | Feedwater heater |
| GA | Genetic algorithm |
| GCC | Gulf Coorporation Council |
| GDP | Generalized disjunctive programming |
| GT | Gas turbine |
| GTE | Gas turbine exhaust |
| HRSG | Heat recovery steam generator |
| HTF | Heat transfer fluid |
| ITM | Ion transport membrane |
| MEB | Multi-effect boiling, also known as multi-effect distillation |
| MED | Multi-effect distillation |
| MEE | Multi-effect evaporation, also known as multi-effect distillation |
| MINLP | Mixed integer nonlinear programming |
| MOO | Multi-objective optimization |
| MSF | Multi-stage flash |
| MVC | Mechanical vapor compression |
| $N_s$ | Transition effect/stage/unit |
| $N_t$ | Total number of effects/stages/units |
| NF | Nanofiltration |
| NLP | Nonlinear programming |
| OT | Once-through (MSF) |
| P | Pump |
| PC | Parallel-cross (MED) |
| PF | Parallel-feed (MED) |
| PR | Performance ratio |
| PWR | Power-to-water ratio |
| Q | Heat stream |
| RR | Recovery ratio |

| | |
|---|---|
| SDI | Silt density index |
| SF | Supplementary firing |
| ST | Steam turbine |
| SWRO | Seawater reverse osmosis |
| TAC | Total annualized cost |
| TBT | Top brine temperature |
| TDS | Total dissolved solids |
| TIP | Turbine inlet pressure |
| TIT | Turbine inlet temperature |
| TVC | Thermal vapor compression |
| UF | Ultrafiltration |
| V | Vapor stream |

## Greek Letters

| | |
|---|---|
| $\lambda$ | Fraction of split flow |
| $\xi$ | Structural binary variable |

## Subscripts

| | |
|---|---|
| b | Brine |
| bd | (Brine) Blowdown |
| d | Distillate |
| di | Discharge stream (TVC) |
| e | Entrained stream (TVC) |
| ev | Evaporation |
| i | Inlet |
| m | Motive stream (TVC) |
| o | Outlet |
| s | Steam |
| td | Thermal desalination |
| v | Vapor |

THIS PAGE INTENTIONALLY LEFT BLANK

# Bibliography


[1] Numerica Technology, JACOBIAN Modeling and Optimization Software, 2009.

[2] N. M. Abdel-Jabbar, H. M. Qiblawey, F. S. Mjalli, and H. Ettouney. Simulation of large capacity MSF brine circulation plants. *Desalination*, 204(1-3):501–514, 2007.

[3] A. Z. Abdullatef, A. M. Farooque, G. F. Al-Otaibi, N. M. Kither, and S. A. Khames. Optimum nanofiltration membrane arrangements in seawater pretreatment: Part 1. In *IDA World Congress, Gran Canaria, Spain.* IDA, October 2007.

[4] A. Z. Abdullatef, A. M. Farooque, G. F. Al-Otaibi, N. M. Kither, and S. A. Khames. Optimum nanofiltration membrane arrangements in seawater pretreatment: Part 2. In *IDA World Congress, Dubai, UAE.* IDA, November 2009.

[5] H. K. Abdulrahim and F. N. Alasfour. Multi-Objective Optimisation of hybrid MSF-RO desalination system using Genetic Algorithm. *International Journal of Exergy*, 7(3):387–424, 2010.

[6] N. Afgan, M. Carvalho, and D. Al Gobaisi. Indicators for Sustainability Assessment of Water Desalination Systems. In *IDA World Congress*, Bahrain, 2002.

[7] S. P. Agashichev. Analysis of integrated co-generative schemes including MSF, RO and power generating systems (present value of expenses and cost of water). *Desalination*, 164(3):281 – 302, 2004.

[8] S. P. Agashichev and M. El-Dahshan. Reverse osmosis incorporated into existing cogenerating systems as a sustainable technological alternative for United Arab Emirates. *Desalination*, 157(1-3):33 – 49, 2003.

[9] S. P. Agashichev and A. M. El-Nashar. Systemic approach for techno-economic evaluation of triple hybrid (RO, MSF and power generation) scheme including accounting of $CO_2$ emission. *Energy*, 30(8):1283 – 1303, 2005.

[10] K. Al-Anezi and N. Hilal. Scale formation in desalination plants: effect of carbon dioxide solubility. *Desalination*, 204(1-3):385 – 402, 2007.

[11] I. S. Al-Mutaz. Simulation of MSF desalination plants. *Desalination*, 74:317–326, 1989.

[12] I. S. Al-Mutaz. The continued challenge of capacity building in desalination. *Desalination*, 141(2):145–156, 2001.

[13] I. S. Al-Mutaz and A. M. Al-Namlah. Characteristics of dual purpose MSF desalination plants. *Desalination*, 166(0):287 – 294, 2004.

[14] A. E. Al-Rawajfeh. Influence of nanofiltration pretreatment on scale deposition in multi-stage flash thermal desalination plants. *Thermal Science*, 15(1):55–65, 2011.

[15] M. Al-Sahali and H. Ettouney. Developments in thermal desalination processes: Design, energy, and costing aspects. *Desalination*, 214(1-3):227–240, 2007.

[16] M. Al-Shammiri, M. Ahmed, and M. Al-Rageeb. Nanofiltration and calcium sulfate limitation for top brine temperature in Gulf desalination plants. *Desalination*, 167(0):335 – 346, 2004.

[17] M. Al-Shammiri and M. Safar. Multi-effect distillation plants: state of the art. *Desalination*, 126(1-3):45–59, 1999.

[18] M. A. K. Al-Sofi, A. M. Hassan, and E. E. El-Sayed. Integrated and non-integrated power/MSF/RO plants. In *International Desalination Water Reuse Quarterly*, volume 2, pages 10–16, 1992.

[19] M. A. K. Al-Sofi, A. M. Hassan, O. A. Hamad, G. M. Mustafa, A. G. I. Dalvi, and M. N. M. Kither. Means and merits of higher temperature operation in dual-purpose plants. *Desalination*, 125(1-3):213 – 222, 1999.

[20] M. A. K. Al-Sofi, A. M. Hassan, O. A. Hamed, A. G. I. Dalvi, M. N. M. Kither, G. M. Mustafa, and K. Bamardouf. Optimization of hybridized seawater desalination process. *Desalination*, 131(1-3):147 – 156, 2000.

[21] M. A. K. Al-Sofi, A. M. Hassan, G. M. Mustafa, A. G. I. Dalvi, and M. N. M. Kither. Nanofiltration as a means of achieving higher TBT of $\geq 120$°C in MSF. *Desalination*, 118(1-3):123 – 129, 1998.

[22] F. Alasfour, M. Darwish, and A. B. Amer. Thermal analysis of ME-TVC+MEE desalination systems. *Desalination*, 174(1):39 – 61, 2005.

[23] F. N. Alasfour and H. K. Abdulrahim. Rigorous steady-state modeling of MSF-BR desalination systems. *Desalination and Water Treatment*, 1:259–276, 2009.

[24] A. Almulla, A. Hamad, and M. Gadalla. Integrating hybrid systems with existing thermal desalination plants. *Desalination*, 174(2):171 – 192, 2005.

[25] H. Alrobaei. Novel integrated gas turbine solar cogeneration power plant. *Desalination*, 220(1-3):574–587, 2008.

[26] N. Aly and A. El-Fiqi. Thermal performance of seawater desalination systems. *Desalination*, 158(1-3, Sp. Iss. SI):127–142, 2003.

[27] N. H. Aly and M. A. Marwan. Dynamic behavior of MSF desalination plants. *Desalination*, 101(3):287–293, 1995.

[28] R. Anantharaman, O. Bolland, and K. I. Asen. Novel cycles for power generation with $CO_2$ capture using OMCM technology. *Energy Procedia*, 1(1):335 – 342, 2009.

[29] J. Andrianne and F. Alardin. Thermal and membrane process economics: Optimized selection for seawater desalination. *Desalination*, 153(1-3):305 – 311, 2003.

[30] K. Ansari, H. Sayyaadi, and M. Amidpour. Thermoeconomic optimization of a hybrid pressurized water reactor (PWR) power plant coupled to a multi effect distillation desalination system with thermo-vapor compressor (MED-TVC). *Energy*, 35(5):1981–1996, 2010.

[31] M. M. Ashour. Steady state analysis of the tripoli west LT-HT-MED plant. *Desalination*, 152(1-3):191–194, 2003.

[32] Aspen Tech®. ASPEN Plus process modeling and optimization software. http://www.aspentech.com. Accessed: 8/01/2010.

[33] G. Assassa and H. El-Dessouky. Dynamic stability of MSF desalination plants. *Desalination*, 45(2):133, 1983.

[34] L. Awerbuch. Power - Desalination and the Importance of Hybrid Ideas. In *IDA World Congress*, volume 4, pages 181–192, Madrid, Spain, 1997. IDA.

[35] L. Awerbuch. Nanofiltration: the great potential in reducing cost of desalination. In *IDA World Congress on Desalination and Water Reuse, Singapore.* IDA, 2005.

[36] L. Awerbuch. Future Directions in Integration of Desalination, Energy and the Environment. Technical report, American Nuclear Society, Seminar, 2009.

[37] L. Awerbuch, S. May, R. Soo-Hoo, and V. Van Der Mast. Hybrid desalting systems. *Desalination*, 76:189–197, 1989.

[38] L. Awerbuch, V. Vandermast, and R. Soohoo. Hybrid desalting systems - A new alternative. *Desalination*, 64:51–63, November 1987.

[39] H. Baig, M. A. Antar, and S. M. Zubair. Performance evaluation of a once-through multi-stage flash distillation system: Impact of brine heater fouling. *Energy Conversion and Management*, 52(2):1414–1425, 2011.

[40] V. Baujat and T. Bukato. Research and development towards the increase of MED units capacity. In *IDA World Congress, Bahamas*, 2003.

[41] J. H. Beamer and D. J. Wilde. The simulation and optimization of a single effect multi-stage flash desalination plant. *Desalination*, 9(3):259–275, 1971.

[42] L. T. Biegler, I. E. Grossmann, and A. W. Westerberg. *Systematic Methods of Chemical Process Design.* Prentice Hall, New Jersey, 1997.

[43] A. O. Bin Amer. Development and optimization of ME-TVC desalination system. *Desalination*, 249(3):1315–1331, 2009.

[44] I. Bolea, J. Uche, and L. Romeo. Integration of MED with captured $CO_2$ flue gas compression. *Desalination and Water Treatment*, 7:124–131, 2009.

[45] P. Budhiraja and A. A. Fares. Studies of scale formation and optimization of antiscalant dosing in multi-effect thermal desalination units. *Desalination*, 220(1-3):313 – 325, 2008.

[46] G. Cali, E. Fois, A. Lallai, and G. Mura. Optimal design of a hybrid RO/MSF desalination system in a non-OPEC country. *Desalination*, 228(1-3):114 – 127, 2008.

[47] E. Cardona, S. Culotta, and A. Piacentino. Energy saving with MSF-RO series desalination plants,. *Desalination*, 153(1-3):167 – 171, 2003.

[48] E. Cardona and A. Piacentino. Optimal design of cogeneration plants for seawater desalination. *Desalination*, 166:411 – 426, 2004.

[49] E. Cardona, A. Piacentino, and F. Marchese. Performance evaluation of CHP hybrid seawater desalination plants. *Desalination*, 205(1-3):1 – 14, 2007.

[50] C. Casarosa, F. Donatini, and A. Franco. Thermoeconomic optimization of heat recovery steam generators operating parameters for combined plants. *Energy*, 29(3):389 – 414, 2004.

[51] R. Chacartegui, D. Sanchez, N. di Gregorio, F. J. Jimenez-Espadafor, A. Munoz, and T. Sanchez. Feasibility analysis of a MED desalination plant in a combined cycle based cogeneration facility. *Applied Thermal Engineering*, 29(2-3):412–417, 2009.

[52] J. Cohen, I. Janovich, and A. Muginstein. Utilization of waste heat from a flue gases up-stream gas scrubbing system. *Desalination*, 139(1-3, Sp. Iss. SI):1–6, 2001.

[53] K. E. Colombo and O. Bolland. Dynamic simulation of an oxygen mixed conducting membrane-based gas turbine power cycle for $CO_2$ capture. *Energy Procedia*, 1(1):431 – 438, 2009.

[54] K. E. Colombo, O. Bolland, V. V. Kharton, and C. Stiller. Simulation of an oxygen membrane-based combined cycle power plant: part-load operation with operational and material constraints. *Energy Environ. Sci.*, 2:–, 2009.

[55] K. E. Colombo, L. Imsland, O. Bolland, and S. Hovland. Dynamic modelling of an oxygen mixed conducting membrane and model reduction for control. *Journal of Membrane Science*, 336(1-2):50 – 60, 2009.

[56] M. Darwish and A. Alsairafi. Technical comparison between TVC/MEB and MSF. *Desalination*, 170(3):223 – 239, 2004.

[57] M. A. Darwish. Thermal analysis of multi-stage flash desalting systems. *Desalination*, 85(1):59–79, 1991.

[58] M. A. Darwish and H. K. Abdulrahim. Feed water arrangements in a multi-effect desalting system. *Desalination*, 228(1-3):30–54, 2008.

[59] M. A. Darwish, F. Al-Juwayhel, and H. K. Abdulraheim. Multi-effect boiling systems from an energy viewpoint. *Desalination*, 194(1-3):22–39, 2006.

[60] M. A. Darwish and N. Al-Najem. Cogeneration power desalting plants in Kuwait: A new trend with reverse osmosis desalters. *Desalination*, 128(1):17 – 33, 2000.

[61] M. A. Darwish, F. A. Asfour, and N. Al-Najem. Energy consumption in equivalent work by different desalting methods: Case study for Kuwait. *Desalination*, 152(1-3):83 – 92, 2003.

[62] M. A. Darwish, M. M. El-Refaee, and M. Abdel-Jawad. Developments in the multi-stage flash desalting system. *Desalination*, 100(1-3):35–64, 1995.

[63] R. Deng, L. Xie, H. Lin, J. Liu, and W. Han. Integration of thermal energy and seawater desalination. *Energy*, 35(11):4368 – 4374, 2010.

[64] Dow Water Solutions, Midland, MI, USA. *FILMTEC Reverse Osmosis Membranes: Technical Manual.*

[65] H. El-Dessouky. Modelling and simulation of the thermal vapour compression desalination process. In *Nuclear Desalination of Seawater*, pages 315–338. International Atomic Agency, 1997.

[66] H. El-Dessouky, I. Alatiqi, and H. Ettouney. Process synthesis: The multi-stage flash desalination system. *Desalination*, 115(2):155 – 179, 1998.

[67] H. El-Dessouky and H. Ettouney. *Fundamentals of Salt Water Desalination.* Elsevier Science B.V., 2002.

[68] H. T. El-Dessouky, I. Alatiqi, S. Bingulac, and H. M. Ettouney. Steady state analysis of the multiple effect evaporation desalination process. *Chemical Engineering & Technology*, 21, 1998.

[69] H. T. El-Dessouky and H. M. Ettouney. Multiple-effect evaporation desalination systems. Thermal analysis. *Desalination*, 125(1-3):259–276, 1999.

[70] H. T. El-Dessouky and H. M. Ettouney. Multiple Effect Evaporation. In *Fundamentals of Salt Water Desalination*, pages 147–208. Elsevier Science B.V., Amsterdam, 2002.

[71] A. M. El-Nashar. Cogeneration for power and desalination – state of the art review. *Desalination*, 134(1-3):7 – 28, 2001.

[72] E. El-Sayed, M. Abdel-Jawad, S. Ebrahim, and A. Al-Saffar. Performance evaluation of two RO membrane configurations in a MSF/RO hybrid system. *Desalination*, 128(3):231 – 245, 2000.

[73] E. El-Sayed, S. Ebrahim, A. Al-Saffar, and M. Abdel-Jawad. Pilot study of MSF/RO hybrid systems. *Desalination*, 120(1-2):121 – 128, 1998.

[74] W. ElMoudir, M. ElBousiffi, and S. Al-Hengari. Process modelling in desalination plant operations. *Desalination*, 222(1-3):431–440, 2008.

[75] H. Ettouney, H. El-Dessouky, and F. Al-Juwayhel. Performance of the once-through multistage flash desalination process. *Proceedings of the Institution of Mechanical Engineers Part A - Journal of Power and Energy*, 216(A3):229–241, 2002.

[76] H. E. S. Fath. The non-equilibrium factor and the flashing evaporation rate inside the flash chamber of a multi-stage flash desalination plant. *Desalination*, 114(3):277–287, 1997.

[77] E. M. Ferreira, J. A. P. Balestieri, and M. A. Zanardi. Optimization analysis of dual-purpose systems. *Desalination*, 250(3):936 – 944, 2010.

[78] D. Fiaschi, F. Gamberi, M. Bartlett, and T. Griffin. The air membrane-ATR integrated gas turbine power cycle: A method for producing electricity with low $CO_2$ emissions. *Energy Conversion and Management*, 46(15-16):2514 – 2529, 2005.

[79] E. Fois, A. Lallai, and G. Mura. Desalted water from a hybrid RO/MSF plant with RDF combustion: Modelling and economics. In L. Rizzuti, H. Ettouney, and A. Cipollina, editors, *Solar Desalination for the 21st Century - A review of modern technologies and research on desalination couple to renewable energies*, Nato Science for Peace and Security Series C - Environmental Security, pages 327–342, 2007.

[80] K. Foy and J. McGovern. Analysis of the effects of combining air separation with combustion in a zero emissions (ZEITMOP) cycle. *Energy Conversion and Management*, 48(11):3046 – 3052, 2007.

[81] A. Ghobeity and A. Mitsos. Optimal time-dependent operation of seawater reverse osmosis. *Desalination*, 263(1-3):76–88, 2010.

[82] A. Ghobeity, C. J. Noone, C. N. Papanicolas, and A. Mitsos. Optimal time-invariant operation of a power and water cogeneration solar-thermal plant. *Solar Energy*, 85(9):2295 – 2320, 2011.

[83] P. Glueckstern, M. Priel, and M. Wilf. Field evaluation of capillary UF technology as a pretreatment for large seawater RO systems. *Desalination*, 147(1-3):55 – 62, 2002.

[84] I. E. Grossmann and J. P. Ruiz. Generalized disjunctive programming: A framework for formulation and alternative algorithms for minlp optimization. In J. Lee and S. Leyffer, editors, *Mixed Integer Nonlinear Programming*, volume 154 of *The IMA Volumes in Mathematics and its Applications*, pages 93–115. Springer New York, 2012.

[85] V. G. Gude, N. Nirmalakhandan, and S. Deng. Renewable and sustainable approaches for desalination. *Renewable and Sustainable Energy Reviews*, 14(9):2641–2654, 2010.

[86] R. Haddada, E. Ferjani, M. S. Roudesli, and A. Deratani. Properties of cellulose acetate nanofiltration membranes. Application to brackish water desalination. *Desalination*, 167(0):403 – 409, 2004.

[87] O. Hamed and H. Al-Otaibi. Prospects of operation of MSF desalination plants at high TBT and low antiscalant dosing rate. *Desalination*, 256(1-3):181–189, 2010.

[88] O. A. Hamed. Overview of hybrid desalination systems – current status and future prospects. *Desalination*, 186(1-3):207–214, 2005.

[89] O. A. Hamed, M. A. Al-Sofi, G. M. Mustafa, and A. G. Dalvi. The performance of different anti-scalants in multi-stage flash distillers. *Desalination*, 123(2-3):185 – 194, 1999.

[90] O. A. Hamed, A. M. Hassan, K. Al-Shail, and M. A. Farooque. Performance analysis of a trihybrid NF/RO/MSF desalination plant. *Desalination and Water Treatment*, 1(1-3):215–222, 2009.

[91] A. M. Hassan, M. A. K. Al-Sofi, A. S. Al-Amoudi, A. T. M. Jamaluddin, A. M. Farooque, A. Rowaili, A. G. I. Dalvi, N. M. Kither, G. M. Mustafa, and I. A. R. Al-Tisan. A new approach to membrane and thermal seawater desalination processes using nanofiltration membranes (Part 1). *Desalination*, 118(1-3):35 – 51, 1998.

[92] A. M. Hassan, A. M. Farooque, A. T. M. Jamaluddin, A. S. Al-Amoudi, M. A. K. Al-Sofi, A. F. Al-Rubaian, N. M. Kither, I. A. R. Al-Tisan, and A. Rowaili. A demonstration plant based on the new NF–SWRO process. *Desalination*, 131(1-3):157 – 171, 2000.

[93] A. M. Hassan, A. M. Farooque, A. T. M. Jamaluddin, A. S. Al-Amoudi, M. A. K. Al-Sofi, A. Rubian, M. M. Gurashi, N. M. Kither, A. G. I. Dalvi, and I. A. R. Al-Tisan. Optimization of NF Pretreatment of Feed to Seawater Desalination Plants. In *IDA World Congress on Desalination and Water Reuse*, San Diego, California, 1999.

[94] M. N. A. Hawlader, J. C. Ho, and C. K. Teng. Desalination of seawater: an experiment with RO membranes. *Desalination*, 132(1-3):275 – 280, 2000.

[95] A. M. Helal. Once-through and brine recirculation MSF designs-a comparative study. *Desalination*, 171(1):33 – 60, 2005.

[96] A. M. Helal, A. M. El-Nashar, E. Al-Katheeri, and S. Al-Malek. Optimal design of hybrid RO/MSF desalination plants Part I: Modeling and algorithms. *Desalination*, 154(1):43 – 66, 2003.

[97] A. M. Helal, A. M. El-Nashar, E. S. Al-Katheeri, and S. A. Al-Malek. Optimal design of hybrid RO/MSF desalination plants Part II: Results and discussion. *Desalination*, 160(1):13 – 27, 2004.

[98] A. M. Helal, A. M. El-Nashar, E. S. Al-Katheeri, and S. A. Al-Maler. Optimal design of hybrid RO/MSF desalination plants Part III: Sensitivity analysis. *Desalination*, 169(1):43 – 60, 2004.

[99] A. M. Helal and M. Odeh. The once-through MSF design. Feasibility for future large capacity desalination plants. *Desalination*, 166:25–39, 2004.

[100] B. Huang, J. Chang, C. Wang, and V. Petrenko. A 1-D analysis of ejector performance. *International Journal of Refrigeration-Revue Internationale Du Froid*, 22(5):354–364, 1999.

[101] A. Husain, A. Woldai, A. Ai-Radif, A. Kesou, R. Borsani, H. Sultan, and P. B. Deshpandey. Modelling and simulation of a multistage flash (MSF) desalination plant. *Desalination*, 97(1-3):555–586, 1994.

[102] F. P. Incropera. *Fundamentals of heat and mass transfer*. John Wiley, Hoboken, NJ, 6th edition, 2007.

[103] International Association for the Properties of Water and Steam. Revised Release on the IAPWS Industrial Formulation 1997 for the Thermodynamic Properties of Water and Steam, 2007.

[104] X. Jin, A. Jawor, S. Kim, and E. M. V. Hoek. Effects of feed water temperature on separation performance and organic fouling of brackish water RO membranes. *Desalination*, 238(1-3):346 – 359, 2009.

[105] I. Kamal. Integration of seawater desalination with power generation. *Desalination*, 180(1-3):217 – 229, 2005.

[106] I. Kamal and G. V. Sims. Thermal cycle and financial modeling for the optimization of dual-purpose power-cum-desalination plants. *Desalination*, 109(1):1 – 13, 1997.

[107] R. Kehlhofer, F. Hannemann, S. F, and B. Rukes. *Combined-cycle gas and steam turbine power plants*. PennWell, Tulsa, 3 edition, 2009.

[108] E. Koutsakos, C. Bartels, S. Cioffi, S. Rybar, and M. Wilf. Membrane innovations ease freshwater shortages in Cyprus. *Water and Wastewater International*, 22(4):27 – 30, 2007.

[109] G. Kronenberg. Cogeneration with the LT-MED desalination process. *Desalination*, 108(1-3):287–294, February 1997.

[110] G. Kronenberg and F. Lokiec. Low-temperature distillation processes in single- and dual-purpose plants. *Desalination*, 136(1-3):189 – 197, 2001.

[111] H. M. Kvamsdal, K. Jordal, and O. Bolland. A quantitative comparison of gas turbine cycles with $CO_2$ capture. *Energy*, 32(1):10 – 24, 2007.

[112] S. Lee and I. E. Grossmann. Global optimization of nonlinear generalized disjunctive programming with bilinear equality constraints: applications to process networks. *Computers & Chemical Engineering*, 27(11):1557 – 1575, 2003.

[113] H. Ludwig. Hybrid systems in seawater desalination–practical design aspects, present status and development perspectives. *Desalination*, 164(1):1–18, 2004.

[114] A. A. Mabrouk, A. S. Nafey, and H. E. S. Fath. Steam, electricity and water costs evaluation of power-desalination co-generation plants. *Desalination and Water Treatment*, 22(1-3):56–64, October 2010.

[115] F. Mahbub, M. N. A. Hawlader, and A. S. Mujumdar. Combined water and power plant (CWPP) - A novel desalination technology. *Desalination and Water Treatment*, 5(1-3):172–177, May 2009.

[116] N. D. Mancini and A. Mitsos. Conceptual Design and Analysis of ITM Oxy-combustion Power Cycles. *Physical Chemistry Chemical Physics*, 13(48):21351–21361, 2011.

[117] N. D. Mancini and A. Mitsos. Ion Transport Membranes for Oxy-combustion Power Cycle Applications: I Intermediate Fidelity Modeling. *Energy*, 36:4701–4720, 2011.

[118] N. D. Mancini and A. Mitsos. Ion Transport Membranes for Oxy-combustion Power Cycle Applications: II Analysis & Comparison of Alternatives. *Energy*, 36:4721–4739, 2011.

[119] M. Marcovecchio, S. Mussati, N. Scenna, and P. Aguirre. Hybrid Desalination Systems: Alternative Designs of Thermal and Membrane Processes. In R. M. de Brito Alves, C. A. O. do Nascimento, and J. Evaristo Chalbaud Biscaia, editors, *10th International Symposium on Process Systems Engineering: Part A*, volume 27 of *Computer Aided Chemical Engineering*, pages 1011 – 1016. Elsevier, 2009.

[120] M. G. Marcovecchio, P. A. Aguirre, and N. J. Scenna. Global optimal design of reverse osmosis networks for seawater desalination: Modeling and algorithm. *Desalination*, 184(1-3):259 – 271, 2005.

[121] M. G. Marcovecchio, S. F. Mussati, P. A. Aguirre, N. J., and Scenna. Optimization of hybrid desalination processes including multi stage flash and reverse osmosis systems. *Desalination*, 182(1-3):111 – 122, 2005.

[122] M. G. Marcovecchio, S. F. Mussati, N. J. Scenna, and P. A. Aguirre. Global optimal synthesis of integrated hybrid desalination plants. In J. Jezowski and J. Thullie, editors, *19th European Symposium on Computer Aided Process Engineering*, volume 26 of *Computer Aided Chemical Engineering*, pages 573 – 578. Elsevier, 2009.

[123] E. Mathioulakis, V. Belessiotis, and E. Delyannis. Desalination by using alternative energy: Review and state-of-the-art. *Desalination*, 203(1-3):346–365, 2007.

[124] R. McGovern, G. Narayan, and J. Lienhard. Analysis of reversible ejectors and definition of an ejector efficiency. *In Press: International Journal of Thermal Sciences*, 2011. doi:10.1016/j.ijthermalsci.2011.11.003.

[125] A. Messineo and F. Marchese. Performance evaluation of hybrid RO/MEE systems powered by a WTE plant. *Desalination*, 229(1-3):82 – 93, 2008.

[126] M. Methnani, S. H. Choi, A. Hussain, and Y. J. Baek. Techno-economics of Hybrid Desalination Systems. In *IDA World Congress, Spain*, 2007.

[127] K. Mistry, M. Antar, and J. Lienhard V. An improved model for multiple effect distillation. In *EDS Conference, Barcelona*, 2012.

[128] A. Mitsos and P. I. Barton. Parametric Mixed 0-1 Linear Programming: The General Case for a Single Parameter. *European Journal of Operational Research*, 194(3):663–686, 2009.

[129] A. Mitsos, B. Chachuat, and P. I. Barton. Methodology for the Design of Man-Portable Power Generation Devices. *Industrial and Engineering Chemistry Research*, 46(22):7164–7176, 2007.

[130] S. Mussati, P. Aguirre, and N. Scenna. Dual-purpose desalination plants. Part I. Optimal design. *Desalination*, 153(1-3):179 – 184, 2003.

[131] S. Mussati, P. Aguirre, and N. Scenna. Dual-purpose desalination plants. Part II. Optimal configuration. *Desalination*, 153(1-3):185 – 189, 2003.

[132] S. Mussati, P. Aguirre, and N. Scenna. Optimization of alternative structures of integrated power and desalination plants. *Desalination*, 182(1-3):123–129, 2005.

[133] S. F. Mussati, P. A. Aguirre, and N. J. Scenna. Novel Configuration for a Multistage Flash-Mixer Desalination System. *Industrial & Engineering Chemistry Research*, 42(20):4828–4839, 2003.

[134] S. F. Mussati, P. A. Aguirre, and N. J. Scenna. A rigorous, mixed-integer, nonlineal programming model (MINLP) for synthesis and optimal operation of cogeneration seawater desalination plants. *Desalination*, 166:339 – 345, 2004.

[135] S. F. Mussati, P. A. Aguirre, and N. J. Scenna. Improving the efficiency of the MSF once through (MSF-OT) and MSF-mixer (MSF-M) evaporators. *Desalination*, 166(0):141 – 151, 2004.

[136] S. F. Mussati, P. A. Aguirre, and N. J. Scenna. Superstructure of Alternative Configurations of the Multistage Flash Desalination Process. *Industrial & Engineering Chemistry Research*, 45(21):7190–7203, 2006.

[137] A. Nafey, H. Fath, and A. Mabrouk. Exergy and thermoeconomic evaluation of MSF process using a new visual package. *Desalination*, 201(1-3):224 – 240, 2006.

[138] A. Nafey, H. Fath, and A. Mabrouk. Thermo-economic investigation of multi effect evaporation (MEE) and hybrid multi effect evaporation-multi stage flash (MEE-MSF) systems. *Desalination*, 201(1-3):241–254, 2006.

[139] G. Narayan, M. Sharqawy, J. Lienhard, and S. Zubair. Thermodynamic analysis of humidification-dehumidification desalination cycles. *Desalination and Water Treatment*, 16:339–353, 2010.

[140] H. Oh, Y. Choung, S. Lee, J. Choi, T. Hwang, and J. Kim. Scale formation in reverse osmosis desalination: model development. *Desalination*, 238(1-3):333 – 346, 2009.

[141] A. Ophir and F. Lokiec. Review of MED Fundamentals and Costing. In *International Conference on Desalination Costing*, Cyprus, 2004. Middle East Desalination Research Center.

[142] A. Ophir and F. Lokiec. Advanced MED process for most economical sea water desalination. *Desalination*, 182(1-3):187 – 198, 2005.

[143] P. Palenzuela, G. Zaragoza, D. Alarcn, and J. Blanco. Simulation and evaluation of the coupling of desalination units to parabolic-trough solar power plants in the Mediterranean region. *Desalination*, 281(0):379 – 387, 2011.

[144] I. Pfaff and A. Kather. Comparative thermodynamic analysis and integration issues of CCS steam power plants based on oxy-combustion with cryogenic or membrane based air separation. *Energy Procedia*, 1(1):495–502, 2009.

[145] F. Rahman and Z. Amjad. Scale Formation and Control in Thermal Desalination Systems. In *The Science and Technology of Industrial Water Treatment*, pages 271–396. CRC Press, Brecksville, Ohio, USA, 2010.

[146] T. Rensonnet, J. Uche, and L. Serra. Simulation and thermoeconomic analysis of different configurations of gas turbine (GT)-based dual-purpose power and desalination plants (DPPDP) and hybrid plants (HP). *Energy*, 32(6, Sp. Iss. SI):1012–1023, 2007.

[147] M. Rosso, A. Beltramini, M. Mazzotti, and M. Morbidelli. Modeling multistage flash desalination plants. *Desalination*, 108(1-3):365–374, 1997.

[148] J. Rovel, P. Mazounie, and M. Sanz. Description of the largest SWRO ever built. In *IDA World Congress on Desalination and Water Reuse*, Bahamas, 2003.

[149] H. K. Sadhukhan and B. M. Misra. Design of a 1.4 MIGD desalination plant based on MSF and RO processes for an arid area in India. *Desalination*, 106(1-3):17 – 23, 1996.

[150] B. Sauvet-Goichon. Ashkelon desalination plant - A successful challenge. *Desalination*, 203(1-3):75 – 81, 2007.

[151] H. Sayyaadi and A. Saffari. Thermoeconomic optimization of multi effect distillation desalination systems. *Applied Energy*, 87(4):1122–1133, 2010.

[152] H. Sayyaadi, A. Saffari, and A. Mahmoodian. Various approaches in optimization of multi effects distillation desalination systems using a hybrid metaheuristic optimization tool. *Desalination*, 254(1-3):138–148, 2010.

[153] N. J. Scenna. Synthesis of thermal desalination processes. Part I. Multistage flash distillation system (MSF). *Desalination*, 64(0):111 – 122, 1987.

[154] N. J. Scenna. Synthesis of thermal desalination processes. Part II. Multi effect evaporation. *Desalination*, 64(0):123 – 135, 1987.

[155] R. Semiat. Energy issues in desalination processes. *Environmental Science and Technology*, 42(22):8193 – 8201, 2008.

[156] M. Shakouri, H. Ghadamian, and R. Sheikholeslami. Optimal model for multi effect desalination system integrated with gas turbine. *Desalination*, 260(1-3):254 – 263, 2010.

[157] M. A. Sharaf, A. S. Nafey, and L. Garca-Rodrguez. Exergy and thermoeconomic analyses of a combined solar organic cycle with multi effect distillation (MED) desalination process. *Desalination*, 272(1-3):135–147, 2011.

[158] M. H. Sharqawy, J. H. Lienhard, V, and S. M. Zubair. Thermophysical properties of seawater: A review of existing correlations and data. *Desalination and Water Treatment*, 16(1-3):354–380, 2010.

[159] E. J. Sheu, A. Mitsos, A. A. Eter, E. M. A. Mokheimer, M. A. Habib, , and A. Al-Qutub. A Review of Hybrid Solar- Fossil Fuel Power Generation Systems and Performance Metrics. *ASME Journal of Solar Energy Engineering*, In Press, 2012.

[160] Silveira, J. L. and C. E. Tuna. Thermoeconomic analysis method for optimization of combined heat and power systems. Part I. *Progress in Energy and Combustion Science*, 29(6):479 – 485, 2003.

[161] A. P. Simpson and A. Simon. Second law comparison of oxy-fuel combustion and post-combustion carbon dioxide separation. *Energy Conversion and Management*, 48(11):3034 – 3045, 2007.

[162] C. Sommariva. Novel Hybrid MED-MSF Concept: Increasing Efficiency and Production in Combined Power and Desalination Plants. In *IDA World Congress Singapore*, 2005.

[163] C. Sommariva and L. Awerbuch. Improving Efficiencies in Thermal Desalination Systems: The Layyah Plant Experience. In *International Water Forum Dubai*, 2006.

[164] C. Sommariva, N. Lior, E. Sciubba, and D. Pinciroli. Innovative Configuration for Multi Stage Flash Desalination Plant. In *IDA Proceedings, San Diego*, volume I, page 16, 1999.

[165] K. Spiegler and Y. El-Sayed. *A desalination primer*. Balaban Desalination Publications, Santa Maria, Italy, 1994.

[166] R. Steeneveldt, B. Berger, and T. Torp. $CO_2$ Capture and Storage: Closing the Knowing-Doing Gap. *Chemical Engineering Research and Design*, 84(9):739 – 763, 2006.

[167] S. G. Sundkvist, S. Julsrud, B. Vigeland, T. Naas, M. Budd, H. Leistner, and D. Winkler. Development and testing of AZEP reactor components. *International Journal of Greenhouse Gas Control*, 1(2):180 – 187, 2007.

[168] M. S. Tanvir and I. M. Mujtaba. Optimisation of MSF desalination process for fixed water demand using gPROMS. In *17th European Symposium on Computer Aided Process Engineering*, volume 24 of *Computer Aided Chemical Engineering*, pages 763 – 768. Elsevier, 2007.

[169] M. S. Tanvir and I. M. Mujtaba. Optimisation of design and operation of MSF desalination process using MINLP technique in gPROMS. *Desalination*, 222(1-3):419–430, March 2008.

[170] M. Turek. Seawater desalination and salt production in a hybrid membrane-thermal process,. *Desalination*, 153(1-3):173 – 177, 2003.

[171] M. Turek and M. Chorazewska. Nanofiltration process for seawater desalination-salt production integrated system. *Desalination and Water Treatment*, 7(1-3):178–181, July 2009.

[172] M. Turek and P. Dydo. Hybrid membrane-thermal versus simple membrane systems. *Desalination*, 157(1-3):51 – 56, 2003.

[173] J. Uche, L. Serra, and A. Valero. Hybrid desalting systems for avoiding water shortage in Spain. *Desalination*, 138(1-3):329 – 334, 2001.

[174] J. Uche, L. Serra, and A. Valero. Thermoeconomic optimization of a dual-purpose power and desalination plant. *Desalination*, 136(1-3):147 – 158, 2001.

[175] F. Vince, F. Marechal, P. Breant, and E. Aoustin. Innovative design and multi-objective optimization of hybrid reverse osmosis and multi-stage flash desalination plants. In *CHISA 2006 - 17th International Congress of Chemical and Process Engineering*, 2006.

[176] P. Voll, M. Lampe, G. Wrobel, and A. Bardow. Superstructure-free synthesis and optimization of distributed industrial energy supply systems. *Energy*, 2012. In Press, DOI=http://dx.doi.org/10.1016/j.energy.2012.01.041.

[177] T. F. Wall. Combustion processes for carbon capture. *Proceedings of the Combustion Institute*, 31(1):31 – 47, 2007.

[178] M. Wilf. *The Guidebook to Membrane Desalination Technology.* Balaban Desalination Publications, L'Aquila, Italy, 2007.

[179] M. Wilf and K. Klinko. Optimization of seawater RO systems design. *Desalination*, 138(1-3):299 – 306, 2001.

[180] S. Wu. Analysis of water production costs of a nuclear desalination plant with a nuclear heating reactor coupled with MED processes. *Desalination*, 190(1-3):287 – 294, 2006.

[181] H. Yeomans and I. E. Grossmann. A systematic modeling framework of superstructure optimization in process synthesis. *Computers & Chemical Engineering*, 23(6):709 – 731, 1999.

[182] T. I. Yun, C. J. Gabelich, M. R. Cox, A. A. Mofidi, and R. Lesan. Reducing costs for large-scale desalting plants using large-diameter, reverse osmosis membranes. *Desalination*, 189(1-3):141 – 154, 2006.